CONTENTS

Aims and scope

Building Materials and Structures aims at providing an international forum for communication and dissemination of innovative research and application in the field of building materials and structures. Journal publishes papers on the characterization of building materials properties, their technologies and modeling. In the area of structural engineering Journal publishes papers dealing with new developments in application of structural mechanics principles and digital technologies for the analysis and design of structures, as well as on the application and skillful use of novel building materials and technologies.

The scope of Building Materials and Structures encompasses, but is not restricted to, the following areas: conventional and non-conventional building materials, recycled materials, smart materials such as nanomaterials and bio-inspired materials, infrastructure engineering, earthquake engineering, wind engineering, fire engineering, blast engineering, structural reliability and integrity, life cycle assessment, structural optimization, structural health monitoring, digital design methods, data-driven analysis methods, experimental methods, performance-based design, innovative construction technologies, and value engineering.

President of ASES
Professor Zlatko Marković
University of Belgrade
Faculty of Civil Engineering
Institute for Materials and Structures
Belgrade, Serbia

CONTACT

EMAIL:
zlatko@imk.grf.bg.ac.rs

FOREWORD

Symposium 2020 of Association of Structural Engineers of Serbia (ASES), that had been postponed because of the pandemic, was finally held between 13th and 15th May 2021 in the „Izvor" hotel in Arandjelovac. It was a combined in-person and online Conference. Despite all the well-known problems caused by the epidemic, the Symposium 2020 was successfully organized. In the proceedings of the national and international conference, 96 papers from 17 countries were published. Most of them were presented directly at the conference venue, and some were presented online, but were also live broadcasted via the Zoom platform. There was also a poster session. Six distinguished keynote speakers presented the most recent papers from the fields of steel and concrete structures, bridge engineering, materials and durability and seismic regulation.

All oral presentations were divided into sessions with different topics such as design and executions of structures, experimental research, assessment, rehabilitation, retrofitting and reconstructions, calculation methods and theoretical aspects, technical regulations, foundation and geotechnical aspects, new materials and technologies and aseismic design (organized in cooperation with Serbian Association for Earthquake Engineering - SAEE).

ASES also takes care of young researchers and engineers (under 30 years), so the best papers of young authors are traditionally published in the Building Materials and Structures Journal. This time, an anonymous jury carefully followed presentations of all young authors and made a choice of five best papers, not only according to the quality of the papers, but also regarding presentation and discussion.

Following papers were chosen: *Effects of material uncertainties on vibration performance of cross laminated timber floors* (authors: *Marija Milojević*, Emilija Damnjanović, Marija Nefovska-Danilović, Miroslav Marjanović)*, Software implementation of section class and resistance calculation for general loading case* (authors: *Tanja Nožica,* Đorđe Jovanović, Drago Žarković) *Influence of cement replacement with limestone filler on the properties of concrete* (authors*: Ksenija Tešić,* Snežana Marinković*,* Aleksandar Savić)*, The new buckling curves for cold-formed stainless steel equal-leg angle columns* (authors: Jelena Dobrić*, Aljoša Filipović,* Nancy Baddoo, Zlatko Marković*,* Dragan Buđevac) and *Vibration serviceability limit state of pedestrian bridges* (authors: *Adam Ramoul,* Milan Spremić).

This issue of Building Materials and Structures is completely dedicated to ASES's Symposium 2020. Beside awarded young researchers' papers, another five representative papers, chosen by Editor-in-Chief, are also published.

Effects of material uncertainties on vibration performance of cross laminated timber floors[*]

Marija Milojević[*1)], Emilija Damnjanović[1)], Marija Nefovska-Danilović[1)], Miroslav Marjanović[1)]

[1)] University of Belgrade Faculty of Civil Engineering, Bulevar kralja Aleksandra 73, 11000 Belgrade, Serbia

A B S T R A C T

Variety of wood species and complexity of their structure make the reliable material properties of cross-laminated timber (CLT) difficult to obtain, which can lead to inaccurate prediction of CLT behavior. Due to high stiffness-to-weight ratio, CLT floors can suffer from vibration serviceability issues. This paper aims to quantify the uncertainties induced by material properties and investigate their effect on vibration performance of CLT floors. Analysis based on Monte Carlo simulations, considering material properties as random variables, is developed. Based on the conducted analysis, appropriate conclusions have been derived.

1   Introduction

During the 20th century, reinforced concrete was found to be the most economical and thus the most commonly used construction material in civil engineering. At the end of the century, as environmental awareness was growing, new materials with low carbon footprint that could be competitive with mineral based materials were needed. This led to renaissance of timber as construction material and development of a novel wood engineering product: cross-laminated timber (CLT). It is a plate-like product, composed of several wooden layers bonded together in a crosswise manner. Modern manufacturing techniques and high structural strength of timber make CLT an element with great stiffness properties and unique aesthetic appeal. CLT structures are characterized by high level of prefabrication, fast and simple transport and assembly, good fire resistance, thermal insulation capacity and ability to tolerate chemically aggressive environments. All these facts increased global interest in CLT and led to many projects on research and development of CLT products [1-2].

One of the main advantages of CLT compared to reinforced concrete is high stiffness-to-weight ratio, which enables large span lightweight floors to be designed. However, CLT floors under human-induced dynamic load may exhibit vibration serviceability issues such as human discomfort and malfunction of vibration sensitive equipment. Consequently, accurate and reliable prediction of dynamic properties of CLT floors is required [3-4].

Variety of wood species and complexity of its structure make the reliable material properties of cross-laminated timber (CLT) difficult to obtain. Effects of annual ring patterns on material properties of wood have been studied by Labonnote et al. [5]. Material uncertainty, as well as

uncertainties in boundary conditions and pedestrian dynamic load can lead to inaccurate prediction of dynamic response of CLT floors [6].

Research in order to quantify the effect of material uncertainty on modal properties of wooden floors has been conducted by Persson el al. [7] and Lim & Manuel [8]. Vibroacoustic response of wooden and CLT floors with material parameter variability has been studied by Persson & Floden [9] and Qian [10]. All analyses demonstrated great influence of material uncertainties on the natural frequencies and acoustic performance of investigated wooden floors.

Currently, material properties of CLT are differently regulated in technical approvals [11], which might lead to significant differences between the actual mechanical properties and those defined in the design guidelines and recommendations. Material properties depend on the strength class of CLT as well as the strength class of the base material.

The aim of this paper is to quantify the uncertainties induced by material properties and investigate their effect on vibration performance of CLT floors. Material properties, in terms of mass density, elastic modulus EL and shear moduli GLT and GRT are considered as random variables, while other properties as deterministic. Two different sampling techniques to generate random variables have been applied and analysis based on Monte Carlo (MC) simulation has been carried out. Numerical modelling and analysis of the investigated CLT floor have been performed using the finite element (FE) models in Abaqus CAE software package [12]. Models have been automatically generated using the Python scripting. Obtained results are statistically analyzed and conclusions have been derived.

---

[*] *Awarded as best young researcher's paper, presented at ASES 2020 Symposium, Arandjelovac, Serbia, May 2021.*
[*] Corresponding author:
   E-mail address: mmilojevic@grf.bg.ac.rs

2 Modal analysis of CLT floor

2.1 CLT properties and numerical model

Wood is an orthotropic material with three principal material axes: the longitudinal axe is aligned with the fiber direction (*L*), while the radial (*R*) and tangential (*T*) axes are orthogonal to annual rings (Figure 1a). Each layer (*k*) of CLT panel exhibits elastic orthotropic material behavior defined as:

$$
\begin{Bmatrix} \varepsilon_L \\ \varepsilon_T \\ \varepsilon_R \\ \gamma_{TR} \\ \gamma_{LR} \\ \gamma_{LT} \end{Bmatrix}^{(k)} = \begin{bmatrix} 1/E_L & -\nu_{TL}/E_T & -\nu_{RL}/E_R & 0 & 0 & 0 \\ -\nu_{LT}/E_L & 1/E_T & -\nu_{RT}/E_R & 0 & 0 & 0 \\ -\nu_{LR}/E_L & -\nu_{TR}/E_T & 1/E_R & 0 & 0 & 0 \\ 0 & 0 & 0 & 1/G_{TR} & 0 & 0 \\ 0 & 0 & 0 & 0 & 1/G_{LR} & 0 \\ 0 & 0 & 0 & 0 & 0 & 1/G_{LT} \end{bmatrix}^{(k)} \begin{Bmatrix} \sigma_L \\ \sigma_T \\ \sigma_R \\ \tau_{TR} \\ \tau_{LR} \\ \tau_{LT} \end{Bmatrix}^{(k)}
\tag{1}
$$

where E_L, E_T and E_R are elastic moduli in the longitudinal, transverse, and radial direction, respectively, ν_{ij} are the Poisson's ratios, and G_{ij} are the Poisson's ratios, and G_{ij} are the shear moduli. CLT floor panel used in the analysis is presented in Figure 1b. Panel's dimensions are 4x8m, and it is composed of 5 layers, bonded in crosswise manner, with stacking sequence (0/90/0/90/0). Height of each layer is 0.03m. Such panel can be used as floor structure in common residential or commercial building. Material properties for C24 timber class [11] are applied (Table 1). The outer layers of CLT panel are oriented in the span direction (L = 4m).

Finite element-based model has been created using Abaqus CAE software package. The finite element mesh consists of 800 S4R shell elements (quadrilateral 4-node shell element with reduced integration) with assigned composite cross section.

Simply supported boundary conditions have been assigned to the two longer floor edges, while the other two remained free. Material axes of the layers are oriented by angle 0° or 90° with respect to the laminate coordinates. Thus, the constitutive relations given in Eq. (1) must be transformed from the material to the global coordinate system, using the well-known transformation matrix.

2.2 Free vibration analysis

Based on the material properties given in Table 1, dynamic properties of CLT floor panel have been determined. Natural frequencies and modal masses of the first five and the twelfth mode, respectively, have been calculated and elaborated in Table 2. First five modes are the bending modes, while the twelfth mode corresponds to the first shear mode. Mode shapes are shown in Figure 2. Calculated modal masses correspond to the unity scaled mode shapes.
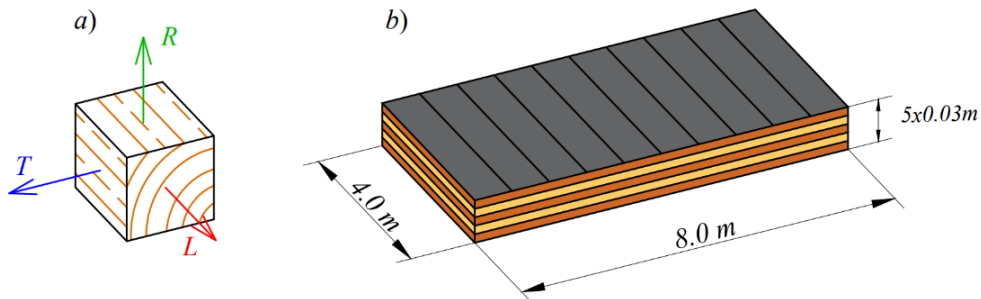
Figure 1. (a) Principal material axes, (b) Layout of CLT floor

Table 1. Mean values of material properties for C24 timber class of CLT panel

ρ [kg/m³]	E_L [MPa]	$E_R=E_T$ [MPa]	$G_{LR}=G_{LT}$ [MPa]	G_{RT} [MPa]	ν_{LT}	ν_{LR}	ν_{RT}
450	11000	370	690	69	0.49	0.39	0.64

Table 2. Dynamic properties of the considered 5-layer CLT floor (4 x 8 m)

Mode No.	Mode type	Natural frequency [Hz]	Modal mass [kg]
1	1st bending	18.06	968.62
2	2nd bending	18.73	403.23
3	3rd bending	21.48	315.45
4	4th bending	28.13	285.69
5	5th bending	39.74	284.05
12	1st shear	77.43	1078.3
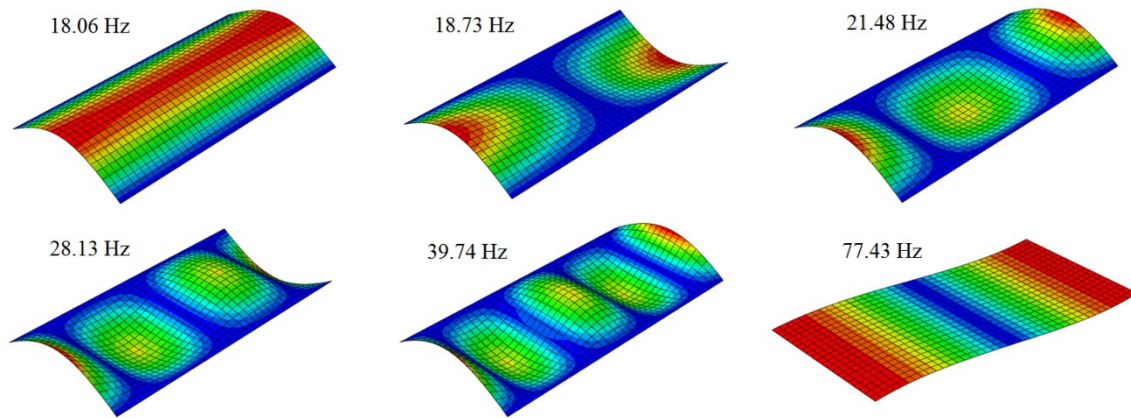
Figure 2. Mode shapes of the considered 5-layer CLT floor (4 x 8 m)

3   Material uncertainty

3.1 Local sensitivity analysis

In order to determine the sensitivity of natural frequencies to random changes in material properties, local sensitivity analysis has been performed. For that purpose, one individual material parameter has been considered as random and all the remaining as deterministic. Normal distribution for four material parameters: mass density ρ, longitudinal elastic modulus E_L, and shear moduli G_{LT} and G_{RT}, respectively, was assumed, with mean values defined in Table 1. Coefficient of variation (COV) of random variables has been increased up to 20% and COVs of the five bending and first shear natural frequencies were calculated. The results after 2,000 conducted MC simulations are presented in Figure 3. Natural frequencies are affected the most by the variability of the mass density. Moreover, it can be noticed that all modes are affected equally by the random change of this parameter. Influence of modulus E_L on the bending modes is significant. The highest influence of E_L is observed in the first mode and it decreases with higher bending modes, while the shear mode has found to be unaffected. On the other hand, variation of the shear modulus G_{LT} has strong impact on the first shear mode and low impact on the natural frequencies of bending modes. The change in the shear modulus G_{RT} induces small change in bending modes, and no change in the natural frequency of the first shear mode.

3.2 Global sensitivity analysis

In the global sensitivity analysis, four material parameters, namely ρ, E_L, G_{LT} and G_{RT}, are simultaneously treated as random variables. It is assumed that all parameters follow the normal distribution, with mean values given in Table 1 and COVs of 10%. Two different sampling techniques have been used: pseudo-random and Latin hypercube. After generating samples of the uncertain parameters, 10,000 Monte Carlo simulations have been performed.

Generation of Abaqus input files with different set of mechanical parameters has been carried out using Python scripting. After the calculation of the natural frequencies, modal masses and (unity scaled) mode shapes, they have been automatically collected from the output files created by Abaqus.

The results of the statistical analysis of the dynamic properties of CLT floor are presented in Figures 4 and 5. COV of 10% for the four input mechanical parameters resulted in the COVs of 6.91%, 6.68%, 6.26%, 6.07% and 6.02% for the natural frequencies of the first five bending modes, respectively, and 7.26% for the first shear mode, following the lognormal distribution when the input parameters are generated by using pseudo-random sampling technique. When Latin hypercube sampling technique is applied, the calculated COVs for the investi-gated natural frequencies are 6.79%, 6.57%, 6.16%, 5.97%,
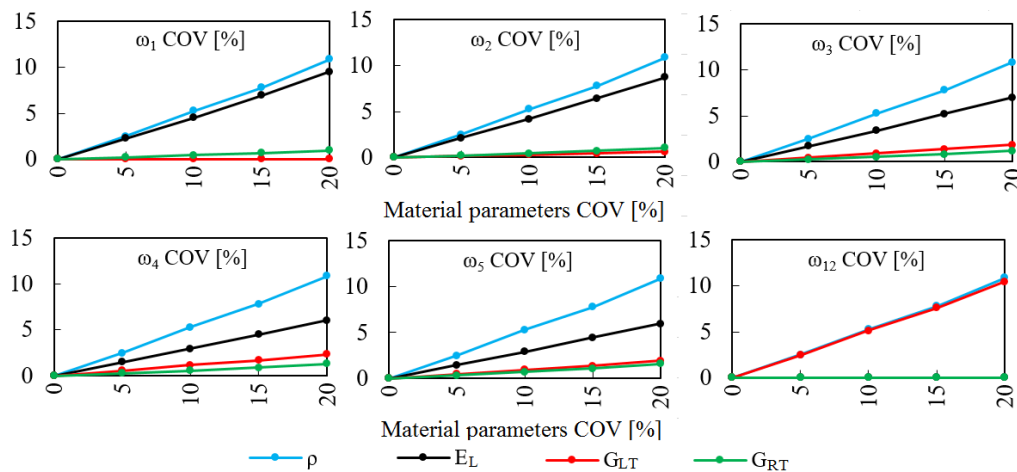
Figure 3. Variation of natural frequency COV with individual change of random variables
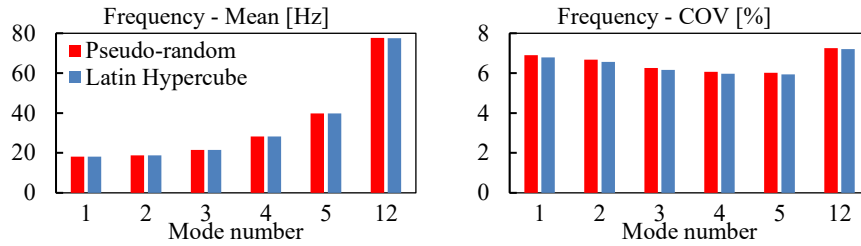
Figure 4. Statistical properties of natural frequencies of CLT floor, considering different sampling techniques
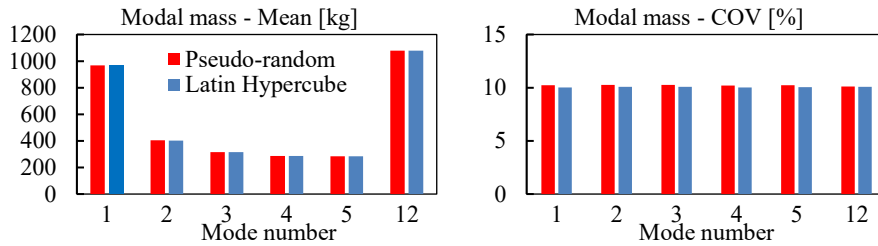
Figure 5. Statistical properties of modal masses of CLT floor, considering different sampling techniques

5.94% and 7.21%. The average difference in the natural frequencies COVs between two sampling techniques is 1.5%. Variations of input parameters resulted in modal masses following the normal distribution, with the COV of 10.27% (pseudo-random) and 10.03% (Latin hypercube).

In addition, the influence of number of simulations on the statistical results for both sampling techniques has been investigated. Mean values and COVs of the natural frequencies regarding the number of simulations are presented in Figure 6 (pseudo-random) and Figure 7 (Latin hypercube). Mean values of the investigated natural frequencies, for both sampling techniques, are nearly constant. The average difference in mean values while comparing 100 and 10,000 simulations is below 1%. The Latin hypercube technique resulted in adequately determined COVs of all investigated natural frequencies after 2,000 simulations.
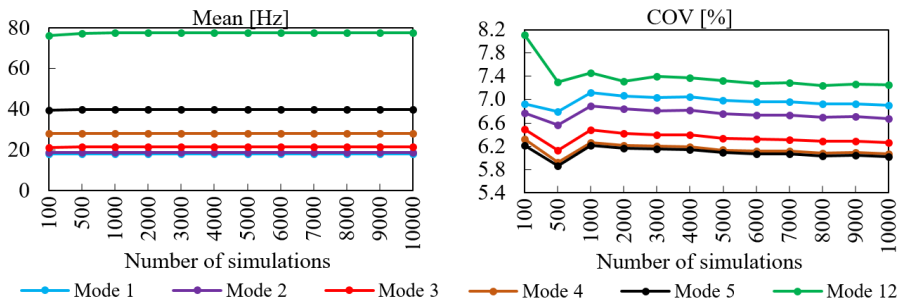
Figure 6. Statistical properties of natural frequencies in regard to number of simulations generated by pseudo-random sampling techique
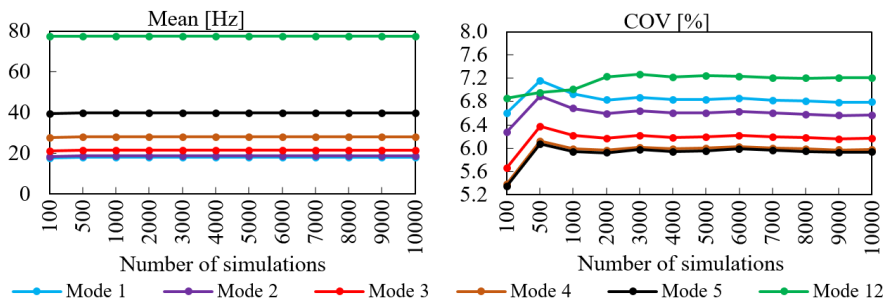
Figure 7. Statistical properties of natural frequencies in regard to number of simulations generated by Latin hypercube sampling technique
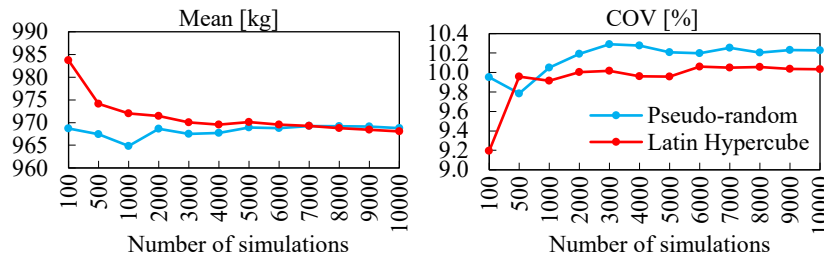
Figure 8. Statistical properties of modal mass of the first mode in regard to number of simulations

The difference between COVs calculated after 2,000 and 10,000 simulations is less than 0.5%. When pseudo-random sampling is used, slight decrease of natural frequencies COVs after 2,000 up to 10,000 simulations is noticeable.

Modal masses of all modes are affected equally by the random changes in material properties. In Figure 8 the mean value and COV of modal mass of the first mode against the number of simulations for both sampling techniques are presented. If less than 2,000 simulations are performed, the differences in mean values and COVs calculated by using two sampling techniques are significant. When number of simulations is greater than 2,000, both techniques resulted in similar statistical parameters.

4   Conclusions

The influence of material uncertainty on the dynamic properties of CLT floor has been investigated numerically. Four material parameters, mass density ρ, longitudinal elastic modulus E_L, and shear moduli G_{LT} and G_{RT}, respectively, are considered as random variables, and the remaining parameters as deterministic. Uncertainty quantification analysis based on Monte Carlo simulations had been performed and the following conclusions were derived:

– Natural frequencies are most affected by the changes in mass density and all modes are equally affected. The longitudinal elastic modulus E_L has great impact on the natural frequencies of bending modes, while the changes in the shear modulus G_{LT} affect only the natural frequency of shear mode.

– Normal distributed uncertain material parameters with 10% COVs resulted in the lognormal distributed natural frequencies and normal distributed modal masses for both sampling techniques. When pseudo-random sampling is used, COVs of natural frequencies are insignificantly higher compared to the Latin hypercube technique. In both cases, COVs are approximately 6-7% for bending modes and 7.2% for the shear mode. COVs of modal masses are also similar for both sampling techniques, about 10%.

– Mean values of natural frequencies can be accurately calculated after 100 simulations, while 2,000 simulations are needed for adequately determination of COVs when both sampling techniques are applied.

References

[1] Brandner R., Flatscher G., Ringhofer A., Schickhofer G., Thiel A.: Cross laminated timber (CLT): overview and development, European Journal of Wood and Wood Products, 74 (3), 2006, 331–351.

[2] Borgstrom E., Frobel J.: The CLT Handbook: CLT structures – facts and planning, Föreningen Sveriges Skogsindustrier, Skogsindustrierna, Sweden, 2019.

[3] Matilainen J. P., Puttonen J.: Free vibration of CLT plates, Journal of Structural Mechanics, 47 (1), 2014, 17-33.

[4] Labonnote N., Malo K. A.: Vibration properties of cross laminated timber floors, 1st International Conference on Structures & Architecture, Guimaraes, Portugal, 2010.

[5] Labonnote N., Malo K. A.: Effect of annual ring patterns on Norway Spruce resulting material properties. 11th World Conference on Timber Engineering – WCTE 2010, Italy, 2010.

[6] Huanga H., Gao Y., Chang W. S.: Human-induced vibration of cross-laminated timber (CLT) floor under different boundary conditions, Engineering Structures, 204, 2020, 110016.

[7] Persson P., Frier L., Pedersen L., Andersen L. V., Manuel L.: Influence of uncertain parameters on modal properties of wood floors, 7th International Conference on Structural Engineering, Mechanics and Computation, Cape Town, South Africa, 2019.

[8] Lim H. U., Manuel L., Persson P., Andersen L. V., A surrogate model to describe uncertainties in wood floor modal frequencies, 7th International Conference on Structural Engineering, Mechanics and Computation, Cape Town, South Africa, 2019.

[9] Persson P., Floden O.: Effect of material parameter variability on vibroacoustic response of wood floors, Applied Acoustics, 146, 2019, 38-79.

[10] Qian C., Menard S., Bard D., Negreira J.: Development of vibroacoustic stochastic finite element prediction tool for a CLT floor, Applied Science, 9(6), 2019, 1106.

[11] Wallner-Novak M., Koppelhuber I., Pock K.: Cross-laminated timber structural design: Basic design and engineering principles according to Eurocode, pro:Holz Austria, ISBN: 978-3-902926-03-6, 2014.

[12] Abaqus, User manual. Version 6.9, Providence, RI, USA: DS SIMULA Corp, 2009.

Software implementation of section class and resistance calculation for general loading case[*]

Tanja Nožica[*1)], Đorđe Jovanović[1)], Drago Žarković[1)]

[1)] Faculty of Technical Sciences University of Novi Sad, Trg Dositeja Obradovića 6, 21000 Novi Sad, Serbia

ABSTRACT

In this paper, the problems arising in implementation of the cross-section class and resistance according to Eurocode, especially for classes 1 and 2 of the steel sections, are presented for general loading case. As Eurocode assumes full plastification of the section, regardless of corresponding strain in the material, it is inevitable to find the position of the plastic neutral axis for ultimate limit state of the section. But, for this purpose, one cannot use the Eurocode's expressions for section resistance. Moreover, solution and strategies used in the steel design module of the Matrix 3D are presented in the paper.

1   Introduction

Trends in modern technical regulations, to which Eurocode belongs, are certainly on the side of almost complete automation of the calculations in the appropriate software. Unfortunately, many of the commercial software don't follow the rules and logic of regulations to their full extent, either due to the complexity of the necessary algorithms or their cumbersome change, frequent changes in regulations, or often insufficient analysis and knowledge of the regulations themselves. In Serbia, in addition to one widespread commercial software, there have been a couple of attempts to develop smaller academic software to the level of comprehensiveness of complete structural calculation with design, but no such project has been completed. At the Faculty of Technical Sciences, the academic software Matrix 3D [5] [6] [7] is being developed, which implements a module for dimensioning steel elements according to Eurocode. The initial problem that arises in this kind of code is described here in more detail and a solution is proposed, mostly for the purpose of encouraging and assisting other similar endeavors. Another reason is that the literature related to this particular problem is scarce, mostly because it is considered as an elementary problem. Furthermore, Eurocode does not give its equations for the resistance of the "U" cross-section, and the assumptions made by [2] [3] papers, regarding the position of the neutral axis, have been proven wrong in this paper. The strategy used in Matrix 3D to efficiently calculate the cross section class but also the resistant surface of the cross section is presented in following chapters, along with the assumptions made during the solution process. It is well documented [2] [3] [4] that the Eurocode expressions for cross section resistance are not very precise, hence there is a justification to use as simple method as possible. Surely, a

more precise solutions are possible, but for the price of more time-consuming computational effort.

2   Problem definition

During the design of each steel element, according to Eurocode, it is first necessary to determine the class of the cross-section, and then the resistance of the cross-section. The class of the cross section depends on the stress distribution in each individual part of the cross-section. For classes 1 and 2, it is necessary to find the position of the plastic neutral axis for each load combination. To do this, it is necessary to know the limit strain state in order to extrapolate strains due to the design values of internal forces. Considering that Eurocode allows for the total plasti-fication of cross-section it is impossible to know the strain state. It is illogical because it is implicitly allowed for strain to reach infinity. This is why the stress state must be found, without firm theoretical background. In other words, it is necessary to know the actual cross-section plastic resistance to determine the position of the plastic neutral axis.

2.1 Resistance of cross-section due to bending and axial force according to en 1993

In order to determine the plastic limit state of the section due to biaxial bending and axial force, Eurocode 3 provides expressions in EN 1993-1-1 [1]. The parameters α and β are included in this approximate expression, which represent the influence of the type of cross section (U, I, L etc.). Based on the expression, an interaction surface that represents the cross-sections plastic resistance, can be created (Figure 1).
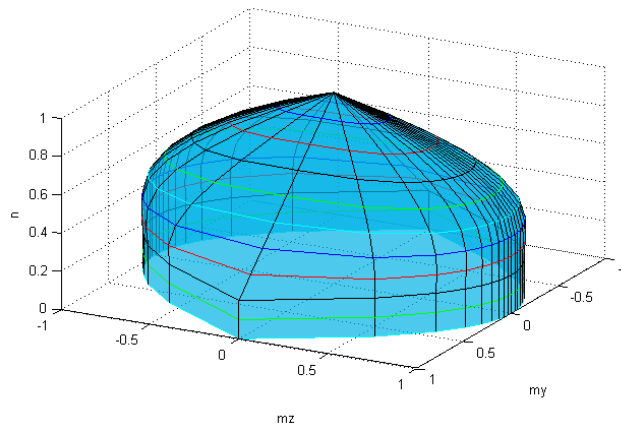
Figure 1. Biaxial bending and axial force interaction surface (EC3) for IPE300 cross-section at axial load levels n=NEd/NRd

The surface defined by Eurocode does not match the real surface because it is a simplified one. Another problem is that there are only expressions for "I" sections and hollow sections, but not for "U" sections.

Anyhow, the internal forces in the section for a given load combination can assume one of the three different position in the force space: 1) inside the resistance surface, 2) on the resistance surface or 3) outside the surface. The case when the point on *N-Mz-My* diagram is outside resistance surface means that this forces cannot be transmitted by the given section, hence there is no need to continue with the classification of the section. The case when it is exactly on the surface is practically almost impossible, but it is trivial to determine the plastic neutral axis in this case. In most of the cases, the point (N_{Ed}, My_{Ed}, Mz_{Ed}) is somewhere inside the surface. In this case, it is necessary to reach the ultimate state by scaling some (or all, or some ratio) of the internal forces. It is not specified which ratio, nor in Eurocode or similar documents. There are several different strategies, and some of the software, such are Dlubal RFEM [8] or SOFISTIK [9] explain their strategies, while majority of others do not mention the problem in their theory reference.

2.2 Neutral axis position for biaxial bending with axial force

The papers [2] [3] show the cross-section resistances due to biaxial bending with the axial force. However, they are calculated on the assumption that in the case of biaxial bending with axial force neutral axis preserve its incline independent of the intensity of the axial force.

In general, when a cross-section which is subjected to a bending moment which does not coincide with the cross-sectional main axes, the neutral axis does not coincide with the angle of the bending axis nor with one of the main axes. Moreover, the neutral axis rotates from the bending axis towards the weaker axis with an increase of the axial force. Hence, when the axial force increases retaining the same bending moment, the plastic neutral axis gains a certain movement, but also the shift of the angle towards the weaker axis of cross section.

3 Method

In order to design the cross-section, it is necessary to define the conditions when the cross section is in the ultimate limit state. The conditions can be set according to the ultimate strain (as it is case for reinforced concrete sections), but the problem with the steel sections defined as they are in EN 1993-1-1 [1] is that the ultimate strain for plastic analysis is not limited. That is why it is necessary to define the ultimate limit state of the cross section using static equilibrium conditions. For creating interaction surfaces, variables *n, mz* and *my,* are needed. *n* represents the ratio of the applied axial load and axial capacity and my and mz represent the ratios of the applied bending moments with the corresponding plastic moment capacities. In order to determine the ultimate limit state, it is necessary to keep one value, the axial force or the ratio between bending moments *My* and *Mz* fixed, and increase the other until the ultimate limit state is reached. Considering this, there are two different strategies to determine the current cross-section state. The first one is to keep the axial force fixed (point 1 in Figure 2), while the second one is to preserve the ratio between axial force and bending moment vectors (point 2 in Figure 2).
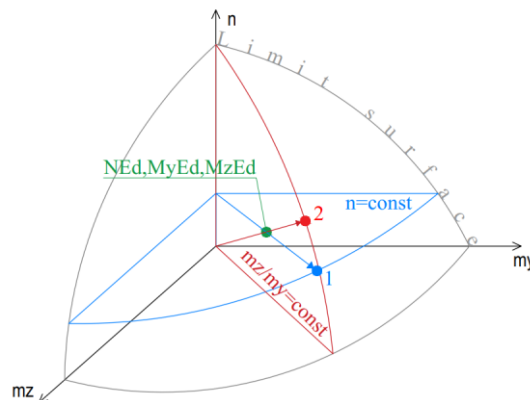
Figure 2. Two strategies to determine the current cross-section state

3.1 Section resistance calculation in Matrix3D

In this research, the interaction surface is calculated by keeping the axial force fixed. This means that for given axial force the horizontal section of the resistance surface is calculated, but due to the symmetry of the standardized steel cross sections, only a quarter or the half of this section needs to be found. Still, it is impossible to find the correct point on this section in the first iteration, because the angle of the neutral axis is not known apriori. There is a possibility to search for the point 1 in the Figure 2 by some sort of numerical strategy, such as halfing method, or to calculate the whole curve (section of the surface) rigorously, and then to find the point that corresponds to the desired ratio between bending moments around M_y and M_z. Since this calculation should be done for each loading combination, and each member, it is desirable to use simplified representation of the section in order to make the computational process less time-consuming. Hence, the usual steel cross sections are represented with the straight lines and the transition zones between web and flanges are disregarded. This does not introduce significant error since the main goal is only to determine the class of the section.

To determine the actual position of the plastic neutral axis for certain internal forces, it is chosen to firstly determine the actual interaction diagram for the cross-section subjected to biaxial bending and given intensity of the axial force.

As mentioned, the simplified line representation of cross-sections was chosen to simplify the determination of the border cases of the position of the plastic neutral axis. Furthermore, the more precise method approaches the fiber beam element [4], and fiber beam-column elements are already implemented in Matrix 3D, and used for materially and geometrically nonlinear analysis [7].

Therefore, the problem consists of calculating two unknowns, the angle of the neutral axis (α) and its position along the z axis (Δ) using three static equilibrium conditions.

The algorithm for determining an actual interaction surface in MATLAB is described through the following steps:
1. The first control is to ensure that the cross-section area is sufficient to transmit the axial force, that is, is the condition $N_{Ed}/f_y < A$ met, if not, the calculation is abandoned.
2. If the condition is met, a control whether the surface of the web itself is sufficient to transmit the axial force or whether it is necessary to include the surface of the flange is performed, depending on that, the expressions for determining the limit values ($α1$ $α2$ $α3$) differ as do their corresponding limit positions of the plastic neutral axis along the z axis ($Δ$).

3. A loop is used to variate the angle α from 0° till 90°, with an appropriate step, in an apt segment.
4. For a single value of α, its corresponding $Δ$ is calculated analytically from the expression obtained from the condition that the difference of the tension and compression areas is sufficient to transmit the axial force.
5. For one value of α and its corresponding $Δ$ bending moments around the main axes are calculated. These moments correlate to one N_{Ed}, one $α$, and its corresponding $Δ$, and represent one point on the interaction surface.

In the next part the limit values ($α1$ $α2$ $α3$) on the example of a "I" section and rectangular hollow section are explained.

The area required to transmit the axial force for "I" section N_{Ed}/f_y can be found in the following intervals: $N_{Ed}/f_y < A$, $A_{web} < N_{Ed}/f_y < A_{web}+A_{flange}$ and $A_{web}+A_{flange} < N_{Ed}/f_y < A$

When calculating the whole interaction curve for a given normal force, it is necessary to algorithmically cover all situations that occur for all angles of the plastic neutral axis, and in parallel, to optimize the calculation time. Therefore, the first step in the algorithm is to divide the cases into those when the normal force can be transmitted by the web, when the web is not enough to transmit the normal force and when the sum of the flange and the web is not enough to transmit the normal force.

This is all necessary in order to analytically write formulas for determining $Δ$, for different ranges of $α$. So, while $α$ varies according to the adopted step, $Δ$ is calculated analytically. This is possible because the stress diagram is very simple - a block diagram. In concrete cross-sections, this is impossible to perform analytically, the position of the neutral axis, $Δ$, is found iteratively in an inner loop, as described in [10].

For a situation where the web can transmit a normal force in the cross-section, there are three limit values for the angle of the plastic neutral axis as shown in Figure 3. For angles less than $α1$, it makes no sense to calculate $Δ$ or divide that interval, because the whole interval has the same values and they represent a segment of the curve on the M_y axis.

When the area required to transmit the axial force is greater than the area of the web but smaller than the sum of the areas of the web and flange, that is, when the condition $A_{web}<N_{Ed}/f_y<A_{web}+A_{flange}$ is satisfied the plastic neutral axis for the value of the angle $α=0$ lies in the flange. In this case the angle $α$ variates between the angle $α3$ and 90°, where the angle $α3$ represents the angle of the plastic neutral axis when the plastic neutral axis intersects the lower flange. In this case as appose to the previous one the plastic neutral axis for the angle of 90° exits the area of the web (Figure 4).

$$N_{Ed}/f_y<A_{web}$$
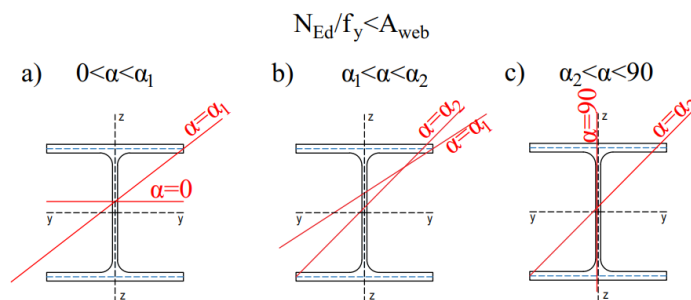
Figure 3. Limit values for the angle of the plastic neutral axis when the web area is sufficient to transmit the axial force for I section

$$A_{web}<N_{Ed}/f_y<A_{web}+A_{flange} \qquad A_{web}+A_{flange}<N_{Ed}/f_y<A$$

$$\alpha_3<\alpha<90 \qquad \alpha=0 \qquad \alpha_3<\alpha<90 \qquad \alpha=0$$
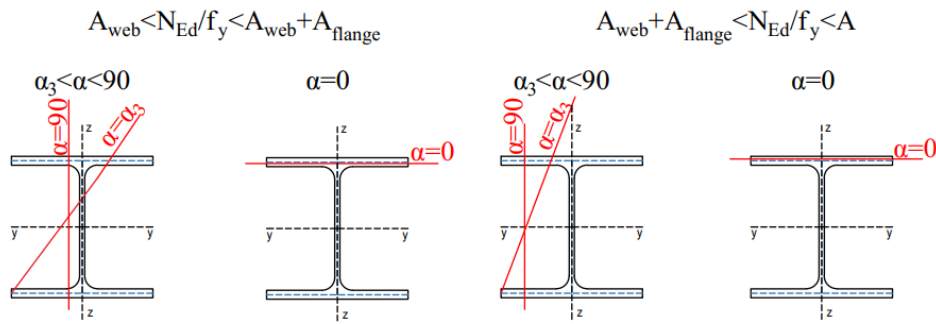
Figure 4. Limit values for the angle of the plastic neutral axis when the web area isn't sufficient to transmit the axial force for I section

In the last case, the sum of the areas of the flange and web is not sufficient to transmit the axial force. Then, just like in the last case, the plastic neutral axis exits the area of the web but the difference being that the plastic neutral axis is located in the upper half of the flange for the value of the angle $\alpha=0$. By variating the value of the angle α from α_3 till 90° the bending moments resistances M_{Rdy} and M_{Rdz} are calculated (Figure 4).

Also by a similar procedure to the previous example, the limit values (α_1 α_2 α_3) and limit areas for rectangular hollow section are determined and shown in Figure 5. With the difference being that in the case of a hollow cross-section, the third case, when the sum of areas of the web and two flanges is not sufficient to transmit the axial force, is not defined, because in that case, the plastic neutral axis varies in the flange for small values of the angle, and for larger values of the angle it varies in the web of the cross-section.

4 Results

The interaction curves for the cross-section IPE 300 made from steel S355 are presented in Fig. 6 and 7. By variating different levels of the axial load, a series of parallel sections of the interaction surface is calculated.

In Figure 6 normalized axial force $n=0.4$ corresponds to the case when the web area is sufficient to transmit the axial force (Figure 3). The value for $n=0.6$ correspond to the case when it is needed more than the area of the web to transmit the axial force but less than the sum of the areas of the web and flange (the first and second case in Figure 4). Lastly the value $n=0.8$ represent the case when is needed more than the sum of the areas of the web and flange to transmit the axial force (the third and fourth cases in Figure 4). Hence,

each of these 3 curves was calculated according to a different case shown in Figures 3 and 4.

The Figure 6 also shows curves calculated by an expression given in EN 1993 [1], for the analyzed section IPE 300. As can be seen from the Figure 5, Eurocodes interaction curve matches the curve obtained by the presented procedure quite well, with some small deviations. The values of bending moment resistances around the stronger axis coincide with the moment resistances calculated by an expression given in Eurocode, while the differences are observed in the bending moment resistances around the weaker axis. The deviations are consequence of the approximate representation of the cross-section with straight lines.

Obtained by the same procedure as the I section, the interaction curves for hollow section RHS 100x100x4 are shown in Figure 7.

The problem with the resistances calculated with the expressions obtained from Eurocode is that the position of the plastic neutral axis cannot be determined. Therefore, the plastic neutral axis can only be determined for an interaction surface that is obtained by the same method that is used to determine the position of the plastic neutral axis.

Figure 8 presents different values of normalized bending resistances (*my* and *mz*) for different values of normalized axial force (*n*) and with the same inclination of the plastic neutral axis ($\alpha=84°$). It is evident that this red curve in Fig. 7 in not a meridian of the resistance surface. This means that by increasing the axial load, the inclination of plastic neutral axis will not be the same for the same direction of applied bending moment.

$$N_{Ed}/f_y<2^*A_{web} \qquad 2^*A_{web}<N_{Ed}/f_y<A_{web}+2^*A_{flange}$$

$$0<\alpha<\alpha_1 \qquad \alpha_1<\alpha<\alpha_2 \qquad \alpha_2<\alpha<90 \qquad \alpha_3<\alpha<90 \qquad \alpha=0$$
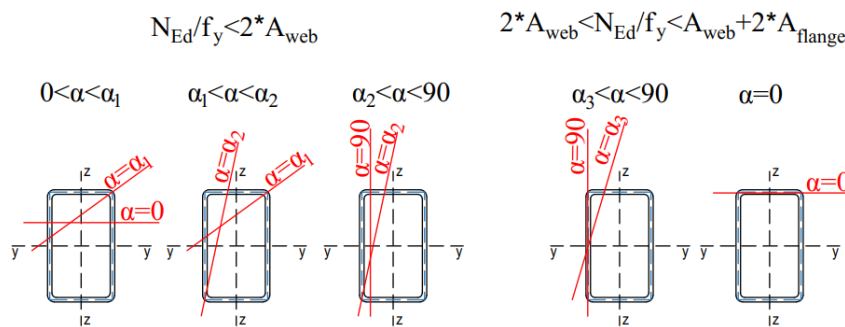
Figure 5. Limit values for the angle of the plastic neutral axis for hollow sections
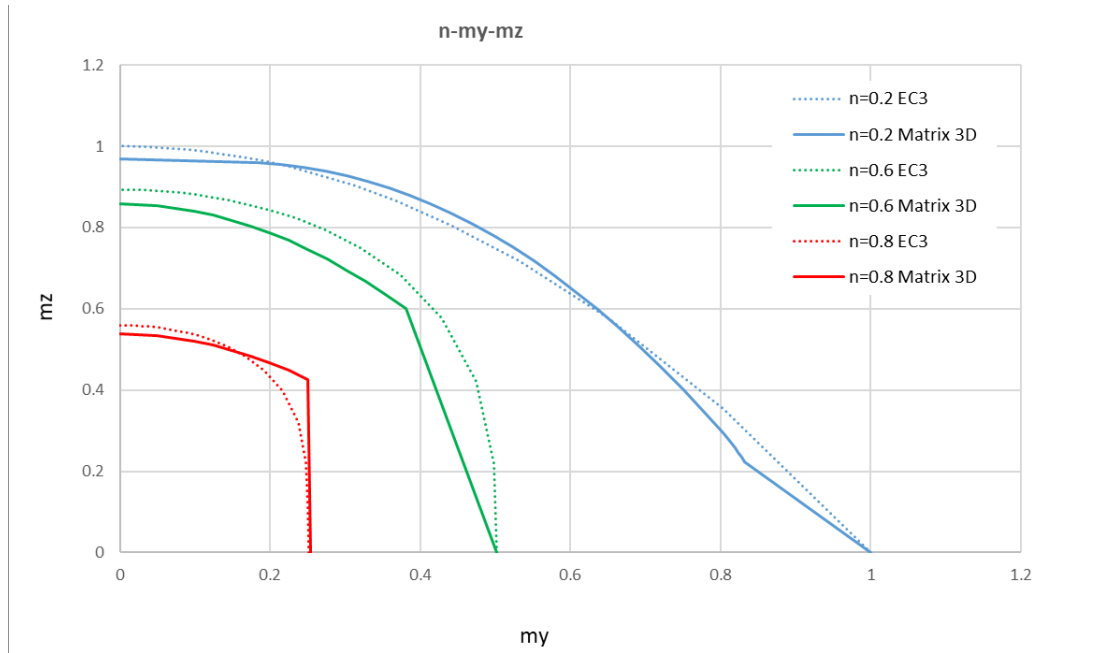
Figure 6. Biaxial bending and axial force interaction curve for IPE300 cross-section at axial load levels n=NEd/NRd
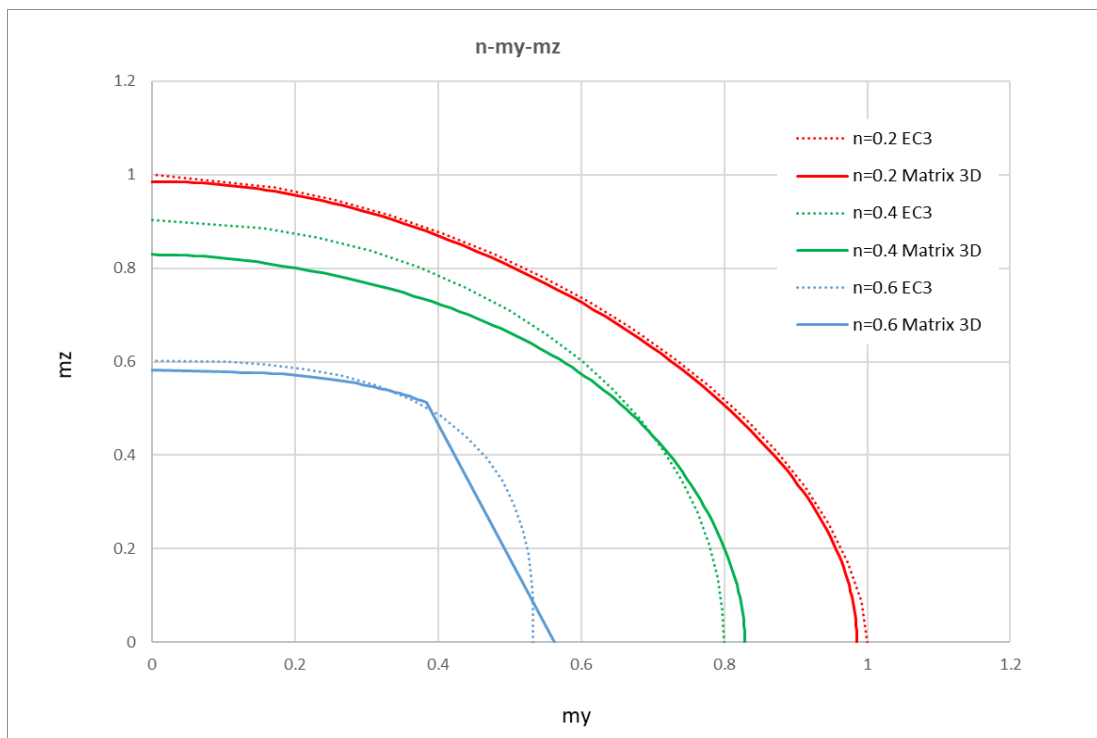
Figure 7. Biaxial bending and axial force interaction curve for RHS 100x100x4 cross-section at axial load levels n=NEd/NRd
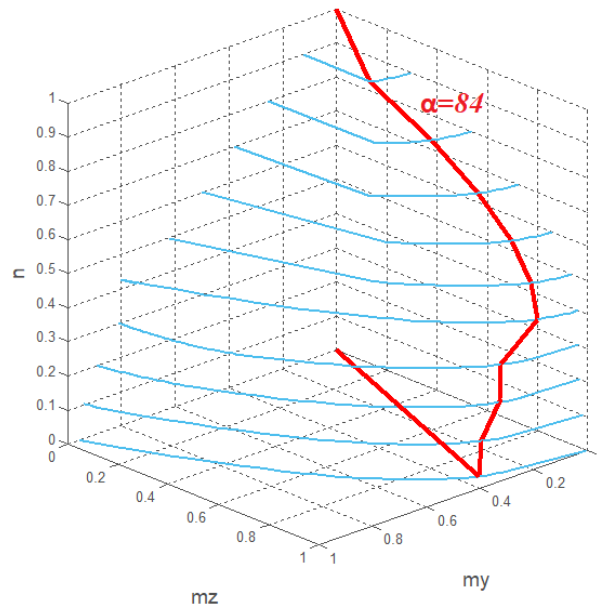
Figure 8. Biaxial bending and axial force interaction curve for IPE 300 cross-section for the angle 84°

5 Discussion and conclusion

The majority of challenges of implementation of the steel section design in software are revisited in this papers. Some of the more involving issues are out of the scope of the paper, such are thin-walled sections and types of buckling there are prone to, or sections loaded by bimoment. Still, even for usual rolled sections, Eurocode tacitly implies that the ultimate resistance for each loading combination should be found in order to determine the class of the cross-section. This can easily become overly time-consuming task, or inadequately solved. It is shown in the paper that for different levels of axial force, the inclination of the plastic neutral axis could not be known a priori. Hence, the algorithm for I and RHS//SHS sections is presented. Further, the approximate resistances of section resistance given in EN 1993-1-1 [1] are compared to ones obtained by this simple algorithm.

References

[1] EN 1993-1-1:2005: Eurocode 3. Design of Steel Structures: General rules and rules for buildings. CEN, 2005.

[2] Baptista A. M.: Resistance of steel I-section under axial force and biaxial bending, Journal of Constructional Steel Research, 72, 2012, 1-11.

[3] Baptista A. M.: Analytical evaluation of the elastic and plastic resistances of double symmetric rectangular hollow sections under axial force and biaxial bending, International Journal of Non-Linear Mechanics, 47, 2012, 1033-1044.

[4] Osterrieder J. K.: First-hinge analysis for lateral buckling design of open thin-walled steel members, Journal of Constructional Steel Research, 62, 2006, 35-43.

[5] Žarković D., Jovanović Đ., Vukobratović V., Brujić Z.: Convergence improvement in computation of strain-softening solids by the arc-length method, Finite Elements in Analysis and Design, 164(1), 2019, 55-68.

[6] Jovanović Đ., Žarković D., Vukobratović V., Brujić Z.: Hysteresis model for beam-to-column connections of steel storage racks, Thin-Walled Structures, 142, 2019, 189-204.

[7] Jovanović Đ., Žarković D., Brujić Z., Lađinović Đ. : Fiber beam-column element implementation in academic CAD software Matrix 3D, Građevinski materijali I konstrukcije, 60, 2017, 57-77.

[8] Dlubal Software : Manual RF-/STEEL EC3. Tiefenbach, 2020.

[9] SOFiSTiK AG.: Sofistic Manual: ASE, AQB, AQUA, BEMESS, DYNA, 2018

[10] Žarković D.: Computer software for structural analysis and design of reinforced concrete structures, Zbornik radova Fakulteta tehničkih nauka, Novi Sad, 24, 2009, 1587-1590.

Influence of cement replacement with limestone filler on the properties of concrete[*]

Ksenija Tešić[*1)], Snežana Marinković[2)], Aleksandar Savić[2)]

[1)] University of Zagreb, Faculty of Civil Engineering, Fra Andrije Kačića Miošiča 26, 10000 Zagreb, Croatia
[2)] University of Belgrade, Faculty of Civil Engineering, Bulevar kralja Aleksandra 73, 11000 Belgrade, Serbia

ABSTRACT

This paper presents an experimental research of one type of green concrete in which Portland cement was replaced with two types of limestone filler of the same origin and mineralogical composition, but with a different fineness of particles. Ten concrete mixtures were designed in which 0%, 15%, 30% and 45% (by mass) of cement were replaced with filler. The water to cement ratio for each mixture was constant (w/c=0.54), and the water to powder ratio was decreasing with increasing cement replacement. Particle size distribution was selected using Funk and Dinger, as well as using Fuller's model. The results showed that it is possible to increase the compressive strength of concrete by reducing 45% of cement, but further research should be focused on improving the workability.

1 Introduction

Concrete is the most widely used building material in the construction industry, with its use increasing steadily over the last 50 years due to its relative ease of production and relatively low price. The production of cement, one of the constituents of concrete, releases a large amount of carbon dioxide (CO_2), one of the gasses most responsible for the negative effects of the greenhouse effect. It is estimated that about 7% of the total carbon dioxide emissions into the atmosphere come from cement production [1]. Reducing its amount in concrete production has a positive impact on the environment. This fact leads to an increased interest in the development of strategies dealing with the partial replacement of cement. Cement can be replaced with by-products of other industries, such as fly ash and slag [2], or by natural raw materials, such as various types of fillers [3]. Fillers are small inert particles where the inert property prevents the binder component of the concrete from being easily replaced by a filler. Therefore, in concretes where the cement has been replaced by a filler, it is necessary to obtain satisfactory physical and mechanical properties by choosing the right amount of material and the type of mix design. In case of these concretes, it is possible to increase the packing density of the solid particles (aggregate, cement and filler) by adding fillers, which reduces the voids between them and thus reduces the water required to fill the remaining voids [4,5]. Since the water to cement ratio is an indicator of the quality of the concrete, it is possible to keep the water to cement ratio constant in the manner previously described, thus ensuring the desired quality of the concrete.

This paper presents experimental studies of concrete in which cement is replaced by limestone filler (by weight) at 0%, 15%, 30% and 45%. In addition, the influence of aggregate particle size distribution on the properties of concrete was considered using different methods. In all mixtures, the water to cement ratio was constant and the water to powder ratio decreased with increasing percentage of cement replacement.

2 Particle size distribution of aggregate

The choice of aggregate particle size distribution is one of the most important tasks in concrete technology. It has been shown that satisfactory properties of fresh and hardened concrete can be obtained if the aggregate particle size composition is selected according to certain optimization curves [6]. They are mainly represented as continuous curves, and one of the most common is the Fuller curve, given by the function:

$$Y(d) = \left(\frac{d}{d_{max}}\right)^{0.5} \tag{1}$$

where:
Y (d) - percentage of passage through the sieve of diameter d,
d -   the diameter of the sieve,
d_{max} - the diameter of the nominally largest particle of the aggregate.

The optimization curve of Funk and Dinger is represented by a modified Fuller curve. The modification refers to the

introduction of the influence of the nominally smallest particle on the particle size distribution. The distribution function is:

$$Y(d) = \frac{d^q - d_{min}{}^q}{d_{max}{}^q - d_{min}{}^q} \qquad (2)$$

where:
d_{min} - the diameter of the nominally smallest particle in the mixture,
q - distribution coefficient.

The value of the distribution coefficient q depends on the desired performance of the concrete mixture; a value of 0.23 is recommended for concretes with a more fluid consistency (self-compacting concretes) and a value of 0.32 is recommended for roller-compacted concretes [7]. The exponent q = 0.37 ÷ 0.4 is the recommended value for mixtures leading to the optimum value of the packing density [8,9], where the packing density is the volume of solid particles per unit volume. The Funk and Dinger curve using the distribution coefficient q gives the possibility to introduce small particles (cement and filler) in the process of particle packing optimization.

3 Green concrete with low cement content and addition of fillers

Considering the mixture of solid particles (aggregate, cement and filler) and water, Figure 1, it can be concluded that in the mixture all voids between the particles must first be filled (void water) and then "additional" water (excess water) must be added. "Additional" water coats the particles with a layer of water and thus ensures workability [5].

As mentioned earlier, fillers have no binding properties, so replacing cement with a filler would result in a proportional decrease in compressive strength. One way to compensate for this decrease is to increase the packing density by adding a filler that is finer than the cement particles while reducing the water content. When the packing density is increased, the content of voids between the solid particles is lower, so less water is needed to fill the voids between the particles. With a reduced amount of cement and a reduced amount of water, it is possible to keep the water to cement ratio constant. However, in these concretes, the presence of very fine particles, the fillers, increases the total specific surface area of solid particles. In this case, more "additional" water is needed to ensure the workability of the mixture [4]. Therefore, instead of increasing the amount of water to

ensure the desired workability, superplasticizers are added, chemical additives that lubricate the particles by coating them with a thin layer [6].

4 Experimental program

Concrete mixtures were prepared to study the influence of cement replacement with limestone filler on concrete properties, as well as the influence of curve selection in the choice of particle size distribution of aggregate. The study was carried out on fresh and hardened concrete.

4.1 Materials

Ordinary Portland Cement CEM I 42.5 R and two types of limestone fillers were used, differing in the fineness of the particles, the larger being referred to as KF1 and the smaller as KF2. The particle size distribution is shown in Figure 2. The cement was larger than the filler particles; the average particle size of the cement was d_{50} = 12.35 μm, the limestone filler KF1 had d_{50} = 4.66μm while the limestone filler KF2 had d_{50} = 2.89μm.

In addition, natural river aggregate distributed in three fractions, (0/4 mm), (4/8 mm) and (8/16 mm), superplasticizer - latest generation hyperplasticizer based on polycarboxylate (SP), and water were used.

4.2 Mixture design

Experimental tests were carried out with a total of ten mixtures which are shown in Table 1. The mixtures were divided into two parts. The first part refers to the optimization of the particle size distribution of cement and aggregate of the reference mixture according to the Funk and Dinger curve, and the second part refers to the optimization of the particle size distribution of aggregate according to the Fuller curve. These two parts were introduced to observe the influence of aggregate optimization by different models. The percentages of the different fractions of aggregate are given in Table 2. In order to consider the influence of the distribution coefficient q of the Funk and Dinger curve, the test of the bulk density of the aggregate in compacted state was carried out for several mixtures. The mixtures had different proportions of aggregate fractions, with each mixture corresponding to one distribution coefficient. The results are shown in Figure 3.
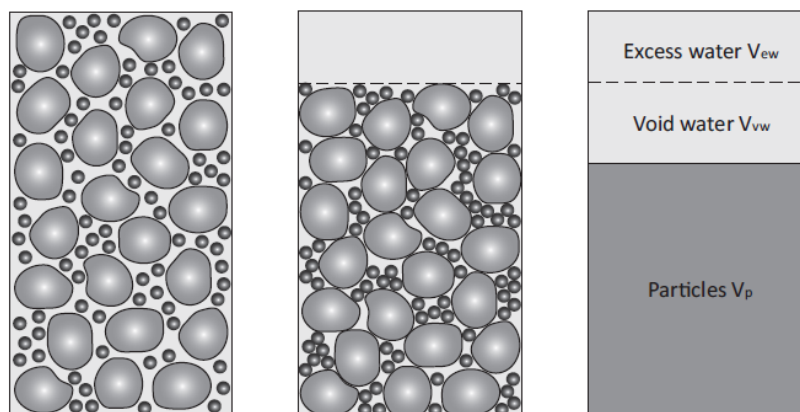
Figure 1. Mixture with its constituents [4]
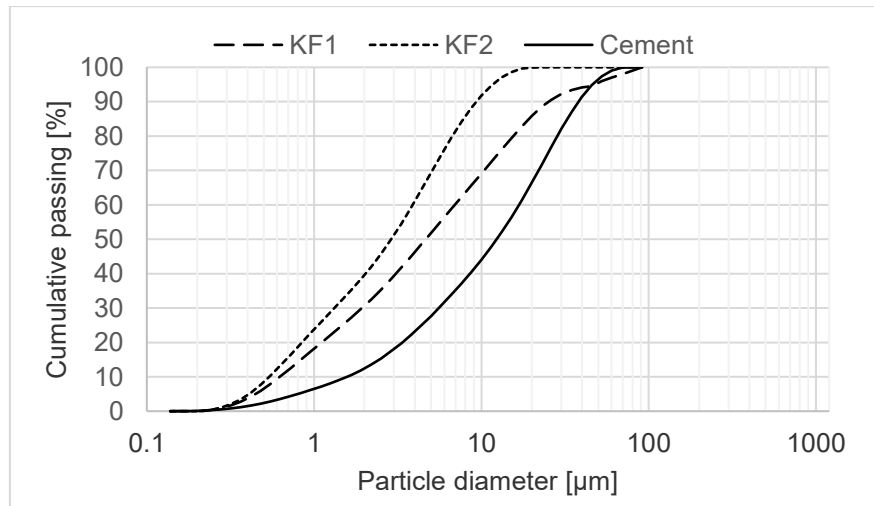
Figure 2. Particle size distribution of cement and limestone fillers
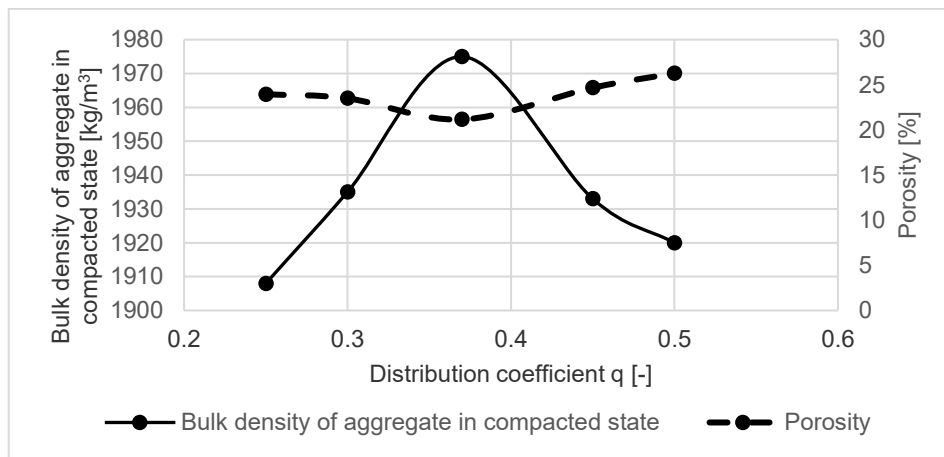
Figure 3. Bulk density of aggregate in the compacted state and porosity for different distribution coefficients of the Funk and Dinger curve

Table 1. Mixture design.

		CEM I 42.5 [kg/m³]	KF1 [kg/m³]	KF2 [kg/m³]	(0/4) [kg/m³]	(4/8) [kg/m³]	(8/16) [kg/m³]	Water [kg/m³]	w/p [-]	SP [kg/m³]
	B-REF	330	-	-	963	387	500	178	0.54	1.16
	BK-15-1	280	50	-	963	387	500	151	0.46	1.32
	BK-15-2	280	-	50	963	387	500	151	0.46	1.32
Funk and Dinger	BK-30-1	230	100	-	963	387	500	124	0.38	6.6
	BK-30-2	230	-	100	963	387	500	124	0.38	6.93
	BK-45-1	180	150	-	963	387	500	97	0.29	10.73
	BK-45-2	180	-	150	963	387	500	97	0.29	11.55
	B-REF-F	330	-	-	738	646	461	178	0.54	1.16
Fuller	BK-15-1-F	280	50	-	738	646	461	151	0.46	1.32
	BK-30-1-F	230	100	-	738	646	461	124	0.38	6.6

Table 2. The percentages of the different fractions of aggregate used in concrete mixtures.

	Aggregate fraction [%]	
	Funk and Dinger	Fuller
(0/4)	52	40
(4/8)	21	35
(8/16)	27	25

The greatest bulk density of the aggregate in compacted state corresponded to the value of the coefficient q = 0.37, indicating the optimal "packing" of the mixture. Therefore, this coefficient value was used in the optimization of the particle size distribution using the Funk and Dinger curve.

Then, in the first part, the cement was replaced with limestone filler at 15%, 30% and 45%. For each replacement, a larger and then a smaller limestone filler was used. In the second part, the cement was replaced with a larger filler at 15% and 30%. As the amount of cement decreased, the amount of water also decreased, so that the water to cement factor (w/c) had a constant value of 0.54. With the increase of cement replacement, the water to powder factor (w / p) decreased, where the powder referred to the cement and filler content. The amount of superplasticizer in the mixture was determined so that the mixture obtained sufficient workability.

4.3 Methods

After the concrete mixtures were prepared, the workability of the concrete was tested using the slump method according to the standard [10]. Then, 10 cm cubes of concrete were made, which were demoulded after one day. They were then stored in water at a temperature of 20 ± 3 °C until the concrete was tested for its compressive strength. This property of the concrete was tested at the age of the specimens of 7 and 28 days according to the standard [11].

5 Results

5.1 Workability

The results of workability test of concrete are presented in Table 3. It was observed that the workability of the mixtures decreases as the cement replacement ratio increases. This phenomenon is expected since the water to powder factor (which can be considered as an indicator of workability) decreases with increasing cement replacement ratio. Even if the mass amount of the powder component of each mixture is constant, the specific surface area of the powder component increases with increasing cement replacement. In this case, the amount of water required to coat all the particles and ensure the "flow" of the mixture increases, further affecting workability.

Table 3. Workability test results.

		Slump Δh [mm]
Funk and Dinger	B-REF	60
	BK-15-1	25
	BK-15-2	25
	BK-30-1	-
	BK-30-2	-
	BK-45-1	0
	BK-45-2	-
Fuller	B-REF-F	80
	BK-15-1-F	40
	BK-30-1-F	-

However, at higher cement replacements (30% and 45%), probably due to the lack of cement paste, an irregular form of slump occurred in the workability test, which is described by the standard as an unacceptable and unmeasurable form of slump. The cause of this phenomenon is most likely the absence of a binder component that provides cohesion and plasticity of the fresh concrete mass. An example of such slump is shown in Figure 4.

a)   *b)*
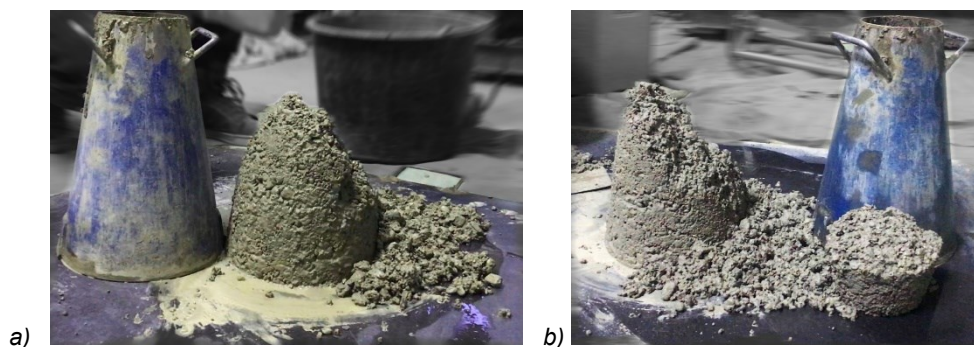
Figure 4. Workability test according to slump method a) BK-30-1 i b) BK-45-2

Considering the results obtained with mixtures where the choice of particle size distribution was made according to two different curves, it is noticed that the mixtures where the Fuller model was applied had better workability. Considering the proportions of the different aggregate fractions given in Table 2, it is concluded that due to the higher proportion of the first fraction in the Funk and Dinger model, a larger amount of water is required to achieve the desired workability, since the specific surface area is larger. This fact is held responsible for the improved workability in mixtures having Fuller optimization curve for the selection of the particle size distribution.

5.2 Compressive strength

The results of compressive strength testing of concrete on 10 cm cube specimens at the age of 7 and 28 days with optimization using the Funk and Dinger curve are shown in Figure 5.

Although all the mixtures had the same water to cement factor, it was observed that the strengths reached higher values for the concrete that had a limestone filler in its composition. The highest strength increase was recorded for the highest percentage of cement replacement (45%) with a smaller filler, and this increase was 22.5% at the age of 7 days and 9.4% at the age of 28 days. All the mixtures showed higher strengths than concrete mixtures without fillers. Considering the compressive strength of concrete as a basic indicator of concrete quality, cement was successfully replaced with limestone filler. A comparative plot of the compressive strength of concrete at the age of 7 and 28 days in mixtures in which the particle size distribution was carried out with two different models is shown in Figure 6. The choice of particle size distribution has an influence on the concrete compressive strength; better packing in mixtures in which the optimization of the solid fractions was carried out according to the Funk and Dinger model contributed to the increase in concrete strength. The largest increase was observed in the

reference mixtures and is 3.9%. However, the tests carried out showed that this increase is not significant and, in some cases, it was even non-existent. This leads to the conclusion that the introduction of fine particles (cement and filler) in optimization curves (Funk and Dinger model) make a more complex particle size distribution process and do little to improve the compressive strength compared to the Fuller curve.

6 Conclusions

The main objective of this experimental research was to investigate the possibility of replacing cement with fine powder material, filler, while maintaining the basic properties of concrete that allow it to compete with traditional concrete, thus offering the possibility of using this type of concrete in reinforced concrete structures. This would lead to an effective reduction in the amount of cement compared to traditional concrete and thus its harmful effects on the environment.

From this study, it was concluded that it is possible to replace up to 45% of the cement with a high fineness limestone filler while maintaining and even increasing the compressive strength. However, the concept of concrete where cement has been replaced with filler requires some reduction in the amount of water, with the reduced amount of cement affecting the workability and cohesion of the mixtures. It was also found that in these concretes, superplasticizer helps to improve these properties, but not enough for such concretes to be competitive with traditional concretes. The impaired workability can be partially compensated by a better choice of aggregate particle size distribution. It is concluded that the value exponent q = 0.37 of the distribution of the Funk and Dinger curves leads to an optimal packing and that this contributes to increasing the compressive strength of the concrete, but not significant compared to the more easily applicable Fuller curve. Since
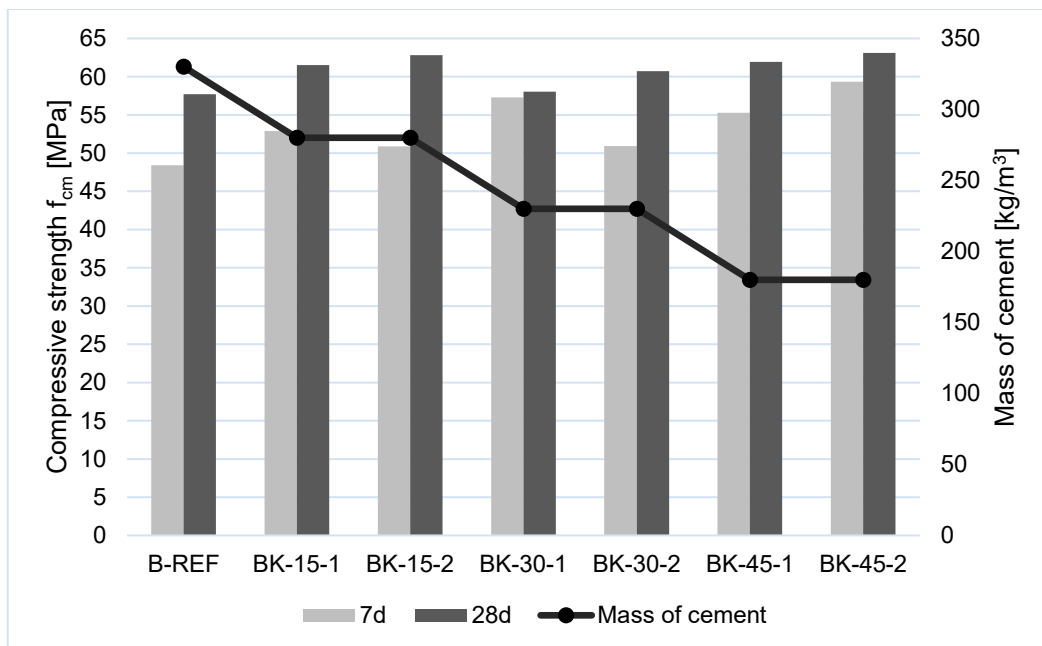
Figure 5. Compressive strength of concrete at the age of 7 and 28 days
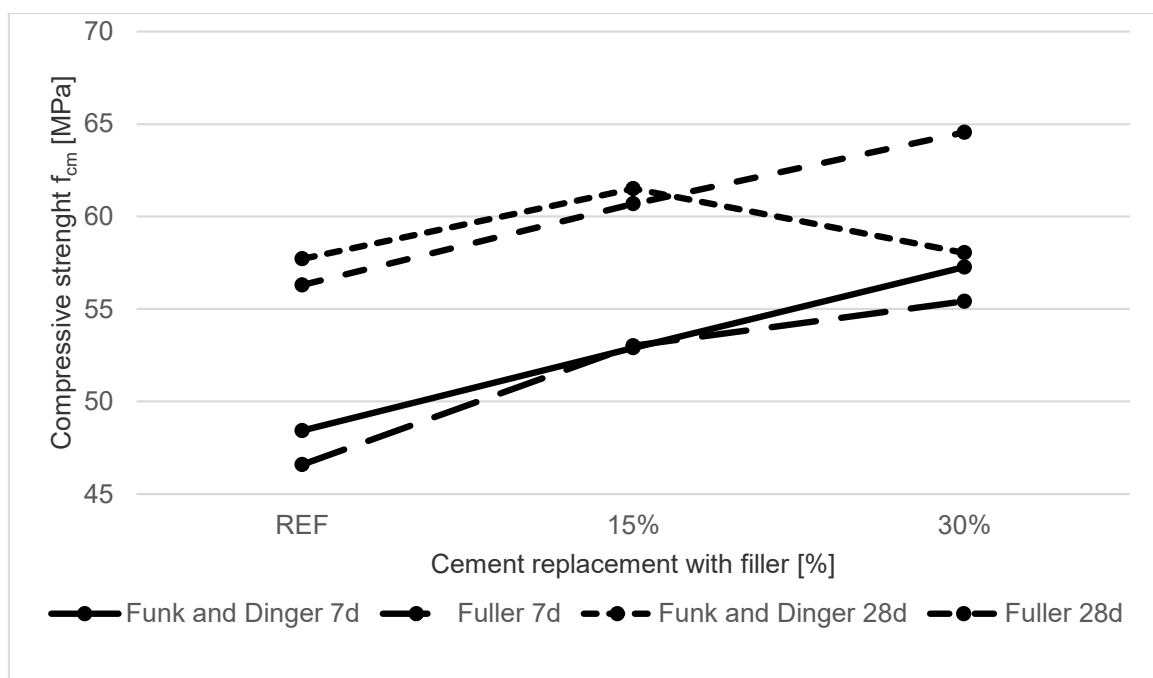
Figure 6. Comparison of the compressive strength of concrete at the age of 7 and 28 days in mixtures where the particle size distribution is selected according to two different optimization curves.

the choice of Fuller curve leads to better workability of concrete mixture with lower percentages of cement replacement, it is recommended to use this, widely used method for the selection of aggregate particle size distribution.

Further research must focus on improving the technological properties of these concretes so that this type of concrete can compete with traditional concrete.

References

[1] IPCC Working group III of the International Panel on climate change: Special Report on Carbon Dioxide Capture and Storage, Cambridge, United Kingdom and New York: Cambridge University Press, 2005

[2] Dragaš J.: Ultimate capacity of high volume fly ash reinforced concrete beams, PhD Thesis, University of Belgrade, 2018.

[3] Scrivener K. L., John V. M., Gartner E. M.: Eco-efficient cements: Potential economically viable solutions for a low-CO2 cement-based materials industry, Cement and Concrete Research, 114 (2), 2018, 2-26.

[4] Fennis S. A. A. M.: Design of Ecological Concrete by Particle Packing Optimization, PhD Thesis, Tehnical University of Delft, 2010.

[5] Vogt C.: Ultrafine particles in concrete - Influence of ultrafine particles on concrete properties and application to concrete mix design, KTH Royal Institute of Technology, 2010.

[6] Muravljov M.: Građevinski materijali, Građevinska knjiga, Beograd, 2002.

[7] Kumar S. V., Santhanam M.: Particle packing theories and their application in mixture proportioning: A review, Indian Concrete Journal, 77 (9), 2003, 1324-1331.

[8] Müller H. S., Haist M., Vogel M.: Assessment of the sustainability potential of concrete and concrete structures considering their environmental impact, performance and lifetime, Construction and Building Materials, 67, 2014, 321-337.

[9] Yousuf S., Sanchez L. F. M., Shammeh S. A.: The use of particle packing models (PPMs) to design structural low cement concrete as an alternative for construction industry, Journal of Building Engineering, 25, 2019

[10] SRPS EN 12350-2:2019 Ispitivanje svežeg betona - Deo 2: Ispitivanje sleganja, Institut za standardizaciju Srbije, 2019.

[11] SRPS EN 12390-3:2019 Ispitivanje očvrslog betona – Deo 3: Čvrstoća betona pri pritisku uzoraka za ispitivanje, Institut za standardizaciju Srbije, 2019.

The new buckling curves for cold-formed stainless steel equal-leg angle columns[*]

Jelena Dobrić[*1)], Aljoša Filipović[1)], Nancy Baddoo[2)], Zlatko Marković[1)], Dragan Buđevac[1)]

[1)] University of Belgrade Faculty of Civil Engineering, Bulevar kralja Aleksandra 73, 11000 Belgrade, Serbia
[2)] Steel Construction Institute United Kingdom

A B S T R A C T

The design rules for centrically compressed stainless steel equal-leg angle members are not explicitly stated in the current European standard SRPS EN 1993-1-4. This paper summarizes the results of extensive research conducted on this type of structural elements aiming to define recommendations for their design. Based on a systematic experimental investigation, a detailed numerical analysis was performed, and a database of columns' resistances were defined. Material and geometric nonlinear analysis included three key stainless steel alloys, austenitic, ferritic and duplex. The design curves for flexural and flexural–torsional buckling check have been proposed in accordance with European codified procedures.

1   Introduction

The compression capacity of the angle column is strongly affected by its geometry. The non-coincidence of the shear centre with the section's centroid and its location at the intersection of angle legs imply a low torsional stiffness and, therefore, a high susceptibility to instability phenomena involving torsion and flexural buckling about major principal axis, namely flexural–torsional buckling (FTB). Since the FTB deformations exhibited by equal-leg angle columns in the intermediate slenderness domain are very similar to local deformations, these members have been also said to fail in "local-global interactive modes". Besides, the short equal-leg angle columns could be susceptible to the torsional buckling (TB) mode whose failure shape corresponds to the cross-section local buckling (LB). However, the slender equal-leg angle columns will fail due to flexural buckling (FB) mode about minor principal axis of the cross-section.

The difficulty in assessing stability of equal-leg angle columns is especially noticeable in the case of slender, thin-walled sections. The deformation and stress redistribution upon the elastic LB of angle legs reduce effective section properties and cause the effective centroid to shift along the axis of symmetry towards the corner, which, in turn, results in an interaction between the axial load and additional bending. Furthermore, the inevitable presence of initial imperfections and end eccentricity of loading acting in combination with the effective centroid shift additionally affects the occurrence of buckling and subsequent failure. As the cross-section is asymmetric, distribution of axial stresses in the cross-section strongly depends on the direction of total eccentricity along the axis of symmetry—towards the tips of

the legs or to the corner (one causing compressive yielding of the leg tips, the other causing compressive yielding of the section corner). Besides, an increase of the leg width-to-thickness ratio increases the tendency of the angle to rotate and increase possibility for FTB failure in the entire global column slenderness range [1], [2].

This paper briefly present key results of a scientific research addressing cold-formed stainless steel equal-leg angle columns with pin-ended boundary conditions, conducted at the University of Belgrade, Faculty of Civil Engineering, aiming to propose procedures for their design taking into account the cross-section slenderness, material non-linearity and initial structural imperfections caused by particular production process. The analytical background, state of art, experimental procedures, numerical studies and used methodologies are described in detail in recently published papers [1], [2].

2   Experimental programme

The experimental programme was performed on press-braked stainless steel equal-leg angle sections with nominal dimensions of 80 × 80 × 4 mm and nominal internal corner radius of 12 mm, and involved material testing, initial imperfection measurements and stub column tests and global buckling tests. The basic material of all tested angle columns was lean-duplex stainless steel grade EN 1.4162 (UNS S32101) with the steel name X2CrMnNiN21-5-1. The lengths of specimens were selected to cover a wide-ranging set of global column slenderness: elastic LB of short specimens, coupled FTB–LB and FB-LB failure modes for

---

the intermediate and long length specimens, respectively. In order to capture material nonlinearity, the tensile tests were performed on coupons extracted from the final press-braked angle sections under strain-control according to the requirements of EN ISO 6892-1 [3]. Two coupons were longitudinally cut from the middle of a leg, and two from the corner regions, to account for the strength enhancement caused by cold-working. Table 1 lists the average values of key mechanical properties, in which f_y is yield strength taken as the 0.2% proof stress, f_u is the ultimate tensile strength, ε_u is the strain corresponding to the ultimate tensile strength, ε_f is the total strain at fracture, E is the modulus of elasticity, and n and m are the strain hardening parameters utilised in the Ramberg–Osgood material model for nonlinear metallic materials [4]. It was found that press-braking method significantly improves material strength in the corner regions — the yield strength is about 38% greater than the yield strength of the flat angle section legs.

Figure 1. Typical stub column failure mode [1]

Table 1. Average measured key material properties obtained from tensile coupon tests [1]

Coupon	f_y (N/mm²)	f_u (N/mm²)	E (N/mm²)	ε_u (%)	ε_f (%)	Strain hardening parameters	
						n	m
Flat leg coupons	517	768	197445	31	45	7.9	3.0
Corner coupons	703	823	199905	17	33	11.0	13.1

The cross-section ultimate resistance and deformation capacity were quantified by stub column tests. A total of three repeated stub column tests were performed under pure axial compression. The nominal length of specimens of 240 mm meets requirements in Clause A.3.2.1 of EN 1993-1-3 [5]. The ends of each specimen were machined flat by a water jet cutter, perpendicular to their longitudinal axes to ensure a uniform distribution of loading during testing. The parallel end plates of the testing machine were fixed against rotations and twist about any axis to achieve fixed boundary conditions. The failure of specimens was governed by local buckling, localised in the middle part of the specimen's height, and characterised by torsional deformations of both angle legs (see Figure 1).

The key experimental results are summarised in Table 2, in which $P_{c,u}$ is the ultimate buckling load, δ_u is the end shortening at ultimate load, σ_{lb} is the LB stress obtained as the ultimate load-to-measured cross-section area ratio of each specimen and f_{ya} is an enhanced average yield strength which accounts for cold working in press-braked sections.

Having established the basic material and cross-sectional response, global buckling tests were carried out on pin-ended angle columns to obtain their compressive resistances and identify key predictors for critical failure modes. The specimens were divided into two test series with nominal lengths of 1000 and 2000 mm and four repeated tests in each of these series. Measurements of specimen geometry and initial global imperfections were performed before tests. A hydraulic testing machine was employed to apply monotonic compression loading to each column specimens. The load was applied through end plates attached to hardened steel knife-edge devices designed to replicate pinned end conditions, allowing rotations about the minor-axis, while restraining major-axis rotations as well as twist rotations and warping. A data acquisition system was used to record the applied load, lateral displacements (measured by linear variable displacement transducers) and axial strains (measured by strain gauges) during the tests. Table 3 provides relevant data obtained for all tested specimen; $P_{b,u,exp}$ is the maximum axial load capacity of the specimens (compressive column's resistance), $d_{u,v}$ and $d_{u,u}$ are respectively the mid-height lateral deflections about minor and major principal axes, and φ_u is the mid-height torsional rotation, all corresponding to the maximum load.

Based on experimental data obtained for global buckling tests, it was conclude following:

– In the intermediate slenderness domain, three repeated specimens failed in an almost identical mode, exhibiting dominant major-axis flexural-torsional deformations, coupled with minor-axis FB and LB, as displayed in Figure 2a. However, the failure of specimen ACF 80 × 80 × 4 – 1000 – 2 was governed by interaction of minor-axis flexural instability FB and local cross-section buckling mode accompanied by significant lateral minor-axis displacements and negligible torsional rotations and major-axis bending (see Table 3).

Table 2. Stub column test results [1]

Specimen	$P_{c,u}$ (kN)	δ_u (mm)	σ_{lb} (N/mm²)	f_{ya} (N/mm²)	σ_{lb} / f_{ya}
ACF 80 × 80 × 4 – 240 – 1	199.0	1.21	327.7	544.1	0.60
ACF 80 × 80 × 4 – 240 – 2	198.2	1.17	320.2	544.2	0.59
ACF 80 × 80 × 4 – 240 – 3	203.7	0.83	328.7	544.2	0.60

Table 3. Global buckling test results [1]

Specimen	$P_{b,u,exp}$ (kN)	$d_{u,u}$ (mm)	$d_{u,v}$ (mm)	φ_u (deg)
ACF 80 × 80 × 4 – 1000 – 1	132.5	+0.335	+0.339	-8.013
ACF 80 × 80 × 4 – 1000 – 2	139.5	-0.156	+8.149	-0.613
ACF 80 × 80 × 4 – 1000 – 3	136.6	-0.468	+1.471	-6.234
ACF 80 × 80 × 4 – 1000 – 4	135.5	-0.288	+0.846	-8.060
ACF 80 × 80 × 4 – 2000 – 1	44.3	-0.053	+31.487	-0.103
ACF 80 × 80 × 4 – 2000 – 2	45.8	+0.229	+23.948	-0.274
ACF 80 × 80 × 4 – 2000 – 3	46.8	-1.132	+29.094	+0.987
ACF 80 × 80 × 4 – 2000 – 4	45.5	-0.023	+21.972	-0.204
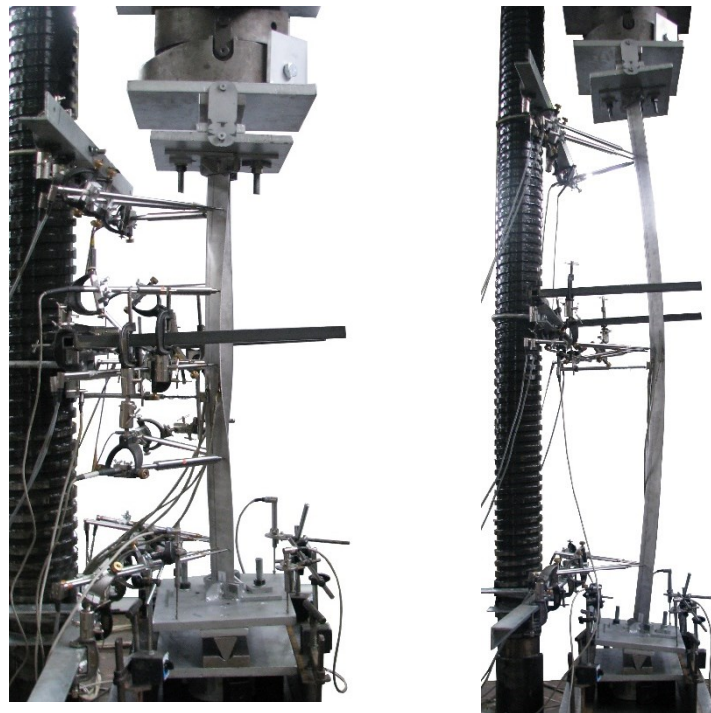
(a) ACF 80 × 80 × 4 – 1000 – 4   *(b) ACF 80 × 80 × 4 – 2000 – 3*

Figure 2. Typical failure modes of intermediate and long length specimens [1]

− As shown in Figure 2b, a dominant failure mode of the long length specimens was global minor-axis FB. The failure pattern involves notable lateral deflections in plane perpendicular to the minor principal axis and negligible twisting in combination with major-axis bending (see Table 3), indicating that the high slenderness specimens are less prone to cross-section LB.

3 Finite element modelling and parametric study

The advanced and realistic numerical simulations of the experiments involved cold-formed equal-leg angle columns were performed using the ABAQUS FE software package [7]. The geometrically and materially non-linear analysis (GMNIA) was developed as quasi-static with the dynamic explicit solver and the variable non-uniform mass scaling technique. The S4R shell elements were used to model the measured geometry of tested columns, as is customary for modelling thin-walled structures. To replicate the realistic pin-ended supporting conditions in global buckling tests, the measured geometry of hardened steel knife-edge devices attached to steel loading plates, together with top and bottom adjustable clamps were additionally modelled using four hexahedral solid elements C3D8R. A linear elastic–perfectly plastic material model with a nominal plateau slope was used to model material properties of steel end adjustable clamps (S275JR) and the hardened steel knife-edges (S355N). The measured stress–strain curves obtained via flat and corner tensile coupon tests on the lean duplex stainless steel grade EN 1.4162 were used to develop the material models of section' flat legs and corner, respectively. The initial geometric imperfections were explicitly modelled by using lowest local (twist imperfection ─ local/torsional mode) and global (bow imperfection about the minor-principal axis) buckling modes obtained via Linear Buckling Analysis (LBA) performed on equivalent FE models with the same mesh. The imperfection amplitudes matched the measured ones.

The qualitative comparisons of the failure modes of the intermediate length specimens occurred in the and the FE modelling are presented in Figure 3.
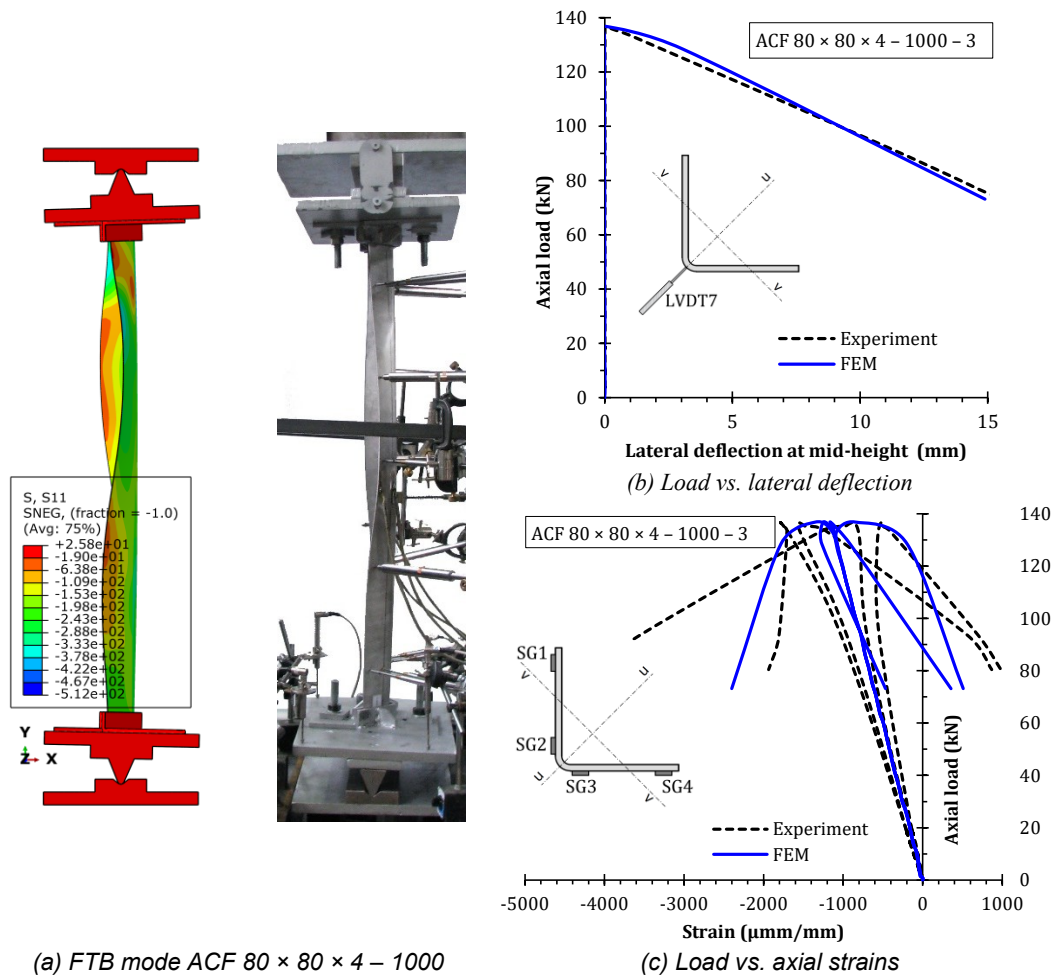
(b) Load vs. lateral deflection

(a) FTB mode ACF 80 × 80 × 4 – 1000

(c) Load vs. axial strains

Figure 3. FE model and experimental buckling mode of intermediate length specimens [2]

Experimentally verified nonlinear FE modelling was used to perform an extensive FE parametric study aiming to thoroughly examine the structural responses of cold-formed equal-leg angle columns and develop a database for their reliability-based design. The wide range of columns' global slenderness was considered in the study to investigate LB, major-axis FTB and minor-axis FB resistances. Furthermore, 27 different equal-leg angle sections were selected providing both slender and non-slender cross-sectional behaviour. The influence of material nonlinearity on column ultimate strength was thoroughly analysed for three primary alloys — austenitic, ferritic and duplex stainless steel using collected data from literature [1], [8], [9], [10].

4   Buckling curve proposal and reliablity assesment

This section addresses the comparison of the generated experimental [1] and FE data [2] with the design buckling predictions determined in accordance with the procedures described in SRPS EN 1993-1-4 [6] and SRPS EN 1993-1-1 [11]. Figures 4 shows the graphical comparisons of the different European buckling with the FE and test ultimate loads normalised by the cross-section yield loads for dominant minor-axis FB. The new buckling curve with the imperfection factor α = 0.92 and non-dimensional limiting slenderness $\bar{\lambda}_0$ = 0.15 for austenitic data set is also depicted in Figure 4.

Table 4 provides a statistical appraisal of the accuracy of the mentioned procedures considering the mean values of FE & test-to-predicted ratios $N_{b,u}/N_{b,u,pred}$ and the corresponded coefficient of variations (CoVs) per stainless steel grade and per cross-section class. The design predictions of columns with slender angle sections (Class 4) were obtained using interaction equation 5.15 of SRPS EN 1993-1-4 [6], to evaluate the influence of the neutral axis shifting along the major principal axis toward the section corner.

The procedure outlined in Annex D of EN 1990 [12] and the methodology described by Afshan et al. [13] were subsequently performed to assess the reliability of the proposed buckling curves for the cold-formed equal-leg angle columns and calculate the values of the partial factors for member resistance γ_{M1} [6]. The key results of the reliability analysis are also shown in Table 4.
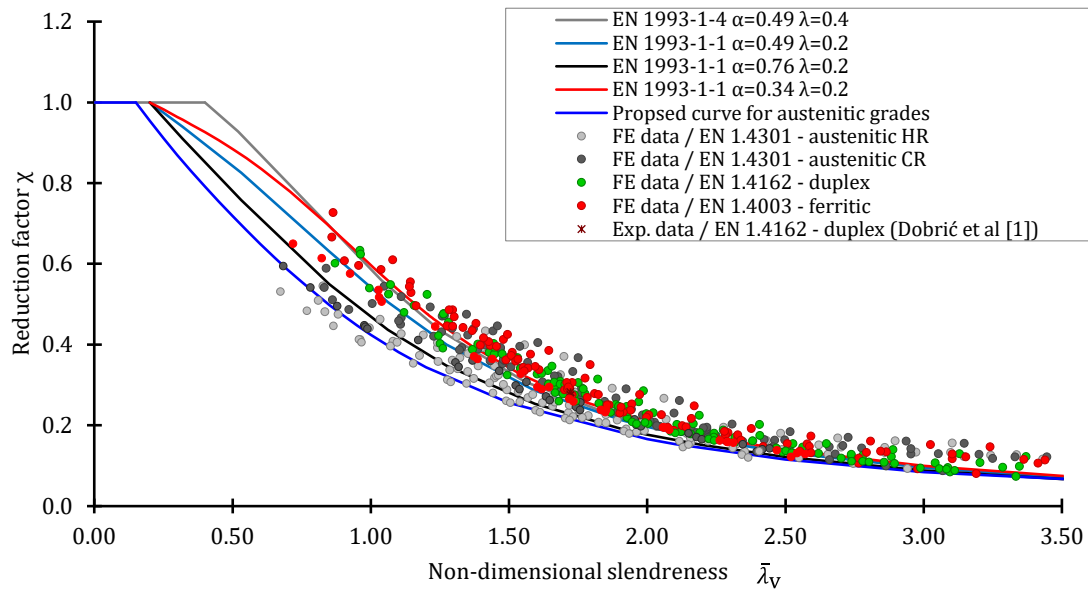
Figure 4. Comparison between normalised FE & test results and European buckling curves for minor-axis FB [2]

Table 4. Comparison between FE & test data and design data and the partial factors for member resistance γ_{M1} obtained in reliability analysis [2]

Grade	Cross-section slenderness	Code	Data no. $\overline{\lambda}_0 > 0.2$	$N_{b,u}/N_{b,u,pred}$		
				Mean	CoV (%)	γ_{M1}
EN 1993-1-4 / minor-axis FB (& minor-axis bending)						
Austenitic	Class 3	$\alpha = 0.76$ $\overline{\lambda}_0 = 0.2$	98	1.181	27.1	1.21
	Class 4	$\alpha = 0.76$ $\overline{\lambda}_0 = 0.2$ & Eq. 5.15	193	1.910	40.6	1.21
	Class 3	$\alpha = 0.92$ $\overline{\lambda}_0 = 0.15$	98	1.198	19.4	1.10
	Class 4	$\alpha = 0.92$ $\overline{\lambda}_0 = 0.15$ & Eq. 5.15	193	2.001	39.8	1.08
Duplex	Class 3	$\alpha = 0.49$ $\overline{\lambda}_0 = 0.2$	21	1.007	2.6	1.09
	Class 4	$\alpha = 0.49$ $\overline{\lambda}_0 = 0.2$ & Eq. 5.15	119	2.054	39.2	1.03
Ferritic	Class 3	$\alpha = 0.49$ $\overline{\lambda}_0 = 0.2$	49	1.159	21.1	1.09
	Class 4	$\alpha = 0.49$ $\overline{\lambda}_0 = 0.2$ & Eq. 5.15	85	1.953	38.4	1.09
EN 1993-1-4 / FTB & minor-axis bending						
Austenitic	Class 4	$\alpha = 0.34$ $\overline{\lambda}_0 = 0.2$ & Eq. 5.15	212	2.892	32.7	1.09
Duplex	Class 4	$\alpha = 0.34$ $\overline{\lambda}_0 = 0.2$ & Eq. 5.15	104	3.779	28.2	0.67
Ferritic	Class 4	$\alpha = 0.34$ $\overline{\lambda}_0 = 0.2$ & Eq. 5.15	104	3.373	29.7	0.83

5 Conclusions

A comprehensive investigation of the structural behaviour of cold-formed equal-leg angle columns members under pure compression, including experiments [1] and qualitative and quantitative numerical studies [2], was carried out with the aim of acquiring a valuable database that enabled the development of an accurate and reliable design method. The following conclusions are drawn from this investigation:

– The failure mode of the short equal-leg angle specimens was governed by elastic local buckling akin to TB, occurring at a stress value that is 40% lower than the measured average yield strength. Elastic FTB coupled with LB and minor-axis FB was the dominant failure mode for specimens in the intermediate slenderness domain. In the high slenderness domain, the failure mode of all specimens was minor-axis FB. The test results also indicate that the long length specimens were not prone to LB.

– Considering the austenitic dataset, comparisons of the test & FE resistances with design predictions obtained for buckling curve *d* ($\alpha = 0.76$ $\overline{\lambda}_0 = 0.2$), demonstrate that the European design method may be either conservative for slender sections (Class 4) or even excessively unconservative, particularly for non-slender sections (Class 3). The unsafe predictions are more significant for columns made from austenitic hot-rolled strips which have noticeably lower structural responses in comparison with their counterparts produced from cold-rolled austenitic strips. Thus, the buckling curve *d* offer unsatisfactory design

predictions with the safety factors γ_{M1} significantly higher than the currently adopted value of 1.10.

− The proposed buckling curve (α = 0.92 $\bar{\lambda}_0$ = 0.15) offers improved fit to available data, providing a higher average ratio of the test & FE resistance-to-design resistance and less scatter across the austenitic datasets both for slender and non-slender angle sections, in comparison with the Eurocode buckling curve *d*. The safety factors γ_{M1} are equal to 1.10 and 1.09 for non-slender (Class 3) and slender (Class 4) angle sections, respectively.

− In contrast to austenitic grade, the predictive curve *c* (α = 0.49 $\bar{\lambda}_0$ = 0.2) is in good agreement with FE & test data for duplex and ferritic grades. The safety factors γ_{M1} are lower than 1.10 for all cross-section classes.

− The FTB response of cold-formed equal-leg angles is strongly associated with their cross-section dimensions. The increasing of the leg slenderness leads to appearing of elastic local buckling accompanied by the torsional rotations of angle section. The comparative analysis shows that the European design method covering the interaction of FTB and uniaxial minor-axis moment gives safe but significantly conservative predictions and safety factors lower than 1.10 for all three stainless steel grades.

References

[1] Dobrić J, Filipović A, Marković Z, Baddoo N.: Structural response to axial testing of cold-formed stainless steel angle columns, Thin-Walled Structures, 156, 2020.

[2] Dobrić J, Filipović A, Baddoo N, Marković Z, Buđevac D.: Design procedures for cold-formed stainless steel equal-leg angle columns, Thin-Walled Structures, 107210, 2020.

[3] EN ISO 6892-1. Metallic materials – Tensile testing. Part 1: Method of test at room temperature. Brussels, Belgium, CEN 2009.

[4] Arrayago I, Real E, Gardner L.: Description of stress-strain curves for stainless steel alloys, Materials and Design. 2015;87:540-552.

[5] Eurocode 3: Design of Steel Structures – Part 1-3: General rules - Supplementary rules for cold-formed members and sheeting EN 1993-1-3, Brussels, Belgium, CEN 2006.

[6] Eurocode 3: Design of steel structures – part 1-4: General rules – supplementary rules for stainless steels, including amendment A1 (2015), EN 1993-1-4:2006+A1:2015, Brussels, Belgium, CEN 2015.

[7] ABAQUS User Manual. Version 6.12. Providence, RI, USA: DS SIMULIA Corp; 2012.

[8] Dobrić J, Buđevac D, Marković Z, Gluhović N.: Behaviour of stainless steel press-braked channel sections under compression, J. Construct. Steel Res. 139 (2017) 236–253.

[9] Lecce M, Rasmussen K.J.: Distortional Buckling of Cold-Formed Stainless Steel Sections: Experimental Investigation, J Struct Eng., ASCE 132 (4) (2006) 497–504.

[10] Rossi B, Jaspart J.P, Rasmussen K.J.: Combined distortional and overall flexural-torsional buckling of cold-formed stainless steel sections: Experimental investigations, Journal of Structural Engineering. 136 (4) (2010) 354–360.

[11] Eurocode 3: Design of steel structures – Part 1-1: General rules and rules for buildings EN 1993-1-1, Brussels, Belgium, CEN 2005

[12] Eurocode: Basis of structural design EN 1990, Brussels, Belgium, European Committee for Standardization (CEN); 2002.

[13] Afshan S, Francis P, Baddoo N.R, Gardner L.: Reliability analysis of structural stainless steel design provisions, J. Construct. Steel Res., 114 (2015) 293–304.

Vibration serviceability limit state of pedestrian bridges[*]

Adam Ramoul[*1)], Milan Spremić[2)]

[1)] *Structural Engineer at Asmec Consultants d.o.o., Belgrade, Republic of Serbia*
[2)] *Faculty of Civil Engineering, University of Belgrade, Republic of Serbia*

A B S T R A C T

Modern conustructions of pedestrian bridges must satisfy functional and increasingly complex architectural requirements. In order to achieve the attractive design of pedestrian bridges, modern constructions generally differ from older, conventional solutions. The vibration problem of such structures shows that the dynamic response of the structure is governing for the design. This paper presents the comparative analysis of several dynamic models of pedestrian loads, described in various standards, guidelines, and recommendations. On the example of an arched pedestrian bridge, comparative analysis of the structure behavior due to the effect of pedestrian load was performed using numerical simulations in the SOFISTIK software, with the results obtained by analytical calculation procedures.

1   Introduction

The development of building materials, construction technologies as well as various design methods result in the construction of attractive, slender structures of a large span. Because of the reduction of the rigidity of the structure, the natural frequencies of the bridge decrease, which increases the risk of uncomfortable vibrations, for example vibrations caused by human walk. The modern approach of checking functionality and comfort as the serviceability limit state implies the analysis of the dynamic response of the structure under the action of the design load, with a frequency corresponding to the natural frequency of the bridge, which causes the most unfavorable response of the structure. Human sensitivity to vibrations is most often expressed by the acceleration of the deck and the time of exposure to vibrations. The criterion of vibrations acceptability of structures is basically a function of frequency and is mainly expressed in units of acceleration [3]. This article was created as a result of a master's thesis defended at the University of Belgrade - Faculty of Civil Engineering.

2   Dynamic loads of pedestrian bridges

The movement of pedestrians on the bridge causes a dynamic force that is variable in time and space, and which has components in three different directions: a vertical component and two components in the horizontal direction - transverse and longitudinal. The force component in the vertical direction is the subject of most studies for the simple reason that it has the largest load magnitude. In recent years, more detailed studies have been done, showing that the lateral component of the force (in the transverse direction)

can also cause problems regarding the serviceability limit state of the structure.

In general, the load caused by the pedestrian movement on the bridge can occur due to various activities such as walking, running or jumping. Each of the possible pedestrian activities on the bridge can be represented by a load curve that includes the intensity and frequency of the pedestrian load.

The intensity of the vertical component of the force due to the pedestrian movement is determined primarily by the weight of the pedestrian, the length of the steps as well as the frequency of walking. The most common frequency range that occurs due to pedestrian movement is 1.6-2.4 Hz.

The horizontal components of the force are much less intense than the vertical component but cannot be ignored. The main reason for transverse vibrations control is the so-called "lock in" effect, when a group of pedestrians, moving at different frequencies, begins to gradually adjust the walking frequency to the natural frequency of the bridge which leads to pedestrian-induced forces resonate with the structure. Small values of transverse vibrations may be sufficient to throw the pedestrian out of balance [3].

Eurocode, EN 1990: 2002 [1] in Annex A2.4.3.2, defines comfort criteria and criteria in which dynamic analysis of the structure is required. The comfort criterion is defined by the maximum allowed structure accelerations. Dynamic analysis is required to prove comfort in cases where the vertical natural frequency of the structure is less than 5 Hz and the horizontal or torsional frequency is less than 2.5 Hz. Vertical accelerations are limited to 0.7 m/s^2, while horizontal accelerations are limited to 0.2 m/s^2 under normal operating conditions and 0.4 m/s^2 for exceptional crowd conditions.

Dynamic load models which should be used in the analysis are not given, it is left to the National Annexes to propose the dynamic load models.

2.1 Dynamic load models

2.1.1 Eurocode 1 Prestandard

Prestandard of Eurocode 1 (pr EN 1991-2:2003) [4] proposed Annex C which provides recommendations for determining the natural frequencies of the structure, damping as well as dynamic load models to be applied in verifying the serviceability limit state. Three load models have been proposed that simulate the movement of a single pedestrian (DLM1), a group of pedestrians (DLM2), and a continuous stream of pedestrians (DLM3). DLM1 and DLM2 are defined as a stationary pulsating force that has two components to be considered separately. Dynamic load model DLM3 consists of a uniformly distributed pulsating surface load [N/m²] with two components also to be considered separately. In the following expressions: f_v , f_h – are vertical and horizontal natural frequency of the bridge, $k(f_v)$, $k(f_h)$ – pedestrian synchronization factors depending on the frequency [4].

2.1.2 UK National annex to EN 1991-2

The UK National Annex to Eurocode 1: Actions on structures - Part 2: Traffic loads on bridges [8] defines dynamic load models to be applied in the design of pedestrian bridges, as well as comfort criteria in the form of limitations of vertical accelerations of the structure. In Chapter NA.2.44.2 bridges are classified into four categories, depending on their usage and location, on the basis of which the number of pedestrians moving on the bridge is determined, as well as the density [ped/m²] in case of crowd loading. Two load models are given that represent the passage of single pedestrian or pedestrian groups as well as the steady state modeling of pedestrians in crowded conditions.

The maximum vertical accelerations that result from single pedestrian or group of pedestrians, should be calculated assuming that these loads are represented by application of a vertical pulsating load $F(N)$ moving across the span of the bridge at a constant speed $v(t)$:

$$F = F_0 \cdot k(f_v) \cdot \sqrt{1 + \gamma \cdot (N-1)} \cdot sin\,(2\pi f_v t)$$

The design maximum vertical accelerations that result from pedestrians in crowded conditions may be calculated by assuming that these are represented by a vertical pulsating distributed load w [N/m²], applied to the deck for a sufficient time so that steady state conditions are achieved as follows:

$$w = 1.8 \cdot \frac{F_0}{A} \cdot k(f_v) \cdot \sqrt{\gamma \cdot \frac{N}{\lambda}} \cdot \sin\,(2\pi f_v t)$$

In the previous expressions: N – is the number of pedestrians determined based on the defined class of the bridge, F_0 – reference amplitude of the pulsating force [N], f_v – natural frequency of the vertical mode under consideration, $k(f_v)$ – combined factor to deal with the effects of a more realistic pedestrian population, harmonic responses and relative weighting of pedestrian sensitivity to response, t – elapsed time [s], γ – reduction factor to allow for the unsynchronized combination of actions in a pedestrian group, is a function of damping and effective span, S_{eff} – effective span (in all cases it is conservative to use $S_{eff} = S$), S – bridge span [m]
ρ – required crowd density obtained from, b – width of the bridge subject to pedestrian loading, λ – factor that reduces the effective number of pedestrians when loading from only part of the span contributes to the mode of interest [8].

2.1.3 Sétra Guide (Service d'Études techniques des routes et autoroutes)
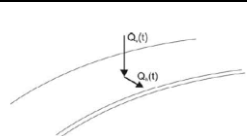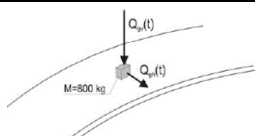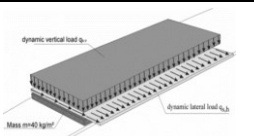
The recommendations given in the Sétra Guide [2] aim to summarize current knowledge on the dynamic behavior of pedestrian bridges due to pedestrian loading.

These recommendations also define bridge classification, as a function of traffic level and location, and the required comfort level which directly depends on the acceleration of the structure. Given the subjective nature of the comfort concept and convenience, the range of acceleration is defined, not the individual value. The methodology proposed by Sétra [2] makes it possible to limit the risk of the occurrence of the resonance caused by the pedestrian load.

The recommendations define three cases of dynamic loading depending on the bridge class and the ranges within which its natural frequencies are situated. Load models for different directions should be considered individually, therefore the dynamic response of the structure should be determined for each load direction separately. The load should be applied to the whole surface of the deck which is intended for the pedestrian movement. Also, the load should be such that the amplitude of the force is always of the same sign as the mode shape. In this way, the maximum response of the structure is obtained, see Figure 1 [2].

The load amplitudes of different dynamic models, for the frequency of the second oscillation mode are shown in Table 2.

Table 1. Dynamic Load Models according to Prestandard of Eurocode 1

Single pedestrian – DLM1	Group of pedestrians – DLM2	Continuous pedestrian stream – DLM3
Vertical component of pulsating force		
$Q_{pv} = 280 sin(2\pi f_v t)$	$Q_{gv} = 280 k_v(f_v) sin(2\pi f_v t)$	$q_{sv} = 12.6 k_v(f_v) sin(2\pi f_v t)$
Horizontal component of pulsating force		
$Q_{ph} = 70 sin(2\pi f_h t)$	$Q_{gh} = 70 k_h(f_h) sin(2\pi f_h t)$	$q_{sh} = 3.2 k_h(f_h) sin(2\pi f_h t)$

Vibration serviceability limit state of pedestrian bridges
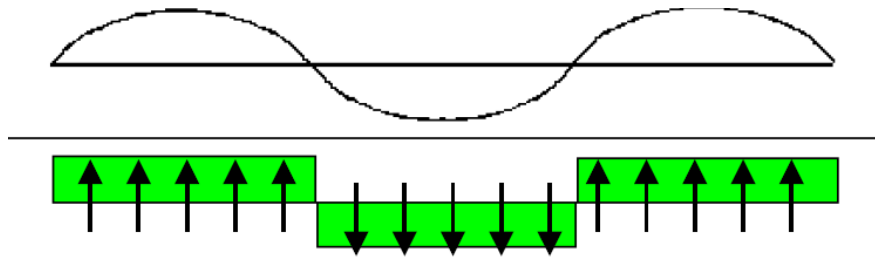
Figure 1. Sign of the amplitude of the load in the case of a mode with several sags [2]

Table 2. Dynamic load amplituedes according to relevant standards

Standard	Load model	Vertical almplitude	Horizontal almplitude
EC 1	DLM1	280 [N]	70 [N]
	DLM2	840 [N]	210 [N]
	DLM3	37.8 [N/m^2]	9.6 [N/m^2]
UK NA	Walking N = 8	434 [N]	/
	Running N = 2	1097 [N]	/
	Pedestrian Crowd	9.0 [N/m^2]	/
Sètra	Walking N = 1	280 [N]	35 [N]
	Pedestrian crowd	14.87 [N/m^2]	1.96 [N/m^2]

3 Dynamic analysis of an arched pedestrian bridge

On the example of one pedestrian bridge, a parametric analysis was performed. It was checked whether the structure meets the serviceability criteria in terms of vibrations induced by pedestrians according to the stated standards and guidelines. A numerical analysis was performed in the SOFISTIK software [7] using time history analysis by step-by-step integration method.

3.1 Technical description of the structure

The conceptual design of the pedestrian bridge over the river Đetinja at the location of Stari grad in Užice was analyzed. The structure of the bridge is formed by two steel arch girders positioned at a distance of 3 m from each other.

The arch span is 70 m while the total length of the bridge is approximately 100 m. The rise of the arch is 12.52 m so that the ratio of the rise and the span *f/L* is 0.18 which corresponds to the recommended values, see figure 2.

The deck structure consists of longitudinal and transverse beams that rest on the main arch girders via the columns. Columns are positioned at a distance of 7m. In order to provide the lateral stability of the bridge, the arches are interconnected by beams at the joints in the zones of columns supports. Vertical bracings are provided between columns and are made in the form of crossed diagonals. The spatial stability is also achieved by a horizontal bracing member at the level of the lower flange of the transverse beam. The longitudinal and transverse beams form a structural system that serves as a support structure for the glass panels that make up the deck for pedestrian movement.
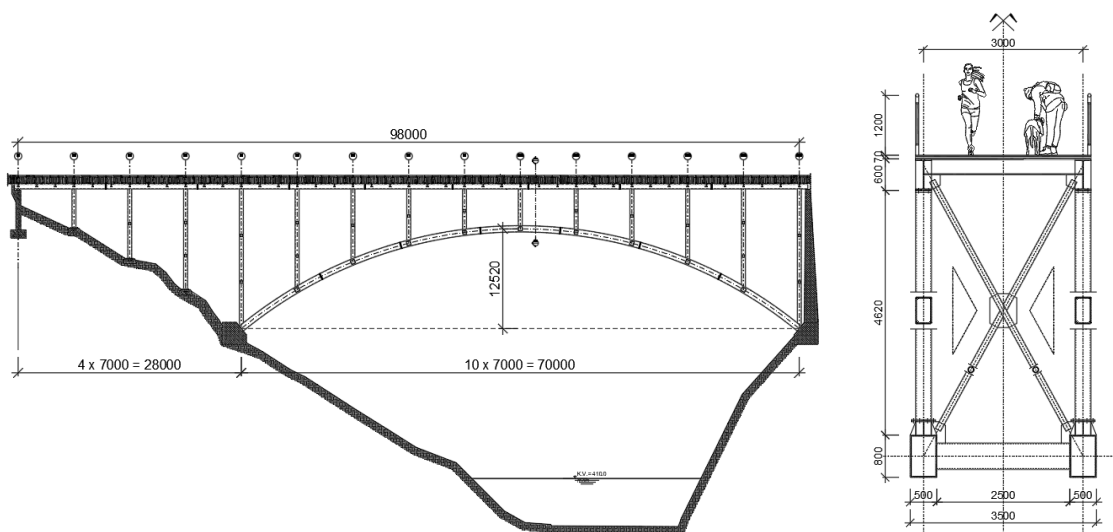
Figure 2. Longitudinal and cross section of the bridge

3.2 Bearing capacity of the glass panel

Glass has been increasingly used as a material in construction in recent years in order to increase the aesthetic value of the buildings. The unique properties of glass, such as unlimited lifespan, transparency, and the ability of letting the light passing through the material lead to the glass being increasingly used not only for non-structural elements but also for structural elements of the buildings. Glass is a brittle material, sensitive to stress concentrations. Laminated glass panels composed of two or more glass panels connected by interlayers of a certain transparent plastic material - glue - are most often used for the glass structural elements. During breakage, cracks appear on the panel constructed in this way and if it disintegrates, pieces of glass will remain attached to the foil layer. The development of standards for the design of glass structures does not keep pace with the dynamic development of the glass industry. The paper analyzes the bearing capacity of the deck in accordance with the draft version of the standard pr EN 13474 "Glass in Buildings" - Part 1 and Part 2 [5] [6].

The behavior of the panel predominantly depends on the properties of the polymer interlayer. The calculation of stresses and deflections is based on the concept of effective thickness [5]. The essence of the concept is to approximate the laminated panel with an equivalent glass panel made of homogeneous material. The structural details of the bond ensure that the panels are loaded only perpendicular to their plane and that the horizontal and vertical loads from pedestrian traffic are transferred to the transverse and longitudinal deck supports. Bearing capacity has been conducted for the dead load and traffic load of $q=5.0kN/m^2$. Rectangular laminated glass panels having dimensions 3.0x2.33m have been adopted. These dimensions were determined by the spacing of longitudinal and transverse beams of the deck structure. The laminated panels are formed from three panels of tempered glass 19mm thick and two PVB interlayers 1.52mm thick. The total thickness of the panel is 60mm. The effective thicknesses for the calculation of deflection and stress are 27.40 mm and 32.91 mm, respectively. For a panel formed in such a way, the ultimate stress values are 39.32 MPa, and the allowable deflection values according to the recommendations of the standard are 10 mm [6]. Table 3 shows the results of obtained stress and deflection.

3.3 Natural frequencies of the structure

Natural frequencies of the structure are determined using the numerical analysis in the SOFISTIK software [7]. Figure 4 shows the relevant vibration modes with vertical frequencies less than 5 Hz and horizontal frequencies less than 2.5 Hz that require additional dynamic analysis.

A very important input parameter for conducting the dynamic analysis is the relative damping of the structure. In the general case, this value can only be estimated. The damping was determined on the basis of the logarithmic decrement δ. The recommended value of this parameter for steel is 0.03 and it was used as input data in the SOFISTIK software [7].

Table 3. Laminated glass panels analysis results

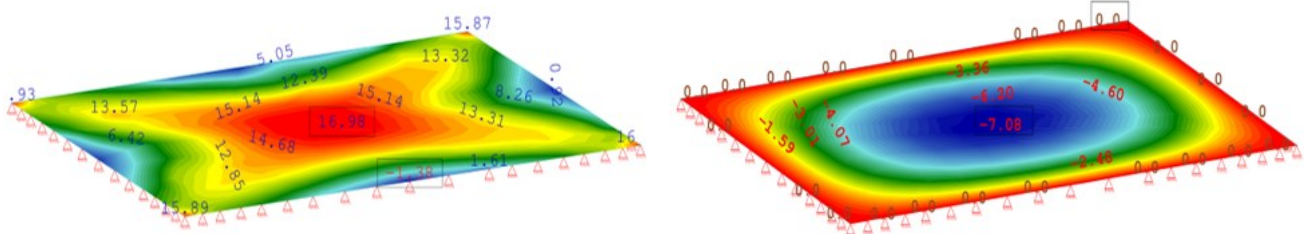| Calculation method	Stress [MPa]	Deflection [mm]
Numerical analysis - SOFISTIK	16.98 < $f_{g.d}$=39.32 MPa	7.08 < 10

Figure 3. Stress and deflection diagrams of glass panel
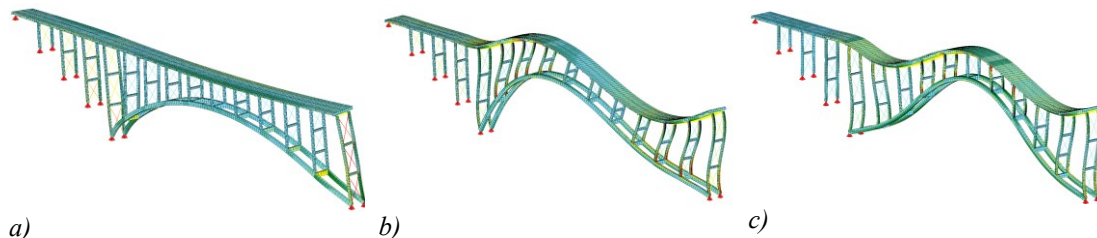

a)   b)   c)

Figure 4. Natural frequencies and mode shapes: a) horizontal - f_h=1.158 Hz, b) vertical - f_{v1}=2.219 Hz, c) vertical - f_{v2}=3.444 Hz

3.4 Dynamic analysis results

Prestandard of Eurocode 1 [4] defines a dynamic load that does not move across the bridge but acts at a single point (DLM1 and DLM2) or as a stationary surface load (DLM3). Load duration is an important calculation parameter. The duration of the load was varied iteratively in order to achieve a steady response of the structure due to the dynamic forces and the adopted damping. The values of the obtained accelerations were recorded after 40,0 s of action of the force. The adopted value of the timestep is Δt=0.02s. The load amplitudes were determined in accordance with the expressions provided in table 1. Coefficients $k_v(f_v)$ and $k_h(f_h)$ were determined based on the diagrams provided in [4]. Based on the results presented in table 4 it can be noticed that the vertical acceleration criteria, defined by the standard, was exceeded in case of the DLM3 load model – continuous pedestrian stream. The vertical acceleration diagram and the function of the dynamic surface load are presented in figure 5.

The UK National Annex to Eurocode 1 [8] defines the vertical dynamic loads to be applied to determine the structural response. Loads are defined for various pedestrian activities such as walking and running. The load amplitudes depend on the adopted bridge class and the obtained frequencies of the structure. Class C was adopted for the considered pedestrian bridge, on the basis of which the sizes of groups of pedestrians for walking, running as well as the density of pedestrians on the bridge in case of a crowd loading were determined.

The load of a group of pedestrians walking or running on the bridge is modeled as a concentrated force moving along a line located in the middle of the deck structure. Dynamic load is defined by a sinusoidal function which means that the amplitude of the load changes over time. The concentrated force acts in the nodes whose distance is defined by the speed of pedestrians as defined by the National Annex [8] and amounts 1.7 m/s for walking, or 3.0 m/s for running and with the load frequency that coincides with the natural frequency of the bridge to obtain the most unfavorable response of the structure.

Table 4. Dynamic analysis results according to Prestandard of Eurocode 1 [4]

Load model	Vertical acceleration [m/s²]	Vertical acceleration criteria [m/s²]	Horizontal acceleration [m/s²]	Horizontal acceleration criteria [m/s²]
DLM1	0.09	0.7	0.02	0.2
DLM2	0.26	0.7	0.05	0.2
DLM3	0.75	0.7	0.36	0.4
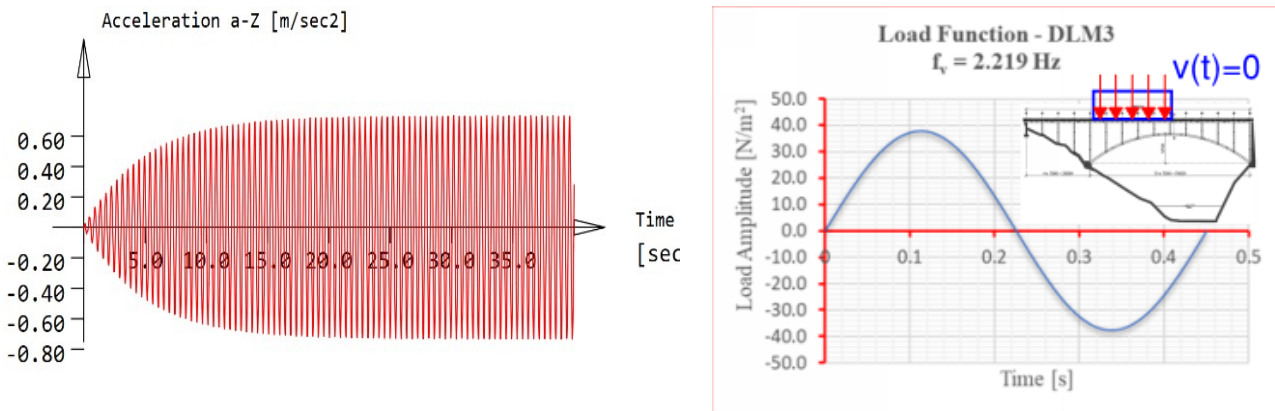
Figure 5. Vertical acceleration diagram (left) and DLM3 load model function (right)

Table 5. Dynamic analysis results according to BS EN1991-2 NA.2.44 [8]

Load model	Natural frequency [Hz]	Vertical acceleration [m/s²]	Acceleration criteria [m/s²]
Walking N=8	2.219	0.10	0.7
Running N=2	2.219	0.22	0.7
Running N=2	3.444	0.09	0.7
Crowd loading [0.8 ped/m²]	2.219	0.35	0.7
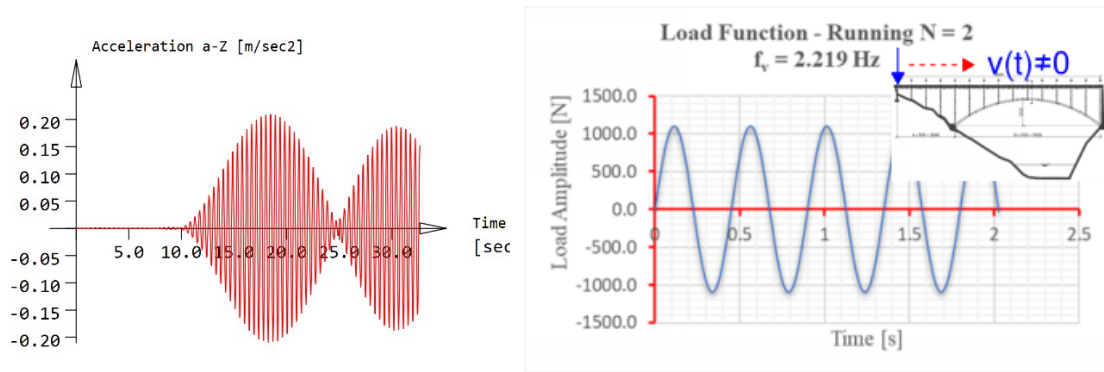
Figure 6. Vertical acceleration diagram (left) and moving force load function (right) – Running N=2

In the dynamic analysis, in accordance with the recommendations of the Sétra Guide [2], bridge class 2 was adopted, which corresponds to the class C given in the UK National Annex [8]. Based on the adopted bridge class and calculated natural frequencies and in accordance with the calculation methodology, load case to be applied to calculate the vertical and horizontal response of the structure was determined. The recommendations given in these guidelines mainly refer to the amplitudes of dynamic loads caused by pedestrian crowd, since this case is usually governing. The load case applied in the dynamic analysis is Load case 1 to which corresponds the pedestrian density of 0.8 ped/m^2.

Having in mind the dimensions of the structure, it is expected that the accelerations caused by the movement of single pedestrian, or a group of pedestrians are significantly below the acceleration criteria, and that the case of a pedestrian crowd loading is most relevant to satisfy the serviceability limit state in terms of vibrations, which is proven by dynamic analysis.

Based on the values shown in Table 7, it can be concluded that the criterion of the serviceability limit state in terms of vibrations is met according to the recommendations of UK NA [8] and Sétra Guide [2] for bridge classes C and 2, respectively, while the vertical accelerations criteria is exceeded according to recommendations given in Prestandard of Eurocode 1 [4].

Table 6. Dynamic analysis results according to Sétra [2]

Load model	Vertical acceleration [m/s^2]	Acceleration ranges and comfort criteria [m/s^2]	Horizontal acceleration [m/s^2]	Horizontal acceleration criteria [m/s^2]
Dense crowd Class 2	0.55	0.0 ÷ 0.5 – max comfort 0.5 ÷ 1.0 – mean comfort 1.0 ÷ 2.5 – min comfort	0.06	0.1
Very dense crowd Class 1	1.23		1.14	0.1
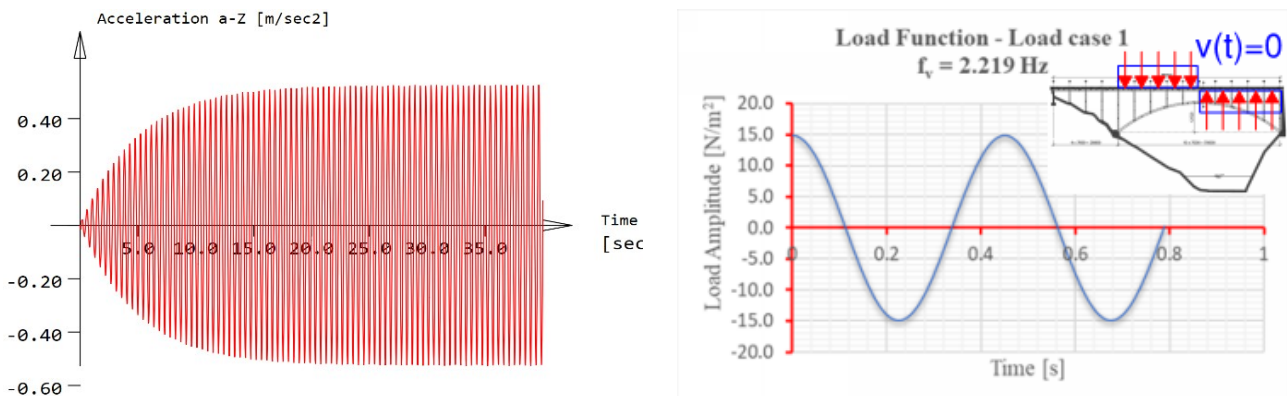
Figure 7. Vertical acceleration diagram (left) and dynamic load function (right) - Sétra Load case 1

Table 7. Comparative analysis for pedestrian crowd case

Standard	EC1	BS NA	Sétra Bridge class 2	Sétra Bridge class 1
Load model	DLM3	Pedestrian crowd	Pedestrian crowd	Pedestrian crowd
Vertical acceleration [m/s^2]	0.75	0.35	0.55	1.23
Horizontal acceleration [m/s^2]	0.36	/	0.06	0.14

According to the comfort criteria defined by Sétra Guide [2], the obtained value of vertical acceleration, in case when a bridge is treated as class 2 bridge, is 0.55 m/s^2 which corresponds to the mean comfort. Taking into consideration the purpose and location of the bridge, the structural response is determined for class 1 bridge too. Such approach to the analysis is justified in certain situations such as the opening day when the bridge is commissioned, when higher densities of pedestrians may occur on the bridge. In this case, vertical acceleration is 1.23 m/s^2 and it corresponds to the minimum comfort, while the horizontal acceleration criteria, which is limited because of the ''lock in'' effect, is exceeded.

4 Conclusions

The very fact that the official versions of Eurocode do not define precise recommendations and data for performing dynamic analysis due to pedestrian load indicates that this is a complex engineering problem. It has been shown that there are differences in the results of the dynamic analysis obtained on the basis of different recommendations and guidelines. The synchronization of a large number of pedestrians, defined through dynamic coefficients, has the greatest impact on the obtained differences. By designing structures according to the UK National Annex and the Sétra Guide, footbridge designs having lower stiffness can be obtained, satisfying the serviceability limit state in terms of vibration. The analysis of the structure according to the Prestandard of Eurocode 1 shows that the adopted solution does not meet the minimum comfort criteria. In this case, an increase in the height of the longitudinal deck girder or the introduction of vibration dampers should be considered.

The obtained results indicate that by using advanced numerical methods, serviceability limit state in terms of vibrations of the lower rank bridges can be satisfied, even when the calculated frequencies of the structure are in critical ranges where there is the maximum risk of resonance occurring. It should be emphasized that the calculation results are very sensitive to the bridge span (dead load of the structure). Also, it is necessary to carefully analyze the class/rank of the bridge, with a precise prediction of pedestrian traffic in the future, so that a bridge that is classified in a lower rank would not move to a higher one and thus potentially endanger the comfort on the bridge.

References

[1] Eurocode 0, EN 1990:2002 – Basis of Structural Design
[2] Footbridges - Assessment of vibrational behaviour of footbridges under pedestrian loading, Sétra, 2006
[3] Marija Spasojević-Šurdilović: Analiza graničnog stanja upotrebljivosti pešačkih mostova u pogledu vibracija indukovanih pešacima, doktorska disertacija – Univerzitet u Nišu, 2013.
[4] Proposal Annex to Eurocode 1991-2:2003 (Not published)
[5] prEN 13474-1. Glass in Building - Design of glass panes - Part 1: General basis of design, 1999.
[6] prEN 13474-2. Glass in Building - Design of glass panes - Part 2: Design for uniformly distributed loads
[7] SOFISTIK Documentation Version 2019
[8] UK National Annex to Eurocode 1: Actions on Structures – Part 2: Traffic loads on bridges (NA to BS EN 1991-2:2003)

Comparative analysis of conventional and new seismically isolated structure[*]

Jelena Ristić[*1)], Miloš Vučinić[2)], Danilo Ristić[3)], Milutin Vučinić[4)]

[1)] Faculty of Engineering, Department of Civil Engineering, International Balkan University (IBU), Skopje, R.N.Macedonia
[2)] Institute for Construction, Sima Barovića 16-18, Podgorica, Montenegro
[3)] Institute of Earthquake Engineering and Engineering Seismology (IZIIS), Ss Cyril and Methodius University, Skopje, R.N.Macedonia
[4)] GP Planum, Beograd, DSD, Podgorica, Veljka Vlahovića 24

A B S T R A C T

Extensive analytical and experimental research has been done by the authors directed to mitigation of the effects of earthquakes on structures. The research results mainly represent parts of the realized several related international projects. A selected part of the analytical studies directed to comparison between conventional and seismically isolated frame structures is presented in this paper. The responses of the applied newly developed advanced seismic isolation system HC-RMS-GOSEB to the simulated input excitation of three representative earthquakes of intensity 0.50g, have shown that it is very effective for construction of vibro-isolated and seismically resistant buildings, providing activated multistage seismic response and globally optimized seismic energy balance. Its application achieves an increase in the vibration period of the structure, far enough from the dominant period of seismic excitation. The results of the research confirm that this system is a potential solution for achieving low-cost and highly efficient protection of buildings.

1   Introduction

Important technological advances and innovations have been created by the authors based on conducted long-term original analytical and experimental research within several international projects, [1], [4-19], focused on efficient mitigation of earthquake effects upon engineering structures. Our studies have been planned and realized considering the most recent analytical advances, [3] & [20], and suitable experimental modeling developments, [2], in this specific field. Presently, the authors are briefly introducing the new specific study results obtained from their recent analytical investigations realized for the purpose of comparison between the main prerequisites regarding construction of seismically safe conventional and innovative seismically isolated RC building structures. The favorable behavior of the applied innovative isolation system HC-RMS-GOSEB under strong input excitation caused by three earthquakes with intensity PGA = 0.50 g has pointed out that this system is very efficient in construction of vibro-isolated and seismically resistant buildings, enabling an activated multistage seismic response and a globally optimized seismic energy balance. The application of this system enables an increase of the vibration period of a structure and avoidance of the range of dominant periods of seismic excitation. The research results have proved that this system

represents a potential, widely applicable solution for achievement of low-cost and very efficient protection of existing and new high-rises. This paper shows the representative part of the comparative results obtained from the performed extensive analytical investigations of the dynamic behavior, the seismic safety and the construction cost of a selected prototype residential structure constructed in Skopje, treating the structure alternatively, first as a structure originally built as a conventional system and then as a structure seismically isolated by application of the originally conceptualized new HC-RMS-GOSEB system.

2   Description of the prototype structure

The building consists of a basement, a souterrain, a ground floor and 5 storeys, with an outline: basement, souterrain and ground floor 68.00x18,50m, gross area of 1258,00 m^2 at plan, Fig. 1. The external dimensions of the characteristic storey are 69,80x20,90, gross area 1371,00 m^2 at plan. The total area of the structure is 3x1258 + 5x1371 = 10629,00 m^2. The storey heights of the basement and the souterrain are 2,65 m. The storey heights of the ground floor and the characteristic storey are 3,20 m and 2,88 m, respectively.

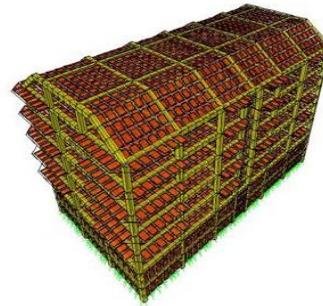*Figure 1. View of the analyzed constructed prototype structure in Skopje*

Figure 2. Formulated 3D linear model for analysis of the structure using SAP2000

Due to its considerably large length, the structure is dilatated into two equal segments of which only one has been analyzed, but the final conclusions refer to both. The main structural system consists of a reinforced concrete 3D frame structure with frames in both orthogonal directions. The staircase area is bounded by reinforced concrete walls. To prevent the negative torsional effect of seismic forces, walls up to half module are inserted at the ends of the structure. The basement and the souterrain walls are constructed of reinforced concrete. The foundation plate has a thickness of 80 cm. All reinforced concrete walls have a thickness of 25 cm. The façade walls are of a "sandwich" type and have a thickness of 30 cm, while the inner walls are constructed of brick blocks with a thickness of 12 cm. The reinforced concrete columns are proportioned 50x60 cm in the basement and 50x70 cm in the souterrain. At the ground floor, they are round Ø 55 cm, while their proportions at the storeys are 50x50 cm. The reinforced concrete beams are proportioned 50x40 cm. The floor structure represents a reinforced concrete slab with a thickness of 16 cm at the basement and the souterrain. Its thickness at the storeys is 14 cm as is also the thickness of the skew roof and staircase slabs. The walls and the slabs are reinforced by meshed reinforcement, with the exception of the foundation slab that is reinforced with ribbed reinforcement. The beams and the columns are reinforced with ribbed reinforcement of quality RA-400/500-2. The concrete class used for all elements is 30 MPa. The bearing capacity of soil is 0,30 MPa. The location of the structure belongs to seismic zone of degree IX according to the MCS scale. Figure 1 shows the view of the constructed building.

3 Seismic responses of the conventional system

a) Linear mathematical model-0 (M0) of the conventional system: The linear mathematical model M0 of the conventional system of the structure has been formulated and analyzed by means of the SAP2000 software, where "frame" elements have been used to model the reinforced concrete beams and columns, while "shell" elements have been used to model the reinforced concrete slabs and walls, Figure 2. Using the standard design procedure according to the current regulations, seismic analysis of the structural system has been carried out according to the ultimate bearing capacity theory. Based on competent results obtained by use of the SAP2000 software [20], proportioning of all RC elements has been done and the necessary reinforcement has been adopted.

b) Nonlinear mathematical model-1 (M1) of the conventional system: The experience that has been gathered so far has led to the conclusion that heavy damages or failure of structures under earthquakes take place due to concentration of damage in some critical points of the structures. Such critical points are usually due to inappropriate design of structural elements and their connections at the joints or due to concentration of seismic forces in these and such connections. One of the prerequisites for calculation of the real seismic response of a structure to a certain earthquake record is formulation of a nonlinear model that includes the real nonlinear effects occurring in the structural and nonstructural elements of the structure. On the other hand, such formulated mathematical model should always be sufficiently simple containing, at the same time, an optimal number of degrees of freedom in order to be suitable for realistic analysis of the dynamic response of the system under the effect of selected recorded characteristic earthquakes.

Considering the above, a two-dimensional analytical model of the structure with reduced number of degrees of freedom has been adopted. In regard to the mathematical model for initial linear analysis, all RC walls have been omitted. This has been done for the purpose of obtaining a model for analysis that has the same 3D frame system and will be able to be compared with the new system with seismic isolation HC-RMS-GOSEB that also has the same 3D system, walls being unnecessary. The nonlinear model of the structure has been formulated in the special software programme NORA2005 developed by the third author, [6]. The effect of all structural elements and their real distribution along storey heights has been simulated by satisfying the previously described criteria. The mathematical model of the prototype structure has been of the "shear type". For such model, some engineering assumptions have been made. The total mass of the structure is concentrated at the level of the RC slabs, namely at the characteristic nodes of the beams, where the horizontal deformation of the structure is independent of the axial forces in the columns. The nonlinear mathematical model of the conventional system with a fixed base for the selected representative prototype residential building (GF+5) is represented by its two representative RC frames RX3, Figure 3, and RY6, Figure 4. Such formulated mathematical models have served for comparative analysis of economic parameters, i.e., cost of construction, which is the main goal of the brief presentation within this work.
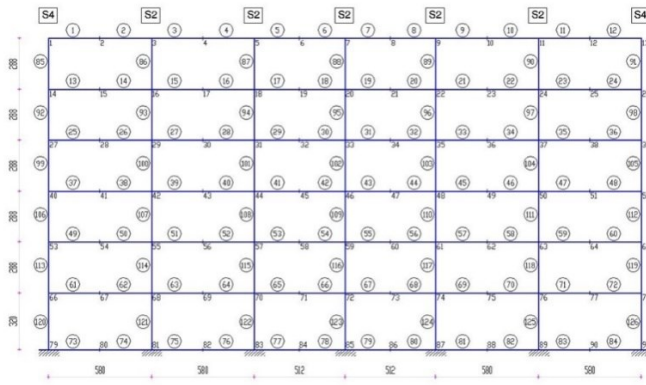
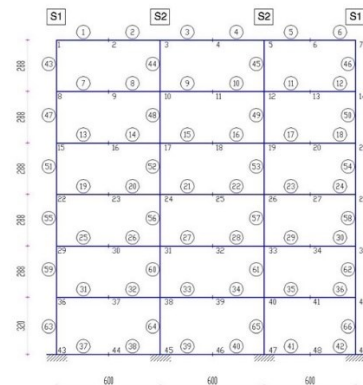*Figure 3. Formulated nonlinear model of the used RX frame of the conventional (C) structure (NORA2005)*

Figure 4. Nonlinear model of the used RY frame of the C-structure (NORA2005)

Using the formulated nonlinear mathematical model, all parametric analyses of the seismic response of the conventional structure have been carried out by taking into account the selected three representative earthquake records scaled to several different intensities. For the purpose of realistic modeling of the nonlinear behavior of the structural elements of the building, the well-known complete hysteretic "TAKEDA" model has been used, [6]. The hysteretic "TAKEDA" model is defined by three pairs of data that determine the characteristic points of the skeleton curve: $C(M_c, F_c)$; $Y(M_y, F_y)$ and $U(M_u, F_u)$. The characteristics of the effective distributed nonlinearity of structural elements for each storey have been modeled through predefined real summary M-ϕ diagrams.

4 Seismic responses of the new HC-RMS-GOSEB system

The HC-RMS-GOSEB system represents a very efficient system [12], applicable for construction of vibro-isolated and seismically resistant buildings, enabling a multistage seismic response and a globally optimized seismic energy balance. It is based on combined application of optimal seismic isolators and optimal multistage dampers – energy

dissipators installed at the base of a structure or in an appropriate space between a defined substructure (lower part) and superstructure (upper part), Figure 5. The objective of the inventive HC-RMS-GOSEB system is to: (a) encourage practical application of a much safer system for construction of vibro-isolated and seismically resistant structures; (b) promote industrialized construction based on optimal components and (c) provide flexible architectural shapes of structures at plan and along height by satisfying the highest standards of the specific architectural requirements. This inventive system enables the achievement of low-cost investment in construction and maintenance of structures during their long serviceability life and exposure to the risk of occurrence of strong earthquakes. The formulated adequate nonlinear mathematical model of the HC-RMS-GOSEB system for the selected representative prototype residential building (GF+5) is presented through the formulated nonlinear models of two representative RC frames, namely RX and RY, Figure 6 and Figure 7.

The applied integral nonlinear model of the new system, Figure 6 and Figure 7, for seismic isolation contains necessary components bellow each column, including both primary base isolators and energy absorbers with activation stages 1 and 2.
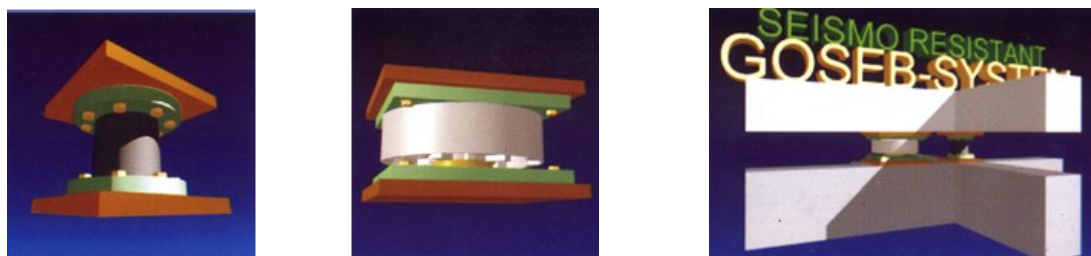
Figure 5. Primary base isolator and energy absorber with view of installation set-up of the two individual components of the invented new isolation (I) HC-RMS-GOSEB system.

The applied new, advanced energy absorbers with two stages of activation, Figure 8a and Figure 8b, have originally been developed and experimentally attested, Figure 9, by the first and the third author. The designations in the figures indicate individual, originally defined, components in the descriptions. The appearance and the mode of installation of the components of the HC-RMS-GOSEB system are presented in Figure 5. The comparison between the

geometrical and stiffness characteristics of both structural systems has shown that the new, inventive system for seismic isolation HC-RMS-GOSEB, has reduced dimensions of most of its structural elements (RC columns and beams). So, in the new structural system, all RC beams with a cross-section of 50/40 cm are proportioned 30/30 cm, while the RC columns at the ground floor proportioned 50/60 cm are proportioned 50/50. In the conventional structural system,
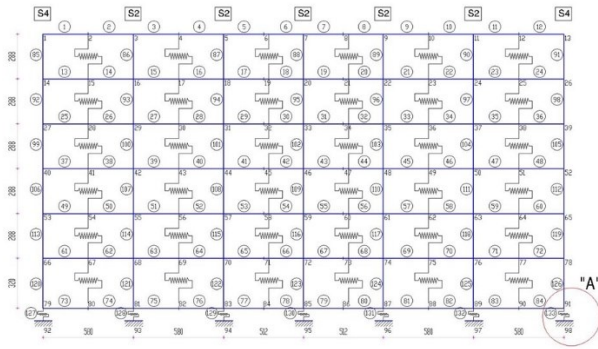
Figure 6. Formulated nonlinear model of the used RX frame of the isolated I-structure (NORA2005)
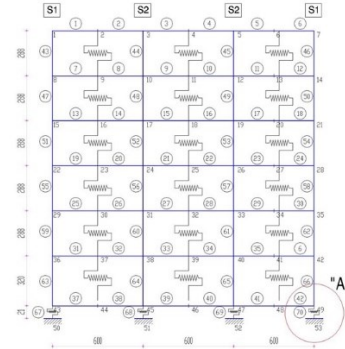
Figure 7. Nonlineardel of the used RY frame of the I-structure (NORA2005)

the RC columns extending from the first to the last storey are with a constant cross-section of 50/50 cm. In the new system, their cross-section has been reduced as follows: 45/45 cm at the first storey, 40/40 cm at the second storey, 35/35 cm at the third storey and 30/30 cm at the remaining storeys. The new specific nonlinear hysteretic models for simulation of nonlinear behavior of individual components are formulated in the computer software NORA2005, [6]. It is essential to note that the procedure of design of new isolators of structures involves definition of their preliminary stiffness characteristics, dynamic analysis of the isolated structure and final definition of stiffness of the bearings. As an input parameter, it is necessary to define the target period

of the structure, namely the period at which the structure exhibits a slight response to a seismic excitation whereat its horizontal displacement at the base should be within the allowable limits. So, for this model, a target period $T_1 = 3,00$ s has been considered. It is known that the intensity of dynamic response of a structure mainly depends on the frequency content of the input excitation and its intensity. To realistically present the dominant frequency content of the expected earthquake ground motions for the considered location of the structure, corresponding knowledge on the regional and particularly local soil conditions is necessary. In some cases, the local soil may cause considerable modification of the input seismic wave.
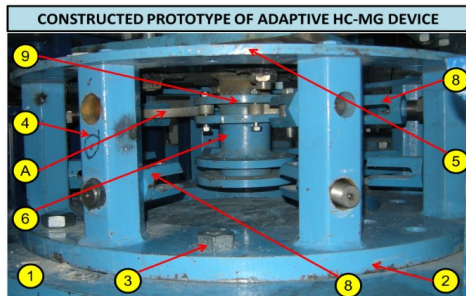
Figure 8a. Original energy absorbers with two stages of activation (Ristic J.; Ristic, D., [17])
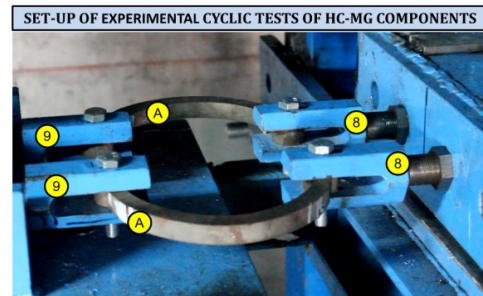
Figure 9. Original attestation of the new energy absorbers (Ristic J.; Ristic, D., [17])
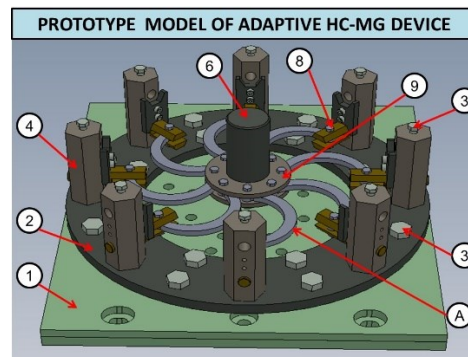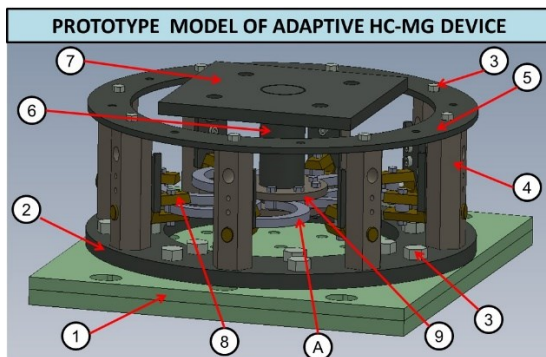
Fig. 8b. Designed experimental prototype model of adaptive HC-MG-device with eight HC-ED components of HC-1.2 type installed at level L1 with gap G1: 1. Bottom fixation plate, 2. Base ring plate, 3. Connecting bolts, 4. Side vertical supports, 5. Upper ring plate, 6. Central support, 7. Upper fixation plate, 8. Gap hinge device, 9. Central hinge device, A. HC-ED components at L1.

For the presented investigations, some possible options of selecting input excitation have been evaluated. However, a set of three recorded real earthquakes involving a considerably wide range of frequency content has been selected as the most representative input. These are: (a) El Centro, component S00E, USA, 1940; (b) Ulcinj-Albatros, component N-S, Montenegro, 1979; (c) Parkfield, component N85E, USA, 1966 (marked with 1 in fig 10 and 11). To define, as precisely as possible, the occurrence of plastic hinges in the model depending on the intensity of input dynamic excitation, the selected three earthquakes have been scaled to five intensities as follows: EQI = 0,10g, 0,20g, 0,30g, 0,40g and 0,50g. This means that 3x5=15 nonlinear dynamic analyses for one direction, i.e., 30 nonlinear analyses have been done for the conventional model of the integral structure. Also, 30 nonlinear analyses have been carried out for the "isolated" model of the integral structure. More precisely, for the purpose of getting a detailed insight into the characteristics of the dynamic response of both structural systems, a total of 60 nonlinear dynamic analyses have been carried out, processed and analyzed, within the presented ample innovative investigations. The dynamic responses of the model have been defined for the first 20s at a calculation step of DT=0,0005s. This means that it has been necessary to perform 40 000 numerical integration steps to realize a single nonlinear analysis. In the considered case, the analyses of the nonlinear seismic response of the structure have been carried out by successful implementation of the special purpose computer programme NORA2005, developed by the third author [6]. The first three vibration modes of both structural systems for longitudinal x-direction of vibration of the structure are shown in Table 1. From each nonlinear dynamic analysis, the time responses of physical parameters

have been obtained as follows: (1) absolute displacement of nodes; (2) node velocities; (3) node accelerations; (4) global reactions; (5) relative displacements of nonlinear structural and nonstructural elements; (6) hysteretic responses of nonlinear structural and nonstructural elements; (6) hysteretic responses of isolation and energy dissipation elements, and secondary responses. A consecutive procedure involving three steps has been applied. First, analysis of the residential structure (GF+5) in the form of a conventional system with the above stated parameters has been carried out.

Then analysis of the same structure (GF+5) constructed as a HC-RMS-GOSEB structural system has been carried out. Finally, a very detailed comparative analysis of the construction costs and the seismic safety (behavior) of the conventional and the new HC-RSM-GOSEB system has been carried out.

5 Results: Conventional and HC-RMS-GOSEB system

The extensive innovative and ample original analytical and experimental investigations discussed and used in this paper were performed during the past longer period [4-19], for the purpose of defining the real potential for practical application of the new HC-RMS-GOSEB system for efficient seismic protection of reinforced concrete and other structures in high rise construction.

Based on the results from the previously conducted studies [12], [17], it has been confirmed that this system enables efficient control of dynamic behavior and successful protection of structures against the strongest seismic effects. Fig. 10 shows the computed maximum absolute displacements of the conventional and seismically isolated structure

Table 1. The first periods of vibration of the conventional and base isolated HC-RMS-GOSEB system

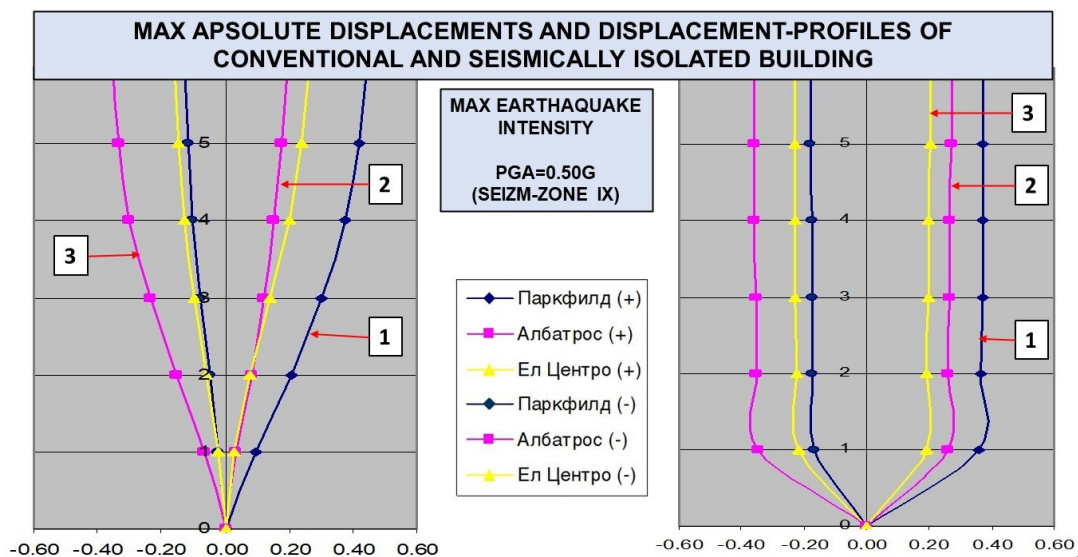| Mode	Conventional system		Base isolated system	
	T (sec)	Direction	T (sec)	Direction
1	0.960	Transverse	2.962	Transverse
2	0.896	Longitudinal	2.934	Longitudinal
3	0.852	Torsion	0.452	Torsion

Figure 10. Maximum absolute displacements (m) of the conventional and seismically isolated structure under the effect of three strong earthquakes with maximum intensity PGA=0.5g (zone IX)
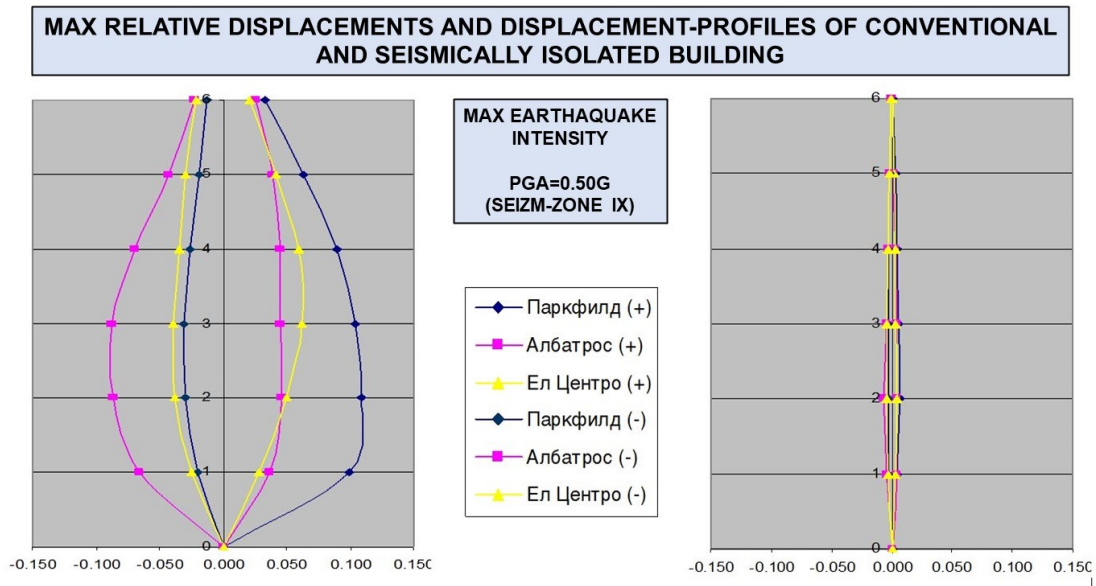
Figure 11. Maximum relative displacements (m) of the conventional and seismically isolated structure due to the effect of three strong earthquakes with maximum intensity PGA=0.5g (zone IX)

due to the effect of three earthquakes with maximum intensity of PGA=0.5g (zone IX). It can be seen that the conventional system suffers large inter-storey displacements causing extensive damage or total failure of the structure. The use of the new HC-RMS-GOSEB system enables compensation of large displacements by isolators and energy dissipaters located at the base of the structure where all storeys remain completely protected, without any possibility for even fine cracks or damage. The same is also confirmed in Figure 11 that shows the maximum relative displacements of the conventional and seismically isolated structure due to the effect of three earthquakes with maximum intensity PGA=0.5g (zone IX). In both figures, Fig. 10 and Fig. 11, characteristic responses to three different earthquakes are respectively marked, namely, 3 for the considered El Centro earthquake, 2 for the considered Ulcinj-Albatros earthquake and 1 for the considered Parkfield earthquake.

The presented characteristics of the seismic response of the seismically isolated structure have been intensively studied and experimentally confirmed, [11] and [12] with the

realized extensive program of dynamic testing of the originally constructed model of the new HC-RMS-GOSEB system [17] in the DYN-LAB laboratory of the Institute of Earthquake Engineering and Engineering Seismology (IZIIS), Skopje, Figure 13. A great number of experimental tests have been realized very successfully by means of the achieved very precise simulation of the selected strong real recorded earthquakes on a large seismic shaking table.

In the framework of the study, a particularly important analyzed parameter has been the cost of construction. Therefore, for the analyzed prototype structure, detailed analysis of actual costs of construction has been performed, following the "element by element" procedure. The final results from the completed comparative analysis of the construction cost of the conventional and seismically isolated RC system are shown in Table 2, and graphically in Figure 12. Detailed descriptions of possible advantages of application of the new HC-RMS-GOSEB system are presented in published lengthy scientific reports, [17]. The authors have particularly been focused on providing a new,.

Table 2. Comparative safety and costs of construction of the RC structural systems of the designed conventional building and the alternatively designed seismically isolated building

COMPARISON OF SAFETY AND COSTS FOR THE BUILDING DESIGNED WITH THE CONVENTIONAL SYSTEM AND WITH THE NEW, SEISMICALLY ISOLATED HC-RMS-GOSEB SYSTEM IN SEISMIC ZONE IX					
Type of construction system of the structure	Concrete (EUR)	Reinforcement (EUR)	Isolators & dissipators (EUR)	Total in (EUR)	Total in (%)
S1 Conventional system	305 887,29	171 198,00	0.00	477 085,29	**100.0**
S2 RMS-GOSEB system	163 858,31	85 466,00	28 000,00	277 324,31	**58.12**
Saving due to reduced material	142 028,98	85 732,00	-28 000,00	199 760.98	**41.88**

Seismic safety: (1) With the conventional system-1, ~90%; (2) With the new isolated system-2~100%
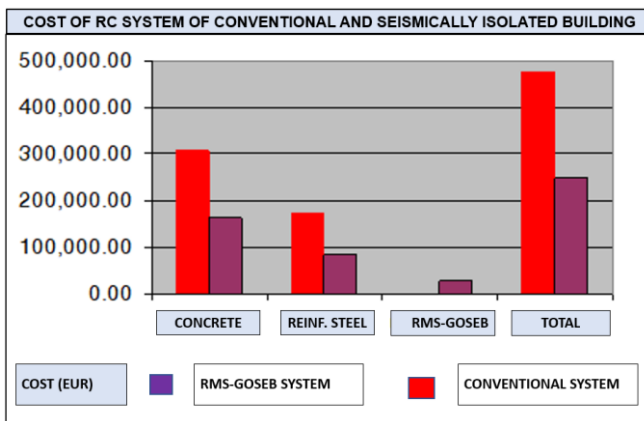

Figure 12. Comparative costs of construction of the alternatively designed RC system of the conventional and seismically isolated building

Figure 13. Testing of the HC-RMS-GOSEB system: (Model in DYN-LAB) IZIIS-Skopje)

general, human, safe and economical construction technology for the users. Special efforts have been made toward obtaining flexible, durable and advanced structures with defined optionally clear composition and flexible design concept. This can be achieved by application of the HC-RMS-GOSEB system, as confirmed by the extensive research experience of the authors and the latest results from the realized investigations. A particular contribution to the recent developments has been made by the first author, who was fully and timely dedicated to innovative work in the field of seismic isolation of bridge structures during the elaboration of her doctoral thesis [12] and continued her research within an international project in the field of development of advanced technologies for seismic isolation of buildings, [17]. The accumulated extensive research results are fully supporting our view that "by building of an isolated structure, we are actually building a seismo-safe structure that possesses high resistance and does not suffer damage under the strongest earthquakes". Today, in most of the developed countries, the method of construction of a conventional structure is most frequently replaced by a new concept of construction of a seismically isolated structure, particularly for structures of some special social importance that have to remain functional even after the strongest earthquakes

Here also belong structures with installed equipment, which is sometimes several times costlier than the construction of the structure itself. Hence, it turns out that investors are somehow forced to increase the level of seismic resistance and safety of structures to protect their investments. The achieved high seismic performances of the new HC-RMS-GOSEB system open the possibilities for consideration of potentials for its future practical application.

6   HC-RMS-GOSEB System: Powerful technological upgrade

The basic performance characteristics and advances of the new HC-RMS-GOSEB system developed on the basis of the conducted long-term innovative investigations can be briefly summarized in the following: (1) General process and knowledge gained from the innovative research; (2) Systematization of the design process for the elements of the

system; (3) Achieved high reliability regarding quality; (4) Possibilities for creation of industrialized processes.

1. General process and knowledge gained from the innovative investigations: (1) By incorporation of the HC-RMS-GOSEB isolation system, possible occurrence of resonance effects due to the short fundamental period of vibration of the structure exposed to the actual frequency content of the seismic excitation is avoided; (2) Through specific dynamic interaction, the HC-RMS-GOSEB system has a direct contribution to reduction of the vibration transfer between the super- and the sub-structure as a result of the discontinuity of stiffness achieved by incorporation of isolation elements; (3) Despite the reduced proportions and reinforcement of columns and beams, the new HC-RMS-GOSEB system is safe even under the highest intensity (0.50g) of any of the three representative earthquakes. Unlike this system, in the case of the conventional system, the first "plastic" hinges and exhaustion of bearing capacity of some structural elements occur as early as under intensity of 0,20g, while total collapse of the structure may take place under peak acceleration of around 0,40g; (4) The new HC-RMS-GOSEB structural system possesses reduced dimensions of its RC columns and beams in respect to the conventional system; (5) Analyzing the behavior of structures with incorporated isolation HC-RMS-GOSEB system exposed to the effect of even the strongest earthquakes, it has been confirmed that the bearing capacity of the reinforced concrete columns and beams is not exhausted. This statement is supported by the fact that the obtained maximum moments in the columns and the beams are within the limits of the bearing capacity of the cross-section, i.e., the columns and the beams as the main bearing elements of the structure remain in the linear range of behaviour; (6) All necessary design parameters are satisfied. The relative storey displacements are within the allowable limits. The maximum relative storey displacement remains small, the largest being recorded at the second storey, amounting to $d_{max}=0.0089m$, in the case of the representative frame Rx exposed to excitation due to the Parkfield earthquake with intensity 0.50g. The maximum allowable storey relative displacement is Hstorey/150 = 0.0192m, meaning that the expected maximum storey relative displacement will be almost twice less than the allowed value; (7) The maximum absolute displacement of the highest point of the nonlinear

system amounts to D$_{max}$=0.357m, for the recorded corresponding shear force of 40.71kN, under the Parkfield earthquake with intensity 0.50g. Considering that the maximum allowed displacement of the isolators defined by the producer is 0.3800m, it turns out that safety of the complete isolation system is provided.

2. Systematization of the design process for the system elements: The design process for the new HC-RMS-GOSEB system for control of vibrations and seismic risk reduction is reduced to the following: (1) The selection of dimensions, stiffness and deformability characteristics of the isolation and vibration control elements directly depends on the dynamic and structural characteristics of each individual RC structure; (2) To provide efficient control of the dynamic behavior of RC structures under strong earthquake effects, the applied elements for isolation and seismic energy absorption must be designed with optimally harmonized stiffness and deformability characteristics; (3) The design of the elements of the HC-RMS-GOSEB system can successfully be carried out and verified based on direct dynamic analyses by use of adequate computer programmes developed for that purpose as is, for example, the developed "NORA2005" computer programme, [6] that has been applied for performance of the analytical investigations discussed in this paper; (4) Using commercially available typified elements for isolation and control of vibrations, their practical design for a specific structure can be reduced only to selection of the necessary number of seismic isolators that have the most favourable characteristics for each specific case; (5) From the aspect of practical application, the design and incorporation of the HC-RMS-GOSEB system elements is simple and particularly economically justified since presently, in the era of developed technology, this does not incur extensive costs; (6) The rubber seismic isolation elements of the HC-RMS-GOSEB system do not exhibit important modification of their main nonlinear behavior characteristics even under great series of repeated dynamic impacts. Therefore, the main criterion for their possible replacement can be the time period of serviceability-life prescribed in the attests; (7) The results from the performed investigations and the derived conclusions provide the possibility for successful practical application of the HC-RMS-GOSEB system in design of reinforced concrete structures.

3. Achieved high reliability regarding quality: For the new HC-RMS-GOSEB system, high reliability and quality of achieved effect have been confirmed as follows: (1) An adequate seismic protection of structures is provided; (2) Low-cost construction and maintenance of structures during their long serviceability life and exposure to the risk of occurrence of strong earthquakes is achieved.

4. Possibility for creation of industrialized processes: The system enables successful control of dynamic behavior and seismic protection of RC structures in high rise construction even under the strongest earthquakes, enabling: (1) introducing of a much safer system of construction of seismically resistant structures into practice; (2) promotion of industrialized construction based on optimized components and (3) providing flexible architectural shapes of structures in plan and along height satisfying, at the same time, the highest standards related to the specific architetural requirements.

7 Conclusions

The original innovative long-term investigations that have been performed so far by the authors can be generally recognized as the *first-key-stage* of a well targeted and successful innovative work resulting in created new advanced technology characterized by the achieved extraordinary seismic safety, rapid practical applicability and cost-effective construction in seismically active regions. In the next phase, there will be a priority need for creation of conditions for providing complete information to design engineers and investors about the advantages of application of the new innovative HC-RMS-GOSEB system for seismic isolation of RC structures. The need and the justification of application of seismically isolated structures in our region are evident since earthquakes occur randomly without warning, while the new system provides total seismic protection of structures in such cases. In addition, the experience that has been gathered so far in the domain of seismic isolation in highly developed countries is quite great and very positive. The most important benefit from the innovation developments that have taken place so far is the successfully opened scientific-research area that offers innovative and advanced quality solutions for direct practical application in design of seismically safe structures. At the same time, by incorporating the HC-RMS-GOSEB system, a considerable reduction of the seismic risk pertaining to existing and new engineering structures is achieved. In addition, the functionality of the structures, particularly those of vital importance, is increased. The development and innovation research that has been done so far marks the real beginning of a new and long-lasting strategy that practically represents a new potential for high reduction of the seismic risk in the region of Southeast Europe.

References

[1] Behrami R., Ristic J., Ristic D., Hristovski V., (2019) The New Uniform VF-EnergyDissipation Device: Refined Modelling, 16 World Conference on SeismicIsolation, Energy Dissipation and Active Vibration Control of Structures, 01.07-06.07.2019, St. Petersburg, Russia.

[2] Candeias, P., Costa, A. C., Coelho, E. (2004): Shaking Table Tests of 1:3 Reduced Scale Models of Four-Story Unreinforced Masonry Buildings, 13th World Conference on Earthquake Engineering, Vancouver, Paper: 2199.

[3] Chopra, A., (2016): "Dynamics of Structures", Pearson, 2016.

[4] Misini, M., Ristic, J., Ristic, D., Guri, Z., Pllana, N., (2019) Seismic Upgrading of Isolated Bridges with SF-ED Devices: Analytical Study Validated by Shaking Table Testing, GRAĐEVINAR, 71 (2019) 4, pp. 255-272;https://doi.org/10.14256/JCE.2274.2017.

[5] Misini M., Ristic J., Guri Z., Ristic D., Pllana N., (2021) Upgrading Seismically Isolated Bridges with Space-Flange Energy-Dissipation Devices, Structures and Buildings, ICE Publishing, January 04, 2021, https://doi.org/10.1680/jstbu.18.00231.

[6] Ristic, D. (1988): Nonlinear Behavior and Stress-Strain Based Modeling of Reinforced Concrete Structures Under Earthquake Induced Bending and Varying Axial Loads, Doctoral Dissertation, School of Civil Engineering, Kyoto University, Japan.

[7] Ristic, D., Kocevski, V., (2006) Evaluation of Economic Feasibility for Application of New Seismic Isolation System for RC Structures, Innovative Emerging Technologies, Institute of Earthquake Engineering and Engineering Seismology (IZIIS), "SS Cyril and Methodius" University, Skopje.

[8] Ristic, D., Iemura, H., Ristic, J., (2008) Innovative Seismic Isolation Systems for Buildings Capable of Full Seismic Energy Control, Special Section "Innovative Emerging Technologies", 14th World Conference on Earthquake Engineering, Beijing, China, 12-17.10.2008.

[9] Ristic, D., Ristic J. (2012): Advanced Integrated 2G3 Response Modification Method for Seismic Upgrading of Advanced and Existing Bridges, 15th World Conf. on Earthquake Engineering, (WCEE), Lisbon.

[10] Ristic D., Uwe D., Ristic J., (2012) Advanced ML-MD GOSEB Seismic Isolation System for Efficient Seismic Protection of Bridges in South East Europe, 9th German-Japanese Bridge Symposium, Kyoto, Japan, 10-11.09.2012.

[11] Ristic, D. et. all. (2014): Innovative Project, SfP 983828: Seismic Upgrading of Bridges in South-East Europe by Innovative Technologies (ISU Bridge), International project (5 countries) financed by NATO Programe Science for Peace and Security, Brussels, Belgium.

[12] Ristic, J. (2016) Modern Technology for Seismic Protection of Bridge Structures Applying Advanced System for Modification of Earthquake Response, PhD Thesis, Institute of Earthquake Engineering and Engineering Seismology (IZIIS), "SS Cyril and Methodius" University, Skopje, Macedonia. (*Innovative Project Supported by NATO (Brussels), Science For Peace and Security Program* 2010-2014).

[13] Ristic, J., Misini, M., Ristic, D., Guri, Z., Pllana, N. (2017): Seismic Upgrading of Isolated Bridges with SF-ED Devices: Shaking Table Tests of Large-Scale Model, *Gradjevinar*, 2147-2017. https://doi.org/10.14256/JCE.2147.2017.

[14] Ristic J., Hristovski V., Ristic D., (2017) "Advanced Seismic Upgrading of Existing Bridges With New Adaptive IMSO-System for Seismic Response Modification", 16th World Conference on Earthquake Engineering, 09.01-13.01.2017, Santiago, Chile.

[15] Ristic J., Hristovski V., Ristic D., (2018) Shaking Table Test of Large-Scale Bridge Model Constructed with New Adaptive IMSO-System for Seismic Protection, 16th European Conference on Earthquake Engineering, 18-21.06.2018, Thessaloniki, Greece.

[16] Ristic J., Ristic D., Behrami R., (2019) The New Uniform VF-Energy Dissipation Device: Prototype Testing", 16 World Conference on Seismic Isolation, Energy Dissipation and Active Vibration Control of Structures, 01.07-06.07.2019, St.Petersburg, Russia.

[17] Ristic, J. (2020) (*Author and Project Leader* 2019-2020): System for Protection of Buildings Against Strong Earthquakes with Uniform HS-MG Energy Control, International Innovative Project Supported by European Union, World Bank and FITR, National Fund for Innovations and Technology Development, Republic of North Macedonia.

[18] Ristic J., Brujic Z., Ristic D., Folic R., Boskovic M., (2020) Upgrading of Isolated Bridges with Energy-Dissipation Devices: Shaking Table Test, Advances in Structural Engineering, Dec. 17, 2020, ASE-20-0787, https://doi.org/10.1177/13694332211013918.

[19] Ristic J., (2021) Heating and Cooling in Passive Building Design, International Conference of Applied Sciences, Engineering and Mathematics (ICASEM 2021), 03-05.06.2021, IBU, Skopje, Macedonia.

[20] Wilson, E.L., (2002): "Static and Dynamic Analysis of Structures: A Physical Approach with Emphasis on Earthquake Engineering", Computers and Structures Inc.

Građevinski materijali i konstrukcije
Building Materials and Structures

journal homepage: www.dimk.rs

Allocation and selection of equipment for concrete works using fuzzy linear[*] programming

Abel Duran[*1)], Nataša Praščević[1)]

[1)] Faculty of Civil Engineering Univeristy of Belgrade, King Alexander Boulevard 73, 11000 Belgrade, Serbia

A B S T R A C T

The aim of this research is focused on the problem of allocation and selection of the construction equipment when construction firms bid for construction projects. The main objective of the selection of construction equipment is to ensure the timely completion of all considered projects, while at the same time the planned budget is fulfilled. In this paper fuzzy linear programming is applied with the fuzzy objective function and fuzzy constrains. The proposed mathematical model is applied for optimal selection and allocation of equipment for five projects with different quantities of concrete works and general budget.

1 Introduction

The optimal selection of construction equipment or complex construction mechanization for the execution of specific construction works is today simply unthinkable without the application of modern methods of analysis during the selection process. The application of fuzzy linear programming as a modern methodology of analysis allows us to, from several alternative solutions, choose the best ones that give optimal results for the appropriate constraints [1].

The problem that big construction companies increasingly encounter in practice is the selection and allocation of construction equipment in the event of the need to implement multiple construction projects simultaneously. Bearing in mind that the works are often performed on foreign markets, often on other continents, the company, when entering a specific market, needs to purchase appropriate construction equipment for specific works. The key reason for analysis of the optimal selection of equipment for concrete works comes from the large number of concrete structures built in the world every year (today, the production of concrete is about 9.4 billion tons per year [2]). The costs of concrete works during the construction of the facility can amount to up to 30% of the total construction costs. Also, during the realization of construction projects in parts of the world with extremely low or extremely high temperatures, these costs are often up to 20% higher than the costs for the same concrete works in Europe [3].

Considering all the data above explaining the concrete usage during the realization of construction projects, as well as share of concrete works in total costs, a quality solution for the procurement of equipment for concrete works is one of the basic prerequisites for submission of quality bid,

winning the project during tender process and make a profit on the project.

In this paper, the process of selection and allocation of construction equipment will be presented on a realistic example from practice which implies a wider choice of equipment (selection of type and category of equipment according to the constructive ability of the machine to perform certain works [4]), determining the optimal number of machines for realization of several construction projects, where the company has a roughly defined budget for the realization of this task.

A systematic solution to this problem is achieved by answering 5 key questions:

− What activities need to be performed on the realization of concrete works,
− What is the scope of work,
− How long it takes to do the work,
− What types and category of machines can perform defined activities (wider choice),
− What is the necessary capacity of the machines that need to be engaged.

As each construction project is emphatically unique [3], the intention of the author is to provide a universal and efficient solution to the problem of allocation of construction equipment for concrete works on several different projects simultaneously using the method of fuzzy linear programming.

2 Problem definiton, analysis of project characteristics and defining the criteria function with constraints

As mentioned earlier, construction companies often face the problem of allocating their resources when biding for

---

multiple construction projects at the same time. For the purposes of this research, we will analyze the case of a representative contracting company that explores the financial aspects and justification of entering the foreign market will be analyzed.

2.1 Problem definition

The contractor has decided to bid for five large projects abroad. As the company has not execute construction works in the country where the projects are being built earlier, it is necessary to envisage the procurement of the necessary construction equipment. As the central concrete plant is rented and not owned by the company, the costs of procurement and operation of this plant will not figure in the analysis of work activities and defining the criteria function with constraints. In addition to the preparation of the concrete mixture in the concrete plant, it is necessary to perform external and internal transport of the concrete mixture and pouring of concrete [5]. The concrete plant is on average 10 km away from the construction site. At the stated distance, the only machine that can perform external transport (from the concrete factory to the construction site [4]) of the concrete mixture in a quality way is the concrete mixer truck [4]. As the quantities of concrete to be poured on each of the construction sites are quite large, it will be necessary to use a mobile concrete pump for the internal transport of the concrete mixture (from the concrete mixer truck to the place where concrete needs to be poured [4]). The consolidation of fresh concrete mixture is performed by concrete vibrators that induce vibrations from 100 to 250 Hz which expels entrapped air from freshly placed concrete and packs the aggregate particles together so as to increase the density of concrete [6].

Furthermore, an approximate budget of between 700 and 800 thousand euros is available to the company for the procurement of construction equipment and for performing concrete works.

2.2 Analysis of project characteristics

Regardless of the place, type and nature of the construction works, each construction project is defined by three important elements: scope of work (subject of the contract), deadline (time for which it is necessary to complete a certain work) and price [3] .

As this specific example considers the selection and allocation of construction equipment for concrete works, the following is a tabular presentation of the project, with the quantities of concrete works to be poured, as well as the deadline within which the aforementioned works should be performed.

In addition to the type of project, the scope of works and planned time for which the works should be performed, the required hourly production $U_{p,req}$ will be calculated and shown in the table for each of the projects. The required hourly production is the minimum performance that each construction machine in combination should achieve in order to complete planned scope of work within a defined period of time and is calculated as:

$$U_{p,req} = Q/t \ [m^3/h] \tag{1}$$

where is:
$Q \ [m^3]$ – quantity of work that needs to be done;
$t \ [h]$ – time for which the works need to be performed.

2.3 Defining criteria function

As the contractor for the procurement of construction equipment for concrete works has an approximate budget of between 700 and 800 thousand euros, it means that the criteria function is an approximate value, i.e., it can be considered as a "fuzzy number" [1].

Having in mind the above, the criteria function will be presented as the amount of available financial resources that will be used for the procurement of construction equipment for concrete works. The criteria function (F) will be presented as the sum of the price of the machine and the number of different types of machines necessary to perform the work and meet the required hourly production on each of the projects:

$$T = P_1N_1 + P_2N_2 + P_3N_3 \tag{2}$$

where is:
T – criteria function,
P_i – the market price of the specific construction machine,
N_i – number of specific construction machines that need to be procured.

Table 1. Information on projects and required hourly production

Project ID	PRO1	PRO2	PRO3	PRO4	PRO5
Project type	*hotel*	*building*	*bridge*	*hotel*	*building*
Quantity of works Q [m³]	*10,500*	*8,400*	*13,500*	*11,200*	*9,000*
Duration of works in days d [day]	*40*	*35*	*30*	*35*	*25*
Shift duration s [h]	*10*	*8*	*8*	*12*	*8*
Number of shifts n [-]	*1*	*1*	*2*	*1*	*2*
Duration of works in hours t=d*s*n [h]	*400*	*280*	*480*	*420*	*400*
Required hourly production $U_{p,req}$ [m³/h]	**26.25**	**30.00**	**28.13**	**26.67**	**22.50**

2.4 Characteristics of available construction machines on the market

Having in mind the ratio of machine dimensions and construction site dimensions, necessary space for maneuver, as well as available manufacturers on the market, the company made a strategic decision to procure machines of the same type and the same manufacturer for each category of machine according to the table below:

3 Definition of the mathematical model

As the financial resources available to the contractor for the procurement of construction equipment are given as an approximate amount between 700 and 800 thousand euros, we can present it in the form of a fuzzy triangular number $T = (t_l, t_m, t_r)$. As the coefficients that have been estimated appear in the formulas for the calculation of machines hourly production, therefore the hourly production can be presented

Table 2. Information on specific machines and their hourly production

ID	Machine type	Manufacturer and label	Market value [€]	Hourly production [m³/h]
CP	concrete pump	Putzmeister BSF 36.16H	180,000	68.00
CM	concrete mixer truck	Mercedes Actross 4841	123,000	7.41
CV	concrete vibrator	Vibrofix IHE 66	1,500	13.28

2.5 Constraints definition

It is necessary to define the appropriate constraint definition for each project respectively. The specific constraint is set on the basis of the rule that the hourly production for each machine type (number of machines multiplied by the corresponding hourly production of the machine) is greater than or equal to the required hourly production for each project [4].

$$PRO1: U_p^{CP}N_1 \geq U_{p,req}^{PRO1} ; U_p^{CM}N_2 \geq U_{p,req}^{PRO1} ; U_p^{CV}N_3 \geq U_{p,req}^{PRO1} \tag{3}$$

$$PRO2: U_p^{CP}N_1 \geq U_{p,req}^{PRO2} ; U_p^{CM}N_2 \geq U_{p,req}^{PRO2} ; U_p^{CV}N_3 \geq U_{p,req}^{PRO2} \tag{4}$$

$$PRO3: U_p^{CP}N_1 \geq U_{p,req}^{PRO3} ; U_p^{CM}N_2 \geq U_{p,req}^{PRO3} ; U_p^{CV}N_3 \geq U_{p,req}^{PRO3} \tag{5}$$

$$PRO4: U_p^{CP}N_1 \geq U_{p,req}^{PRO4} ; U_p^{CM}N_2 \geq U_{p,req}^{PRO4} ; U_p^{CV}N_3 \geq U_{p,req}^{PRO4} \tag{6}$$

$$PRO5: U_p^{CP}N_1 \geq U_{p,req}^{PRO5} ; U_p^{CM}N_2 \geq U_{p,req}^{PRO5} ; U_p^{CV}N_3 \geq U_{p,req}^{PRO5} \tag{7}$$

where is:
PRO_i – project ID,
U_P^{XX} – specific machine hourly production,
$U_{p,pot}^{PROi}$ – required hourly production for specific project,
N_i – number of specific construction machines that need to be procured.

also in the form of a fuzzy triangular numbers $U_p^{XX} = (u_l^{XX}, u_m^{XX}, u_r^{XX})$ [1].

The financial resources and hourly production of the machines presented in the form of a fuzzy triangular number are shown in Table 3:

As the financial resources and practical effects for the concrete pump, concrete mixer truck and concrete vibrator are presented in the form of fuzzy triangular numbers, after re-arranging of mathematical equations following mathematical model is defined [1]:

$$max\ F = h \tag{8}$$

$$P_1N_1 + P_2N_2 + P_3N_3 \geq t_l + h(t_l - t_r) \tag{9}$$

$$P_1N_1 + P_2N_2 + P_3N_3 \leq t_r + h(t_r - t_l) \tag{10}$$

$$U_p^{CP}N_1 \geq max_{CP}(U_{p,req}^{PROi}) \tag{11}$$

$$U_p^{CM}N_2 \geq max_{CM}(U_{p,req}^{PROi}) \tag{12}$$

$$U_p^{CV}N_3 \geq max_{CV}(U_{p,req}^{PROi}) \tag{13}$$

The equations shown from (9) to (13) can be represented in a generally derived fuzzified form as follows:

$$u_m^{XX}N_i + (1 - k_i)(u_r^{XX}N_i - u_l^{XX}N_i) \geq max_{XX}(U_{p,req}^{PROi}) \tag{14}$$

Table 3. The total budget and hourly production in the form of a fuzzy triangular number

fuzzy label	Total Budget T [€]	U_p^{CP} [m³/h]	U_p^{CM} [m³/h]	U_p^{CV} [m³/h]
LEFT [80%] $(t_l;u_l)$	700,000	54.50	5.93	10.62
MIDDLE [100%] $(t_m;u_m)$	-	68.00	7.41	13.28
RIGHT [110%] $(t_r;u_r)$	800,000	74.80	8.15	14.61
fulfilment level $[k_i]$	-	0.8	0.8	0.8

4 Results and discussion

The initial step for solving the aforementioned equations is that the degree of satisfaction k_i (which is directly related to the hourly production of construction equipment for concrete works) is previously set, and that the degree of satisfaction of the requirements h is maximized.

When the corresponding numerical data previously obtained in points 2.2., 2.4 and Table 3 of this paper are inserted into equations (8) to (13), i.e. equations (8) to (10) and equation in the generally derived fuzzified form (14), we obtain the following system of equations:

$$max\ F = h \tag{15}$$

$$180,000N_1 + 123,000N_2 + 1,500N_3 - 100,000h \geq$$
$$\geq 700,000 \tag{16}$$

$$180,000N_1 + 123,000N_2 + 1,500N_3 - 100,000h \leq$$
$$\leq 800,000 \tag{17}$$

$$N_1 \geq 0,32 \tag{18}$$

$$N_2 \geq 3,82 \tag{19}$$

$$N_3 \geq 2,13 \tag{20}$$

It is recommended to solve this problem with the help of modern software solutions, and in this paper the problem is defined in the software package "Matlab" by defining the parameters of the ***itlinprog*** function [7]. The following solutions were obtained:

$$N_1 = 1 \tag{21}$$

$$N_2 = 5 \tag{22}$$

$$N_3 = 3 \tag{23}$$

$$max\ F = h = 0.99 \tag{24}$$

$$T = 799,500\ € \tag{25}$$

where is:
N_1 – number of concrete pumps
N_2 – number of concrete mixer trucks
N_3 – number of concrete vibrators
T – Financial resources necessary for the procurement of all construction equipment.

It can be noticed that the calculated amount of financial resources meets the pre-set constraints in terms of available financial resources, as well as that the number of necessary machines multiplied by their hourly production meets the required hourly production to meet all 5 considered projects.

The amount of available funds is presented in the form of a range between two acceptable values because in practice it is not considered appropriate to buy either too cheap or too expensive equipment and for such a situation the application of the considered target function as a fuzzy number proved to be justified. In case only the maximum value is set as a constraint condition, it would be necessary to observe the criteria function in a different way, because the fuzzy number method when it is not a range of acceptable values is not adequate

In case the projects did not take place abroad and new equipment did not need to be procured (equipment from the company's existing fleet would be used) the problem that the company should solve is the choice of the optimal combination of machines that can complete all necessary operations and meet the required hourly production for each of the projects. To solve this problem, one of the ways would be to apply the method of linear programming.

5 Conclusion

This paper analyzed a practical example from construction industry that contractors encounter very often when entering a new market and when they are bidding for the several similar construction projects at the same time. The example from this paper, which analyzes the procurement of necessary construction equipment for concrete works on 5 different construction projects, was solved by applying fuzzy linear programming with the fuzzy objective function and fuzzy constrains. As a solution to the problem, it was obtained that, at the degree of satisfaction of the requirements h = 0.99, it is necessary to procure:
- − 1 concrete pump (Putzmeister BSF 36.16H) with a purchase value of € 180,000
- − 5 concrete mixer trucks (Mercedes Actross 4841) with a purchase value of € 123,000
- − 3 concrete vibrators (Vibrofix IHE 66) with a purchase value of € 5,000

Regardless of the applied model and the specific problem that is being solved, when it comes to the analysis of construction equipment, it is necessary to perform a permanent fine-tuning of the mathematical model and input parameters. The authors recommend that the hourly production construction equipment, as well as their purchase values, be observed in real time and that the mathematical model be fine-tuned in a timely manner through input parameters and constraints.

The mathematical model presented in this paper on one practical problem can be considered sufficient and general, because a simple substitution of input parameters and constraints gives a model for any other similar case that the contractor may encounter in practice.

The model presented in this paper has limitations in its application if the projects under consideration are located close to each other, i.e. when it is possible to apply the same machine to several construction sites at the same time.

One of the directions for future researches is to compare the solution obtained by applying fuzzy linear programming with the solution obtained by another optimization method.

Acknowledgment

References

[1] Tiodorović D., Kikuchi S.: Fuzzy sets and application in transport industry, Faculty of Transport and Traffic Engineering University of Belgrade, Belgrade, ISBN 86-80897-42-6, 1994.

[2] Marinković S.: Design of concrete structures with regards to their impact on the environment, Conference proceedings, National Symposium of the Association of Structural Engineers of Serbia, Zlatibor, ISBN 978-86-850073-04-05, 2008.

[3] Ivković B., Popović Ž.: Construction project management, Građevinska knjiga, Belgrade, ISBN 86-395-0447-4, 2005.

[4] Mirković S.: Construction equipment, Građevinska knjiga, Belgrade, ISBN 86-395-0434-2, 2005.

[5] Praščević Ž.: Organization of construction works, Zavod za udžbenike, Belgrade, ISBN 86-17-022-57-4, 1992.

[6] Arizanović D., Petronijević P., Beljaković D.; Technology of construction works, Faculty of Civil Engineering University of Belgrade, Belgrade, ISBN 978-86-7518-157-6, 2015.

[7] Klem N., Kovačević M., Praščević N., Nedeljković Đ.: Basis of programming in MATLAB, Građevinska knjiga, Belgrade, ISBN 978-86-395-0609-4, 2010.

Static and dynamic approach to the analysis of wind gusts in case of a tower H=110 m[*]

Todor Vacev[*1)], Stanko Brčić[2)], Andrija Zorić[1)], Miloš Milić[1)], Ivan Nešović[1)], Slobodan Ranković[1)]

[1)] University of Niš, Faculty of Civil Engineering. and Architecture, Aleksandra Medvedeva 14, 18000 Niš, Serbia
[2)] University of Belgrade, Faculty of Civil Engineering, Bulevar kralja Aleksandra 73, 11000 Belgrade, Serbia

ABSTRACT

Steel lattice towers have large application in meteorology, and are regularly exposed to loads difficult to determine reliably, like wind and ice, and especially wind gusts and accompanied structural vibrations. EN 1993-3-1 treats such structures and requires checking of vibrations, but does not supply methodology for it, neither allowed values for deformation and vibrations. The paper presents analysis of a tower 110 m high using the Finite Element Method (FEM), in case of wind gust, for iced and non-iced structure, both statically and dynamically. The results were compared and recommendations for future treatment of such sensitive structures were given.

The meteorological tower structure

The analysed structure is a triangular lattice tower with total height of 110 m, and base length of 4.40 m (Fig. 1). The location of the tower is Vršac, Serbia, a region with severe winds. The structural and load data are taken from the expertise [2].

1   Wind and ice loads on towers

In this analysis, attention is paid to loads dominant for this type of structure: self-weight and wind action. Wind action is often associated with icing, which increases the self-weight and aerodynamic drag. Besides, the wind action itself is a highly stochastic phenomenon. Usually it consists of some steady air stream, known as "wind mean action" (WM), and intermittent wind gusts (WG), which can cause significant vibrations of the structure. Both components are commonly calculated using static analysis, and superimposed.

The standard [4] requires that towers and masts be examined for gust induced vibrations in the wind direction. However, it does not specify the methodology for such checking.

The idea of this investigation was to compare structural behaviour of a realistic sample structure applying two different approaches:

1. Analysis of the load case self-weight + wind mean action + wind gust (G+WM+WG) using FEM static analysis.

2. Analysis of the load case self-weight + wind mean action (G+WM) using static approach, and then applying the wind gust load (WG) on such deformed structure, using FEM dynamic time-history analysis (Specific details of the methodology used for this approach are given in further text).

Both approaches are conducted for ice-free and for iced tower, in order to investigate the influence of icing on the structure. The ice loading was taken from the expertise [2], with adopted ice density of ρ=900 kg/m³, as the most unfavourable value. Modelling of the iced tower showed significant mass increase. Namely, the structural mass was 18270 kg, mass of the ice 8960 kg, (additional 46%), and total mass 27230 kg. Ice also affects the natural frequency of the structure, altering it from f_1=0.5012 Hz (ice-free) to f_1=0.3869 Hz (iced).

2   FE analysis of the tower

2.1 FE modelling and analysis parameters

The tower structure model is based on the model analysed in [5], and using the standard [1]. The adopted FE mesh was obtained by division of every structural member into eight FE.

The dynamic analyses were conducted for a series of ten load frequency values, ranging from 10 % of the resonant frequency (K = 0.1) up to 100 % of the resonant frequency (K = 1.0), see *Table 2, 3*. The idea was to investigate the influence of different excitation frequencies, including the resonant one, on behaviour of the structure and on its serviceability and strength.

The overall structural damping factor (G) is calculated based on the relationship between the structural damping coefficient (G) and the relative damping (ξ):
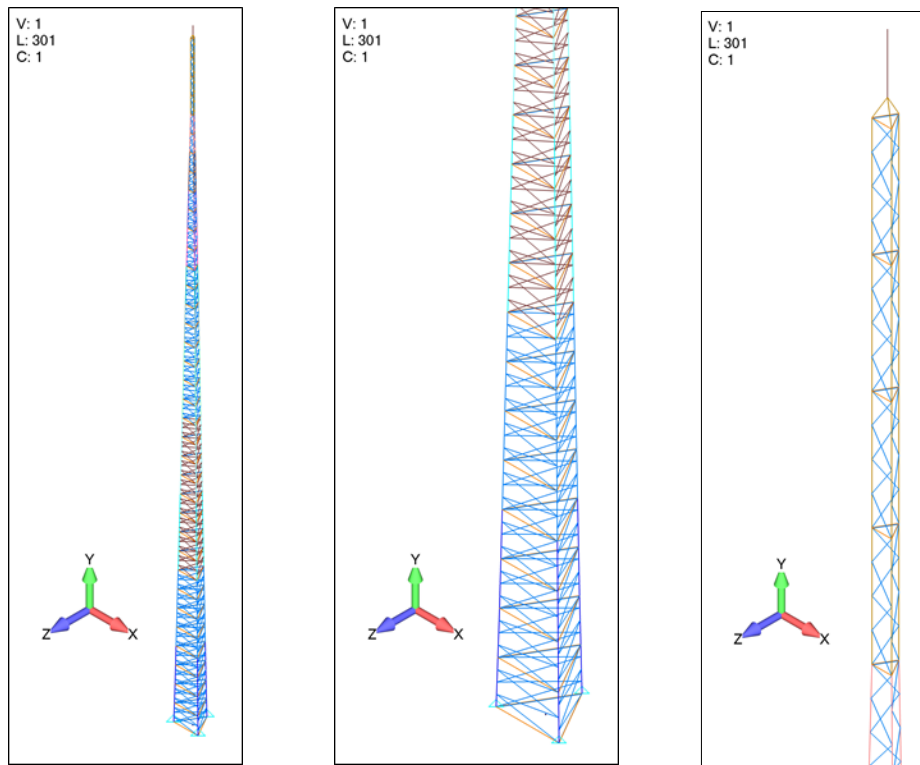
$$\xi = \frac{G}{2} \Rightarrow G = 2\xi \tag{1}$$

Figure 1. Tower geometry; a) global view; b) bottom part - detail; c) top part - detail

Based on the equation (1) and adopted relative damping ξ = 0.05, recommended for steel structures, the overall structural damping factor is calculated as G = 0.10. The system damping frequency (denoted as *W3* in [6]) was adopted based on the frequency of the 1st mode of oscillation, that is, W3 = 0.5013 Hz (ice-free tower), and W3 = 0.3869 Hz (iced tower).

As mentioned, the main idea was to superimpose the dynamic action of the wind gust on the tower structure that is already statically deformed by the basic load case (G+WM). For that purpose, a set of two load functions were created. The first function, simulating static G+WM action was defined as time-dependent, using bilinear function. According to this, the load rises linearly from zero to full value in a relatively short period, t=5 s, and from then on holds this steady value.

The time interval between t_1=5 s and t_2=20 s is intended for damping of the oscillations which unavoidably arise by applying this part of the load. Consequently, the G+WM load function is formally a dynamic one, although its action on the structure has static character. For the purpose of clarity, we denoted it as quasi-static (Table 3, 4). The second function that simulates the gust wind action is a sine function, and has a zero value from t_0=0 s to t_2=20 s. At t_2=20 s starts the sine function and lasts for one oscillation period (T_c). Lasting time of this period varies depending on the excitation frequency of the wind gust, which was varied as described above. After one sine period, the wind gust function takes zero value in order to enable damping of the structure, and it ends at t_3=60 s. The complete loading process is presented on diagrams in Figures 2 and 3.
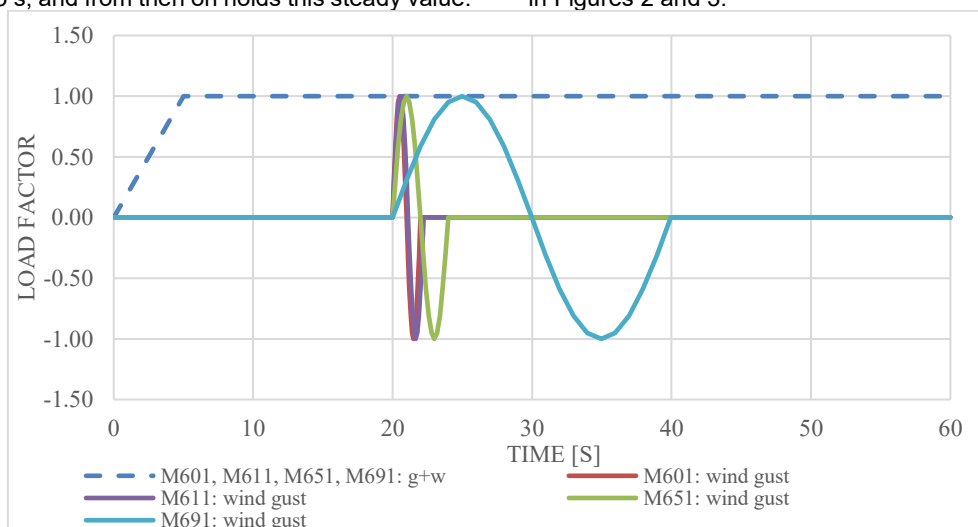

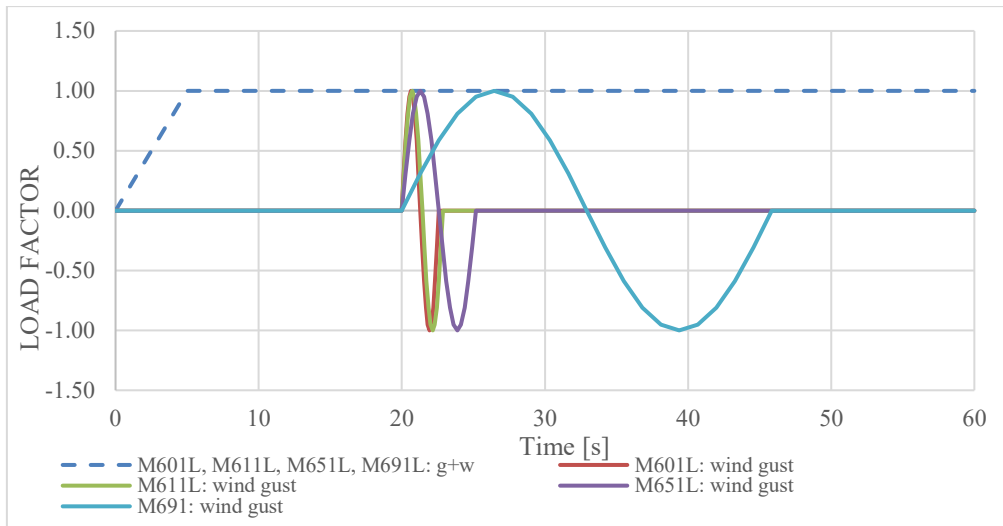*Figure 2. Ice-free tower: load factor vs. time*

Figure 3. Iced tower: load factor vs. time

2.2 FEM analysis results and discussion

The structural displacements of the top of the tower in the wind direction (Z) were selected as main serviceability value, and the max. and min. stresses were taken as strength check data.

Characteristic input and output analysis data are presented in the Tables 1 and 2 and on diagrams in Fig. 4 and 5.

Table 1. Ice-free tower – static and dynamic analysis; f_1=0.5013 Hz; G=0.1; W_3=0.5013 Hz

Model	Load freq. factor K [-]	Total load duration ts [s]	No. of steps n [-]	Zmax [m]	Smax [MPa]	Smin [MPa]
M601	1.00	60	600	6.203	211	-412
M611	0.90	60	600	**6.345**	**219**	**-426**
M621	0.80	60	600	6.293	217	-423
M631	0.70	60	600	5.735	197	-383
M641	0.60	60	600	4.970	162	-316
M651	0.50	60	600	4.907	157	-307
M661	0.40	60	600	4.740	150	-292
M671	0.30	60	600	4.432	138	-270
M681	0.20	60	600	3.918	121	-238
M691	0.10	60	600	3.887	120	-235
M600	G+WM	STATIC	1	**2.176**	**79**	**-157**
M600	G+WM+WG	STATIC	1	**3.816**	**135**	**-263**

G= Self-weight; WM= Wind mean value; WG= Wind gust

Table 2. Iced tower – static and dynamic analysis; f_1=0.3869 Hz; G=0.1; W_3=0.3869Hz

Model	Load freq. factor K [-]	Total load duration ts [s]	No. of steps n [-]	Zmax [m]	Smax [MPa]	Smin [MPa]
M601L	1.00	60	600	7.810	277	-542
M611L	0.90	60	600	**7.970**	**286**	**-559**
M621L	0.80	60	600	7.893	284	-555
M631L	0.70	60	600	7.337	262	-514
M641L	0.60	60	600	6.532	223	-437
M651L	0.50	60	600	6.452	217	-427
M661L	0.40	60	600	6.267	209	-411
M671L	0.30	60	600	5.931	196	-387
M681L	0.20	60	600	5.398	179	-353
M691L	0.10	60	600	5.393	178	-350
M600L	G+WM	STATIC	1	**3.624**	**143**	**-285**
M600L	G+WM+WG	STATIC	1	**5.266**	**202**	**-389**

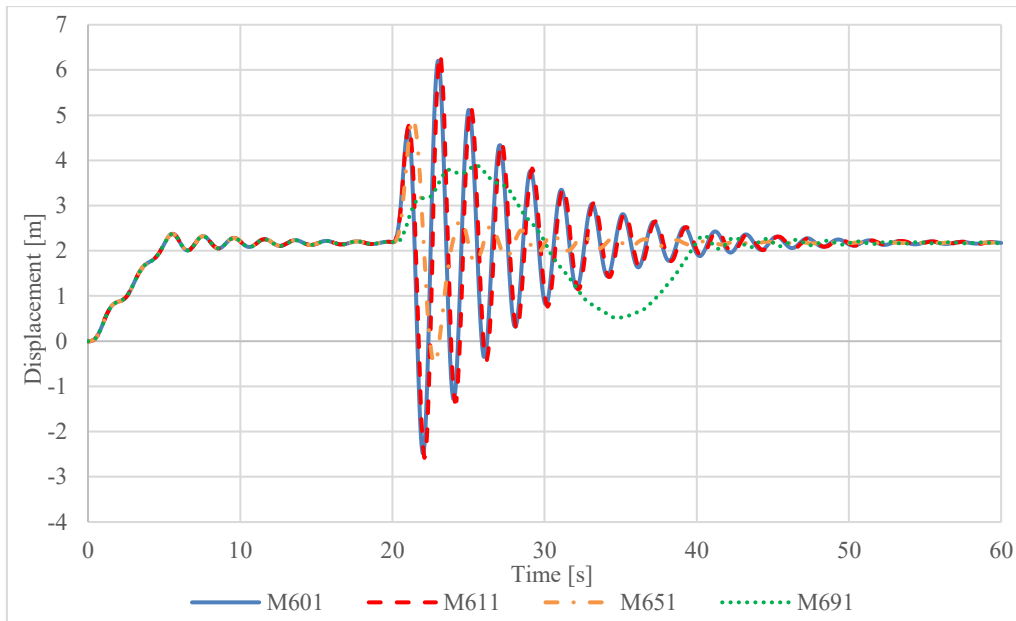G= Self-weight; WM= Wind mean value; WG= Wind gust

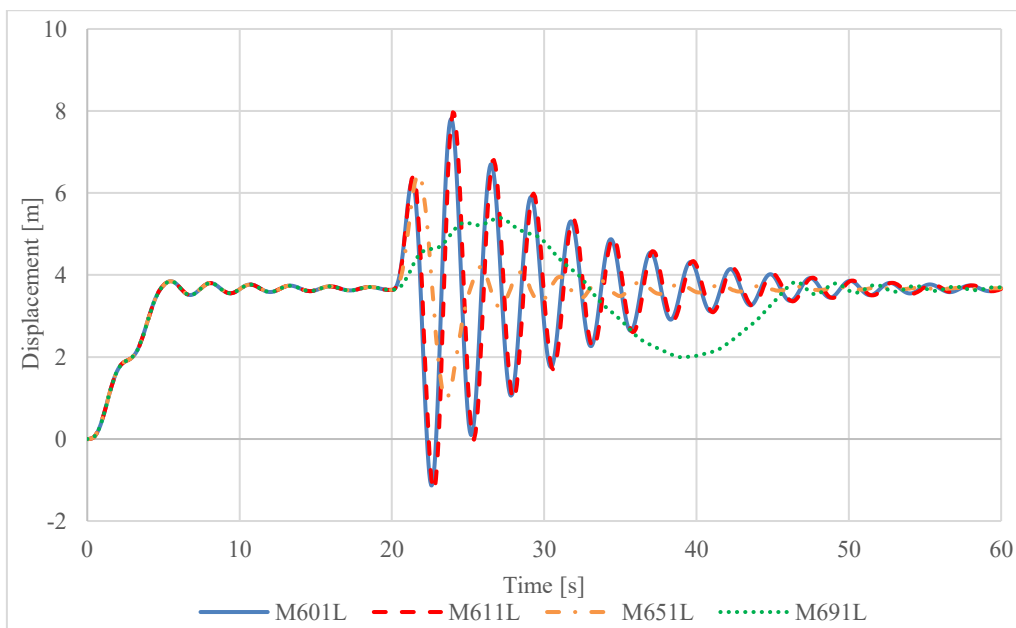*Figure 4. Ice-free tower: displacements of the top of the tower*

Figure 5. Iced tower: displacements of the top of the tower

Based on the obtained analysis results presented in tables 1 and 2 and in figures 4 and 5 a comparison was done, separately for the ice-free and the iced tower (Table 3 and 4). For comparison extreme values of displacements and stresses were taken. The load case G+WM, analysed statically, was adopted as a starting point, and its results were declared as 100 % value. In the second step, the wind gust was added, and this load case (G+WM+WG) was again analysed statically. The third step in fact represents the focal point of this paper. Here the wind gust was analysed using dynamic time-history analysis.

Table 3. Ice-free tower – comparison of results

Load and analysis method	Zmax [m]	Zmax [%]	Smax [MPa]	Smax [%]	Smin [MPa]	Smin [%]
G+WM (STATIC)	2.176	**100**	79	**100**	-157	**100**
G+WM+WG (STATIC)	3.816	**175**	135	**171**	-263	**168**
G+WM(QUASI-STATIC) + WG(DYNAMIC)	6.345	**192**	219	**277**	-426	**271**

Table 4. Iced tower – comparison of results

Load and analysis method	Zmax [m]	Zmax [%]	Smax [MPa]	Smax [%]	Smin [MPa]	Smin [%]
G+WM (STATIC)	3.624	**100**	143	**100**	-285	**100**
G+WM+WG (STATIC)	5.266	**145**	202	**141**	-389	**136**
G+WM (QUASI-STATIC) + WG (DYNAMIC)	7.970	**220**	286	**200**	-559	**196**

The first observation is that wind gust, even taken as a static load, increases all relevant output data, e.g., displacements rise for 75 % (ice-free tower) and 45 % (iced tower). The stresses were also significantly higher (see Table 3 and 4). That points to a strong recommendation that such high and slender structures should be obligatory checked under gust action, according to the standards [3].

However, the third analysis step, with the dynamic approach to gust action shows further considerable increase in displacements and stresses. This poses a very important question: is static analysis of wind actions satisfying for towers and similar structures? The obtained results obviously show that the answer is – no. Here must be noticed that Tables 3 and 4 present the most unfavourable results, which arise at frequencies of the gust excitation close to the resonant ones. But, a close look into the output data given in Tables 1 and 2 shows that displacements start to rise even if the gust excitation is only 10 % of the resonant frequency, compared to the static approach to gust action.

The results of the dynamic analysis are expected, but with one unexpected anomaly – the maximal displacements do not occur for the excitation frequency (K=1.0), but for a little lower value (K=0.9). This can be ascribed to some numerical error of the software, and certainly indicates that smaller frequency increments around resonance should be applied in the analysis, which will be the subject of the further investigations.

General view on the analysis results, especially the stresses, show that the selected structure could not satisfy criteria for safety and strength. Regardless of that, it was used for demonstration purposes of the importance of appropriate structural analysis method. Also, it must be noted that all analyses were done as linear, meaning that stability problems were nor treated. By all means, including of nonlinearity would be the next step of this research. It is reasonable to expect that noticed differences between the static and dynamic approach be even higher.

3 Conclusions

Based on the presented research, the following conclusions are drawn:

− Towers, masts, and similar structures are exposed to severe meteorological loads, and the most critical are wind, ice, and wind gust;

− Eurocode standards provide checking of towers and masts on wind gust induced vibrations in the wind direction, but do not supply concrete procedures for this;

− In this paper is developed an FEM model and load functions that enable a dynamic analysis of the wind gust, combined with the static action related to self-weight of the structure and wind mean action;

− The proposed method showed that application of dynamic analysis of the wind gust is strongly justified, because it showed significantly higher values of displacements and stresses compared to static wind gust analysis, mostly in the resonant domain, but also out of it;

− The FEM and application of advanced engineering software are a powerful tool for more reliable analysis of sensitive classes of structures like towers and masts, and make the approximate methods like the quasi-static method unjustified.

References

[1] EN 1993: Design of steel structures - Part 1-14: Design assisted by finite element analysis (draft material)

[2] Brčić, S., Met Lattice Tower H=110 m - Analysis Report Summary, Belgrade, 2019

[3] EN 1991: Actions on structures - Part 1-4: General actions - Wind actions

[4] EN 1993 - Design of steel structures - Part 3-1: Towers, masts and chimneys - Towers and masts

[5] Vacev, T., Brčić, S., Milić, M., Zorić, A., Nešović, I., Standard EN 1993-1-14: Design of Steel Structures Assisted by FEM in Case of a Tower H=110 m – ASES Symposium, 2020, Serbia

[6] FEMAP WITH NX NASTRAN Software Documentation

Performance of RC frames in 26.11.2019. Albania earthquake: effects of irregularities and detailing[*]

Ivan Milićević[*1)], Marko Marinković[1)], Nikola Blagojević[2)], Svetlana Nikolić-Brzev[3)]

[1)] University of Belgrade, Faculty of Civil Engineering, Bulevar kralja Aleksandra 73, 11000 Belgrade, Serbia
[2)] ETH Zurich, Department of Civil, Environmental and Geomatic Engineering, 8093 Zurich, Switzerland
[3)] University of British Columbia, Department of Civil Engineering, Vancouver, Canada

A B S T R A C T

The collapse and damage of large number of buildings during the November 26, 2019 (Mw 6,4) Albania earthquake caused 51 fatalities and injuries to at least 910 people. Most of collapsed or heavily damaged buildings were RC frame buildings. Although RC frame system is considered as very ductile seismic force-resisting system, its behaviour during earthquake highly depends on: (1) regularity in plan and elevation, and (2) global and local ductility. Based on the authors' visit to the earthquake-affected area on behalf of the Serbian Association of Earthquake Engineering and observations of collapsed and damaged buildings, it was concluded that among main reasons for underperformance of these flexible systems were inadequate analysis of interaction between infill walls and RC frames and reinforcement detailing of RC members.

1 Introduction

Located in a seismically active area, the territory of Albania has been exposed to 7 earthquakes of magnitude greater than 6.0 in the last 100 years. Only two months after two earthquakes of magnitude M_w larger than 5.0 that occurred in September 2019 (M_w = 5.6 and M_w = 5.1), at 3:45 a.m. on November 26, 2019 the western part of central Albania was hit by an earthquake of magnitude M_w 6.4 [1]. This was the strongest earthquake to hit Albania in the last 40 years. The epicentre of the earthquake, with a focal depth of 22 km, was 15 km from Mamurras, 22 km from the city of Durrës and 30 km from the capital Tirana (Fig. 1(a)). The main shock was followed by about 20 aftershocks of magnitude greater than 4.0.

As a result of the collapse and damage of a large number of buildings, 51 people were killed and over 910 were injured, while more than 200,000 people were affected by the earthquake [2]. In total, about 95,000 housing units (18% of the total number in the affected municipalities), 321 educational institutions (24%) and 36 health institutions were damaged, with total losses of 985 million euros. Majority of collapsed and significantly damaged buildings were located in the city of Durrës, which were predominantly constructed of reinforced concrete, and in the town of Thumanë, which were predominantly masonry buildings with prefabricated hollow reinforced concrete floor and roof systems.

The Serbian Association for Earthquake Engineering (SUZI-SAEE) formed a four-member team that visited the areas affected by the earthquake a month after the earthquake. The SUZI-SAEE team, which consisted of the authors of this paper, visited several villages and towns, including Tirana, Durrës, Krujë, Fushë-Krujë, Thumanë and Bubq.

After the survey of the damaged buildings, it was concluded that most buildings that experienced collapse or significant damage were constructed using the system of monolithic reinforced concrete (RC) frames, which had several structural deficiencies. Note that many RC frame buildings in Durres which suffered severe damage during the November 26, 2019 earthquake, were not damaged in the lower intensity earthquakes that occurred only two months earlier [6]. The main reason for severe damage of these RC frame buildings in the November 2019 earthquake was spectral accelerations which were higher than expected for flexible structures. The earthquake also revealed detailing deficiencies and effect of structural irregularities which negatively affected the seismic performance of these buildings. Fig. 1(b) shows that the spectral accelerations of November 26 earthquake were approximately equal to the elastic spectral accelerations according to the KTP-N.2-89 code. It can be seen from the chart that the predominant period corresponding to the peak spectral acceleration was in the range of 1.0 sec, with the peak ground acceleration (PGA) of 0.196g and the maximum spectral acceleration of more than 0.5g. It should be noted that the response spectrum for the Durrës station shown in Fig 1(b) was derived using the ground acceleration records corresponding to the initial 15 seconds of the main shock (the recording was discontinued due to a power outage in the station caused by the earthquake) [3].
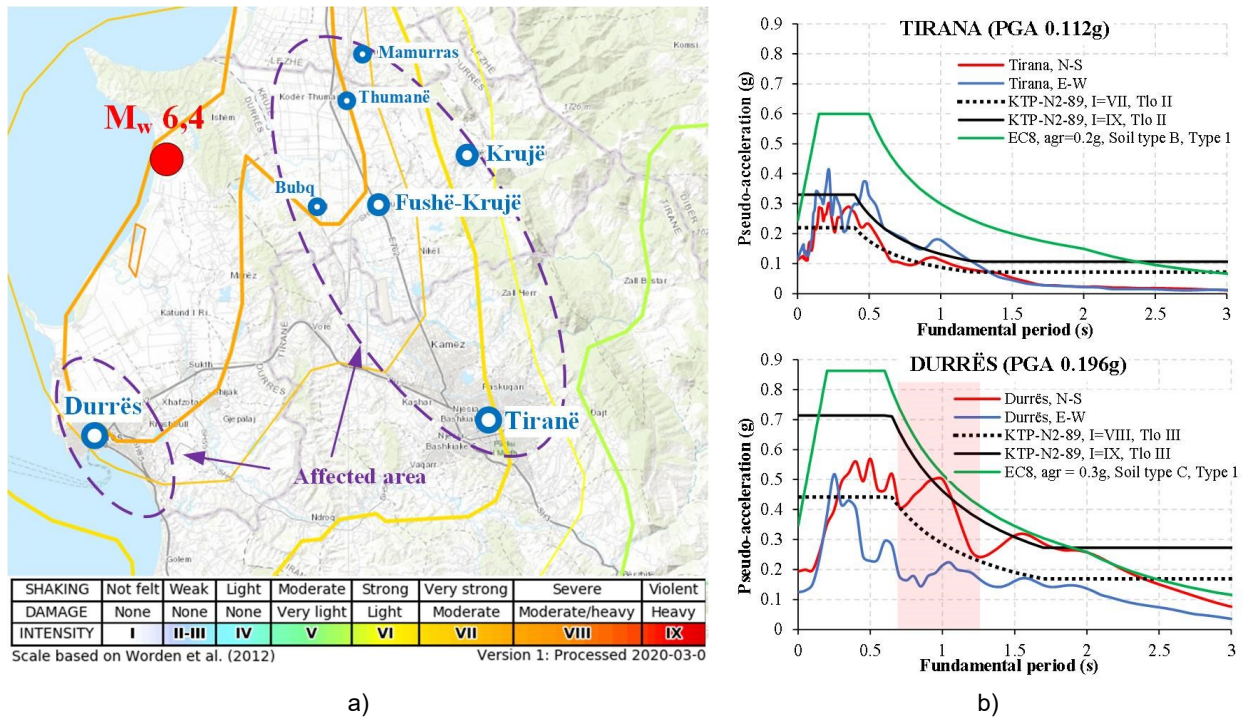
---

a)

b)

Figure 1. Earthquake in Albania 26.11.2019: a) Map of the affected area [1], b) Comparison of the earthquake spectrum with elastic spectra, according to [3], [4] and [5]

This paper presents observations and conclusions of the SUZI reconnaissance team pertaining the causes of collapse and damage of buildings with RC frame structures in the November 26, 2019 Albania earthquake. Since over 30 damaged buildings were completely demolished and the ruins were cleared before the arrival of the SUZI team in Albania, the conclusions were made based on a visual inspection of the remaining damaged buildings and information gathered in the field, various reports and analysis of seismic regulations and construction practices in Albania. The aim of this paper is to highlight negative consequences of inadequate reinforcement details for local ductility of RC elements, as well as inadequate treatment of irregularities in flexible RC frame systems. These irregularities were caused by inadequate building configuration and unfavourable influence of elements which are usually disregarded in seismic design, e.g., masonry infill walls, stairs, etc.

2 Construction practice and regulations in Albania: reinforced concrete frames

Before 1990s, unreinforced masonry buildings and prefabricated large panel RC buildings prevailed in Albanian construction practice. At the beginning of the 1990s, the construction of buildings with monolithic RC frame structures became prevalent. This structural system became dominant in construction practice after the adoption of the Albanian seismic code KTP-N.2-89 [5]. In most cases, RC frame buildings had one-way or two-way ribbed RC slabs with polystyrene or clay masonry infills, as shown in Figs. 2(a) and 2(b), respectively. In this floor system wide/shallow beams span between interior columns while in some cases deeper beams may be provided at the perimeter. The depth of these shallow beams is equal to the total floor thickness (on the order of 300 mm), which matches the minimum required

a)

b)

Figure 2. Typical examples of RC frame buildings in Albania:
a) a building during construction, b) interior of an existing building

depth of RC beams prescribed by the KTP-N.2-89 code [5], while the beam width is greater than or equal to the corresponding column dimension. In Albanian engineering practice, these shallow beams are often designed in the same manner as deeper RC beams. These buildings are usually designed and constructed either without any RC structural walls or with a relatively few walls, even in case of taller multi-storey buildings which are more than 10-storey high. As a result, the seismic force resisting system of these buildings consists of rather flexible RC moment-resisting frames (also known as bare frames).

Masonry infills, used as partition and façade walls, are in the form of multi-perforated clay blocks with horizontally aligned holes which is not common in practice other countries (e.g. in Serbia). Layout of the masonry infills in elevation and plan of the building depends on its function and position in relation to other buildings. There were many cases of buildings with open ground and first floors, with infills existing only at the higher floors. In other cases, masonry infills are unevenly distributed in plan (usually in buildings located at corners of a building block).

This structural system is addressed by the seismic code KTP-N.2-89 [5], which was published in 1989. According to KTP-N.2-89, seismic analysis and design of a structure is based on the reduced seismic load compared to a system with linear elastic behaviour. The values of the reduction factor depend on the type of the structural system and its presumed ductility. For RC frames with masonry infills which do not participate in resisting of seismic forces, the value of the reduction factor is between 2.63 and 4.0 (depending on the flexibility of RC columns). It should be noted that this is usual approach, although it is well-known that infill walls participate in resisting seismic forces, thus bring additional stress to the surrounding frame. The presumed ductility of the system is ensured by meeting the relatively strict detailing requirements for reinforcement in RC columns and beams, e.g. reduced spacing of stirrups/ties in critical areas and at splices of longitudinal reinforcement, minimum diameters of stirrups, maximum distances between restrained and unrestrained longitudinal bars in columns, lap splice lengths, etc. For buildings irregular plan or elevation, the code requires the application of a more accurate calculation method, which takes into account the contribution of higher vibration modes through multi-modal analysis (without increasing the seismic load). The displacement control is ensured through limiting inelastic displacements (the principle of "equal displacements"); however, the code does not explicitly prescribe displacement limits.

It is important to emphasize that, according to local experts, the code KTP-N.2-89 [5] was seldom applied in Albanian engineering practice in the period 1990-2000 (although its application was mandatory). The extent of KTP-N.2-89 code in the period 2001-2012 is also unknown. In addition to KTP-N.2-89, seismic design codes from other countries such as American design codes (since 1995) and Eurocodes (since 2005) have been applied on a voluntary basis on some projects.

3 Types and causes of damage of buildings with RC frame system

High spectral accelerations, combined with characteristic structural deficiencies, led to the collapse and damage of large number of buildings with RC frame structures in the November 26, 2019 earthquake. The inspection of damaged buildings revealed that each building had two or more deficiencies, such as:

– Irregularity in plan and/or elevation of flexible seismic-force-resisting system, most often due to the influence of masonry infills or staircases,
– Inadequate reinforcement detailing for local ductility of RC frame elements,
– Interaction of RC frames and masonry infills,
– Insufficient width of seismic gaps, which caused pounding of the adjacent buildings.

3.1 The effect of irregularities in RC frame structures

In most cases, structural irregularities of buildings located in the area affected by the November 26 earthquake were caused by the interaction of highly flexible RC frame structures with masonry infills or stair cases. In engineering practice, stiffness of these elements is often neglected in design of RC buildings. The most common types of irregularities were "soft storey", "short"/"captive" column effects, and asymmetrical stiffness distribution in plan which caused torsional effects during the earthquake.

Examples of collapsed buildings in Albania due to the November 26 earthquake are shown in Fig. 3. The "soft storey" collapse was caused by a large difference in the lateral stiffness between adjacent floors-usually ground floors that were more flexible than upper floors. This behaviour is typical for flexible RC frame systems, which are common in Albania. Vertical irregularities were caused by unevenly distributed masonry infills in buildings, with open spaces at the ground floor level (garages, office space, shops, restaurants, etc.), while at the other floors there was a masonry infill (usually housing units). Due to presence of masonry infills and the resulting increased stiffness at higher floor levels, deformation demands on RC columns at open lower floors were significantly increased, which most likely resulted in structural damage and collapse. It should also be noted that Hotel Ljubljana (see Figure 3(d)) had three added floors (vertical extension). The other cause for significant damage of RC columns is their smaller dimensions compared to dimensions of RC beams, as shown in Fig. 6(a).

The "short-column" effect most often occurs when some parts of staircase (usually on intermediate landing) are supported by the RC columns or a partial masonry infill is constructed up to a certain height of the RC column due to openings (e.g. windows), acting as a lateral restraint along the column height. Damaged RC columns caused by this effect are presented in Figs. 4(a) and 4(b), respectively. Due to the lateral restraint of RC column provided by the staircase or the partial masonry infill, the column height is smaller. Shortening of RC column leads to increased localized stiffness and internal forces in the column itself (usually shear forces), for which RC column is usually not designed.

Fig. 5 shows significant earthquake damage and collapse of flexible structures due to torsional effects. The damage was caused by "secondary elements", specifically masonry infills and stairs, which are often neglected in seismic design practice. Fig. 5(a) illustrates the effect of shifting the position of the centre of stiffness of the structure due to the restrained RC columns at the stair support locations. Torsional effects caused an increase of forces in elements on the opposite side, and significant damage of the RC columns along the façade. The damage of an RC column which supports the staircase in this building is shown in Fig. 4(a). The building also had an open space at the ground floor. Fig. 5(b) shows the collapse of a corner building that had two adjacent open sides at the ground floor level with masonry infill walls along the other two sides. The ruins were cleared before the authors' reconnaissance, but it is believed that the collapse

a)

b)

c)

d)

Figure 3. Examples of building collapses due to "soft storey" effect in the November 26, 2019

Shear failure of
RC column

a)

b)

Figure 4. Examples of RC column damage due to "short column" effect in the Albania earthquake caused by: a) intermediate staircase landing, b) partial masonry infill due to openings

was primarily due to inadequate detailing of RC members and torsional effects caused by a significant increase in stiffness on sides with masonry infill and an eccentricity of the centre of mass (CM) relative to centre of stiffness (CK).

3.2 Inadequate reinforcement detailing of RC frame elements

Apart from structural irregularities, several typical flaws in reinforcement detailing for the local ductility of the elements of RC frames (columns and beams), were observed in most of the damaged and collapsed buildings. Examples of these flaws are shown in Fig. 8. The authors believe that the most common detailing flaws were:

(1) A single perimeter tie in RC columns in "critical" regions (according to [5], for RC columns with cross section dimensions larger than 30 cm, there should be at least 2 ties);

(2) Widely spaced stirrups/ties in "critical" regions and/or outside the "critical" regions of beams and columns (according to [5], for IX seismic zone spacing of ties in RC columns should be less than 8 diameters of longitudinal bars or 10 cm);

(3) Lack of or complete absence of stirrups in beam-column joint regions;

(4) Ties with 90° hooks and insufficient anchorage length (according to [5], 135° hooks with straight part not shorter than 10 tie diameters are mandatory);

(5) Ties with 6 mm diameter in RC columns (according to [5], for seismic zone IX diameter of ties should be at least 8 mm);

(6) Insufficient lap splice length when (often 100% spliced reinforcement at one floor);

(7) Insufficient anchorage length of longitudinal beam reinforcement (without hooks).

A few examples of highlighted detailing flaws are shown in Fig. 6.

a) b)
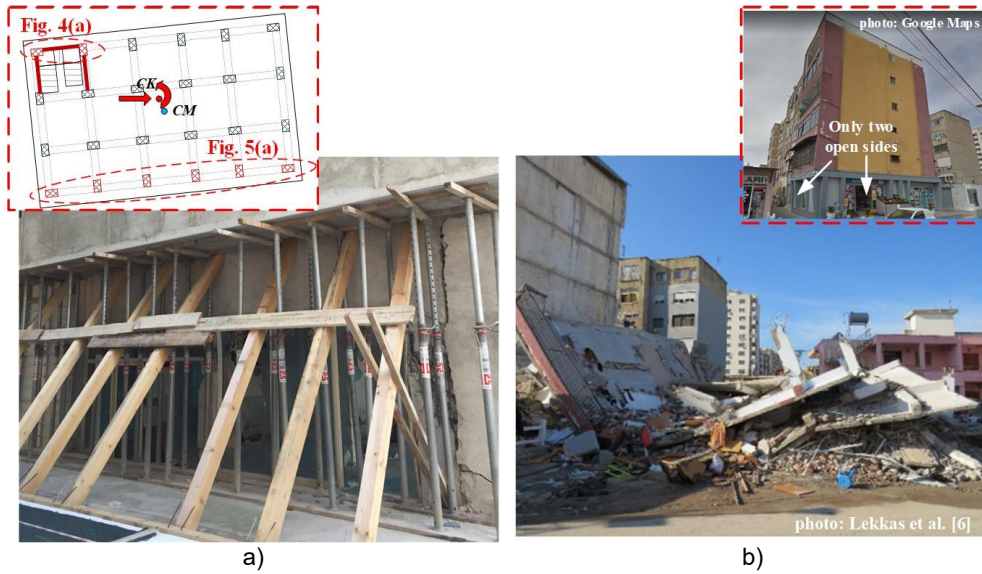
Figure 5. Examples of damage and collapse of a building in Durres due to torsional effects: a) shifting of centre of stiffness due to the corner staircases, b) the influence of masonry infills

Figure 6. Examples of inadequate detailing of reinforcement in RC columns and beams

3.3 Pounding of RC buildings and damage of RC columns due to interaction with infill walls

Several buildings suffered minor damage in the earthquake due to pounding, which was caused by insufficient width or absence of seismic gaps. An example of damage caused by this effect is shown in Fig. 7. In this case, the building experienced permanent inter-storey drifts. The interaction caused damage such as crushing of concrete cover (see Fig. 7(b)) and cracking of infill walls made out of concrete blocks as well as RC columns (see Fig. 7(c)) is the result of their interaction. This mechanism is explained in detail in [8].

3.4 Behaviour of RC frame structures of newer buildings with damaged masonry infill walls

Most of the buildings that sustained significant damage or collapse during the November 26 earthquake were built between 1990 and 2010. Although the buildings built after 2010 also sustained damage in the earthquake, the level and extent of damage to the structural elements of these buildings were relatively small. The masonry infills suffered most of the damage. Although these (mostly tall) buildings had flexible RC frame structures, the authors believe that RC elements with large dimensions had a significantly higher load-bearing capacity compared to the masonry infills. Therefore, due to large inter-storey drifts at lower floor levels (typical for frame structures), only masonry infills experienced significant damage (see Figs. 8(a) and 8(b)).

Minor damage of RC elements can be attributed to adequate detailing of reinforcement for local ductility (see Fig. 8(c)).

4 Conclusions and recommendations for seismic design

Many buildings in the western part of central Albania were damaged by the November 26, 2019 earthquake. Despite the existence of the Albanian seismic code which prescribes detailed provisions for design and detailing of reinforcement in RC frame elements, many buildings with this structural system experienced significant damage or collapse. Given the high demands in terms of spectral accelerations that were approximately equal to the design accelerations for flexible systems corresponding to fundamental periods of 0.8 to 1.2 s, several key "weaknesses" of RC frame structures came to the fore. One of the main reasons for the damage was inadequate analysis of various irregularities caused by the unfavourable influence of "secondary elements" - masonry infills and staircases, which completely changed the assumed behaviour of flexible RC frames. The second reason was poor detailing of reinforcement in RC columns, beams and beam-column joints. As a result, the provided ductility of the structures was significantly less than expected. Since, in the Republic of Serbia, RC frame structures are quite common in residential and commercial buildings and the maximum ground acceleration in Durres was 0.196g (according to Eurocode 8, for the large part of Serbia peak ground acceleration is in
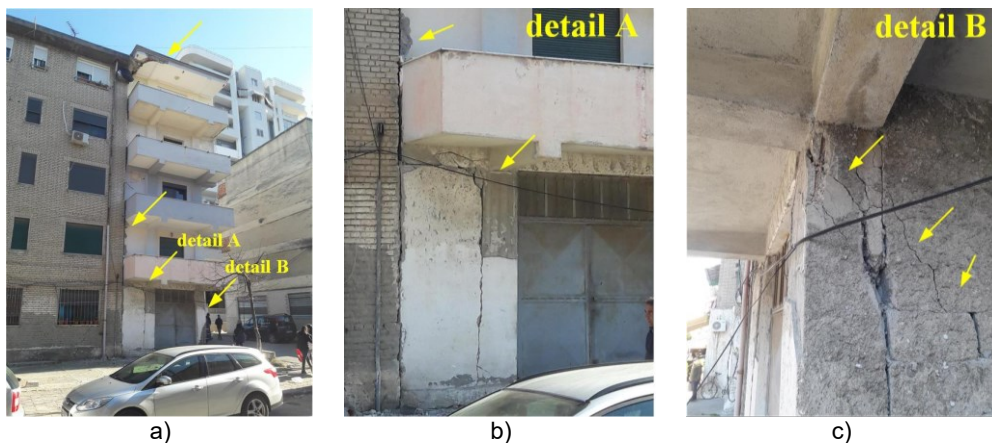

Figure 7. Example of damage caused by pounding of adjacent buildings (a, b) and interaction between RC frames with infill walls (c)
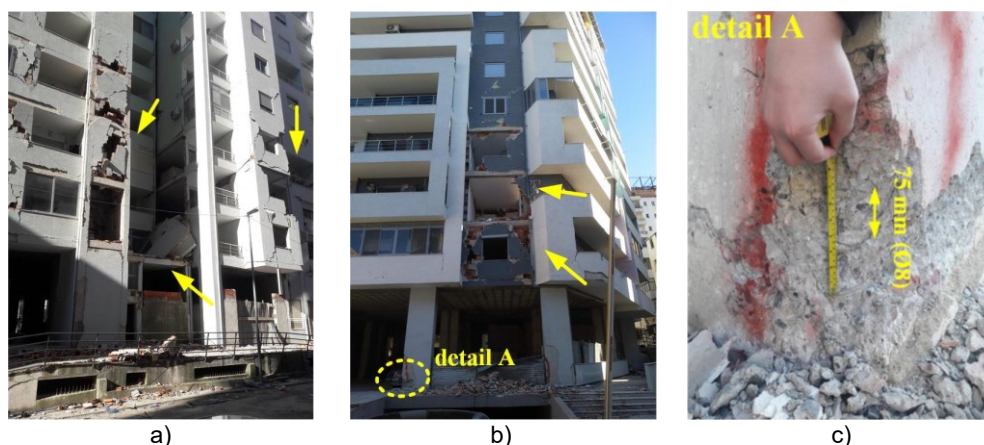

Figure 8. Examples of damage to modern buildings with RC frame structure

range 0.15g-0.20g), experiences from this earthquake are relevant to Serbian engineering practice. In contemporary seismic design codes (such as Eurocode 8) detailed engineering analysis is required to ensure reliable behaviour of RC frame structures during earthquakes. Alternative solution is to provide sufficient amount of RC walls, which would reduce the flexibility of the entire structure and mitigate highlighted problems.

Acknowledgement

References

[1]   U.S. Geological Survey (USGS): M 6.4 - 15km WSW of Mamurras,   Albania, https://earthquake.usgs.gov/earthquakes/eventpage/us70006d0m/executive, (22.4.2020.)

[2]   UNDOP, WB & EU: Post-Disaster Needs Assessment – Albania. United Nations Development Program, World Bank and European Union, 2020.

[3]   Duni L., Theodoulidis N.: Short note on the November 26, 2019, Durres (Albania) M6.4   earthquake: strong ground motion with emphasis in Durres city, Institute of Engineering Seismology and Earthquake Engineering (ITSAK), 2019.

[4]   Institute of GeoSciences, Energy, Water and Environment: StrongMotionRecords_Durresi earthquake_26November2019,https://geo.edu.al/newweb/?fq=november&gj=gj2, (22.4.2020)

[5]   KTP-N.2-89: Kusht teknik projektimi per ndertimet antisizmike, Akademia e Shkencave (Qendra Sizmologjike) & Ministria E Ndertimit (Drejtoria e Projektimeve), 1989.

[6]   Lekkas E., Mavroulis S., Papa D., Carydis P.: The November 26, 2019 Mw 6.4 Durrës (Albania) earthquake, Newsletter of Environmental, Disaster and Crisis Menagment Stategies, 2019.8

[7]   McKenney C,: Reconnaissance Observation Report Albania M6.4 Earthquake on November 26, 2019, 2019.

[8]   M.Marinković, S. Brzev, M. Baballëku, B. Isufi, N. Blagojević, I. Milićević, Ž. Žugić, P. Bursać, Out-of-plane behaviour of loadbearing and non-structural masonry walls during recent earthquakes, 1st Croatian Conference on Earthquake Engineering, Zagreb, Croatia, 22-24 March, 2021.

Repair of RC structure of road-pedestrian bridge over Lepenica river in Kragujevac*

Vlastimir Radonjanin*[1], Mirjana Malešev[1], Ivan Lukić[1], Slobodan Šupić[1]

[1] Faculty of Technical Sciences University of Novi Sad, Trg Dositeja Obradovića 6, 21000 Novi Sad, Serbia

A B S T R A C T

The paper gives an overview of the repair solution of the RC structure of the bridge over the Lepenica River in Kragujevac with a detailed description of the adopted solution for the repair/strengthening of the main RC girders. All necessary parameters (degree of environment aggressiveness, classes of exposure, the thickness of the concrete cover, principles and methods of repair, etc.) for the proper selection of products (materials) and the techniques of repair, were defined according to the Regulations on technical standards for concrete structures exposed to aggressive environments, EN 206, EC 1992-1-1 and standard EN 1504..

1   introduction

After 60 years of service a severe damage of the reinforced concrete bridge have been occurred. The main causes that have led to significant damage appearance are: direct exposure to weathering, a numerous defects originating from the period of bridge construction, poorly solved bridge drainage system and lack of maintenance. By the survey of the bridge load-bearing structure and in-situ testing of built-in materials it was concluded that the designed load-bearing capacity and durability of the bridge can be restored by appropriate repair measures.

2   Basic data on the bridge structure

The road-pedestrian bridge is a RC structure, a static system of a continuous girder on three-span continuous beam (23.5m+28.2m+23.5m), with total length of 75.20m. The superstructure consists of: 3 main longitudinal and 13 cross girders, bridge deck and cantilever slabs. The main longitudinal girders are located in the axes "A", "B", and "C" at a distance of 3m from each other (Fig. 1). The height of the main longitudinal girders in the axes "A" and "C" is 140cm, and in the axis "B" is 145cm. In the zone of middle supports (above the river pillars) the main longitudinal girders in the axes "A" and "C" are 190cm high, and the girder in the axis "B" is 195cm (due to the transverse slope of the pavement). The width of the main longitudinal girders is constant - 40cm.

Cross girders were constructed at quarters of each span. The width of those girders is 25cm, and their height is 125cm.

The thickness of the bridge deck is 17cm. The slope of the deck is 2% to both sides. Along with the bridge deck,

1.5m wide cantilever pedestrian paths were constructed on both sides, with variable height from 25cm to 10cm.

The elements of substructures are: 2 RC pillars and 2 abutments. The abutments are constructed as massive elements, 8m long and of variable width from 4.30m to 1.95m at the top. Both river pillars are constructed as RC panels, 80cm thick, with variable width (maximum 6.40m). The height of the river pillars is 10.40m. The wing walls are constructed as hanging RC wings (tied to the abutments).

Three supports of the main girders are roller supports, and the fourth one on the abutment in the axis "3" is pin support. The roller support on the abutment in axis "0" is built of reinforced concrete in the form of a pendulum, while the supports on the river pillars are built of crossed reinforcement.

The foundation of the bridge was derived on a single stepped footings made of plain concrete. The dimensions of the foundations under the river pillars are 400x700cm in the base (height 270cm) and under the abutments 515x800cm (height 160cm).

3   Assessment of the bridge structures

The process of assessment of the load-bearing RC structure and other elements of the bridge included:

– review and analysis of available bridge documentation,

– control of the dimensions of the bridge and the basic elements of the load-bearing structure,

– detailed visual inspection with registration and classification of characteristic defects and damages of the load-bearing structure elements,

---

* *Paper presented at ASES 2020 Symposium, Arandjelovac, Serbia, May 2021.*
* Corresponding author:
   E-mail address: radonv@uns.ac.rs

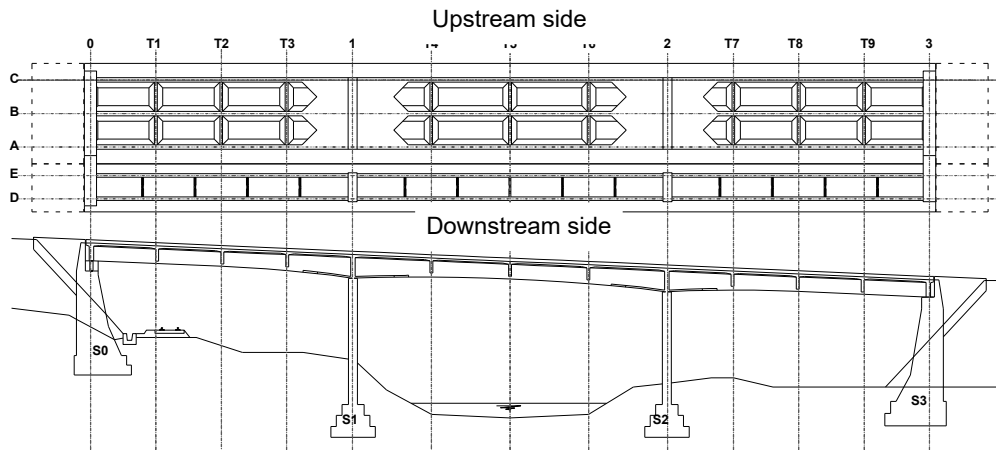Upstream side

Downstream side

Figure 1. The base and longitudinal cross section of the bridge with the adopted axis labels

− subsequent determination of the quality of the built-in concrete;

− determining the depth of the concrete carbonation,

− checking the arrangement of built-in reinforcement in main and transverse girders,

− geodetic survey of the bridge and

− control calculation of the load-bearing capacity of the bridge.

The aim of all these activities was to obtain a sufficient number of reliable data for an realistic assessment of the condition of the bridge structure in terms of its load-bearing capacity, stability, serviceability and durability [1], [3].

Based on the obtained results of the current condition of the bridge the following conclusions were derived:

− The load-bearing structure of the bridge corresponds to the designed values of the bridge in terms of shape and dimensions.

− The assessed class of compressive strength of built-in concrete in the tested RC elements of the bridge structure corresponds to the designed one.

− The type and arrangement of the installed reinforcement in the tested structure elements correspond to the details of the reinforcement from the project.

− The control calculation confirmed the load-bearing capacity and stability of the bridge except in the upper zone of the bridge deck, where approximately 5% of reinforcement is missing.

− The reinforcement lost its passive protection due to the concrete carbonation and the insufficient thickness of the concrete cover.

− The stability of the bridge is not endangered.

− The load-bearing capacity of the two main longitudinal girders (in axes "A" and "C") is reduced due to heavy corrosion of reinforcement and loss of adhesion between reinforcement and concrete, thus reducing the load-bearing capacity of the bridge as a whole (Fig 2 and 3).

− The durability of the bridge is reduced due to numerous defects, such as the insufficient thickness of the concrete cover, improper reinforcement arrangement, honeycombing, etc., as well as carbonation, damages of the concrete in the form of cracked and fallen parts of concrete and improper drainage of atmospheric water from the bridge.

− The serviceability of the bridge is partially endangered on pedestrian paths due to deep damages in asphalt concrete and precast RC slabs, and on the pavement slab, because of the reduced load-bearing capacity of the superstructure.

Figure 2. Severe corrosion of reinforcement, broken stirrups, longitudinal girder in axis "A"

Figure 3. Severe corrosion of reinforcement, broken stirrups, deep spalling off of concrete, longitudinal girder in axis "C"

4 Repair design

In order to ensure the designed load-bearing capacity, serviceability, and durability of the bridge, the following repair solutions [2], [4] were proposed:

– general reprofiling of abutments,

– local reprofiling and surface protection of river pillars,

– replacement of bearings (3 pendulums) on the abutment in the "0" axis,

– repair and strengthening of the main RC longitudinal girders in axes "A" and "C", new protective layer and surface protection,

– structural repair of the main RC longitudinal girder in the "B" axis and new protective layer,

– local reprofiling and surface protection of transverse girders,

– local reprofiling, application of a new protective layer or application of a protective coating on the underside of the RC slab;

– structural repair of the top side of the RC slab,

– removal of edge RC girders of pedestrian path and construction of new edge girders and slabs of pedestrian path,

– other works (drains and atmospheric sewers, waterproof membrane, ...)

Here are presented repair solutions for main structural elements: longitudinal RC girders, replacement of bearings and repair of RC slab.

The appearance of main cross sections is presented in Figures 4 and 5.

4.1 Main longitudinal girders

The repair method of the main edge girders in axes A and C includes cleaning and protection of the reinforcement bars affected by moderate or surface corrosion (principle 7, method 7.2), replacement of main reinforcement bars and stirrups affected by strong corrosion (principle 4, method 4.1), execution of a new protective layer of concrete (principle 4, method 4.4 and principle 7, method 7.1), reinforcement with CFRP composites (principle 4, method 4.3), and application of a protective coating which additionally prevents the penetration of water, CO_2, chloride and other aggressive substances into the concrete interior (principle 1, method 1.3).
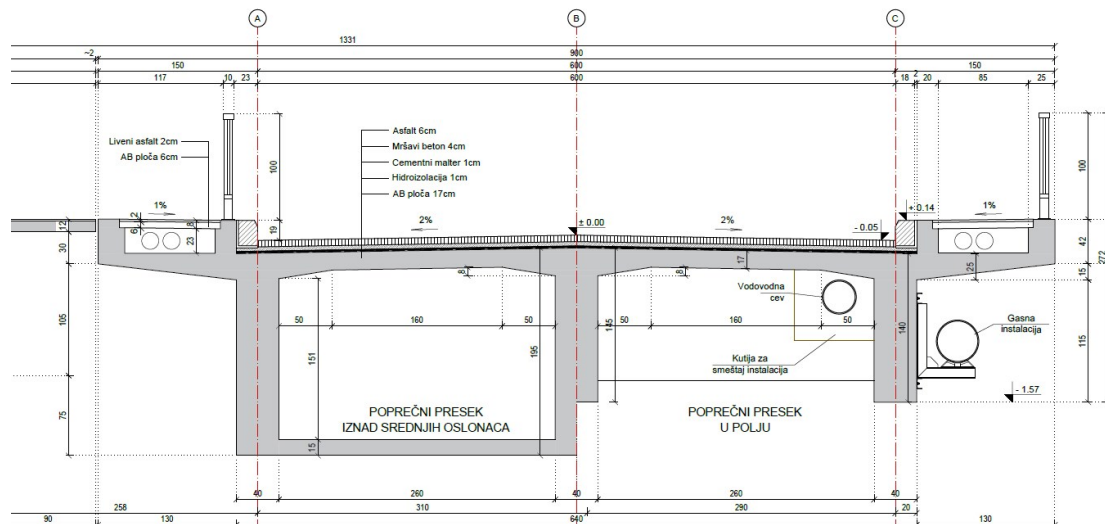
Figure 4. Main cross section of bridge before repair
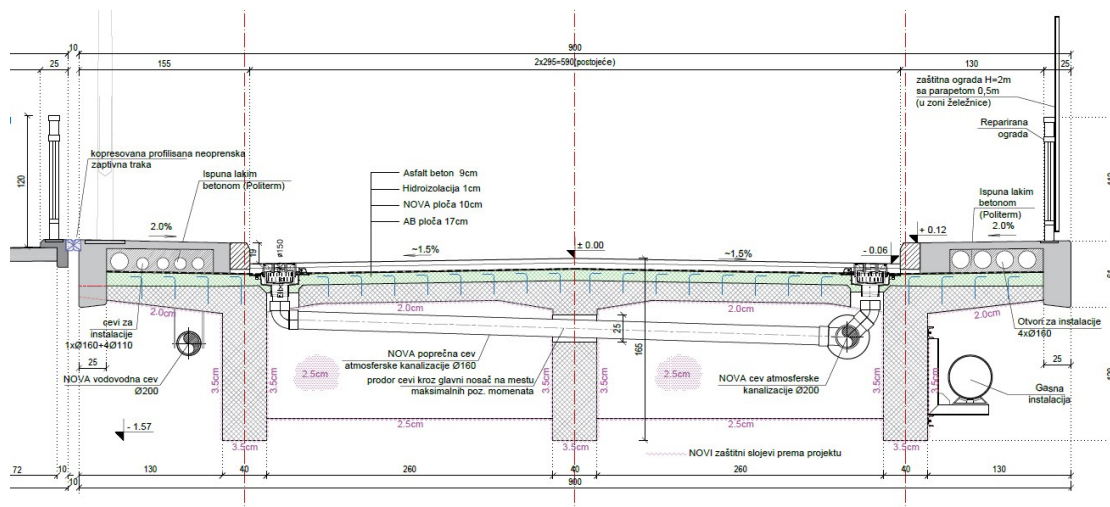
Figure 5. Main cross section of bridge according to repair design

Depending on the degree of damage, the repair solutions of main girders are divided into two groups:

− Girders in axes A and C on which the following procedures are applied: repair of reinforcement affected by moderate or surface corrosion, replacement of rods of main reinforcement and stirrups affected by strong corrosion, execution of a new protective layer of concrete, strengthening with CFRP strips and application of protective coating.

− Girders in the B axis on which the following procedures are applied: repair of reinforcement affected by moderate or surface corrosion, construction of a new protective layer of concrete and strengthening with CFRP strips.

Taking into account extent of damage and position of damaged zone, four different repair solutions are designed (Figure 6).

4.1.1 D2/D4: Repair of reinforcement bars affected by moderate or surface corrosion and construction of a new protective layer

Local repair of corroded bars is applied at the places of visible corrosion of reinforcement and stirrups and at the places of cracks along corroded bars of reinforcement, and includes the following operations:

− Marking of zones for repair of corroded reinforcement bars on the sides, while for the lower side it is planned to remove the protective layer of concrete over the entire surface.

− Removal of the existing protective layer of concrete on the underside of the girder and locally, around the corroded reinforcement bars on the underside and on the sides, including areas with cracked concrete. The depth of the removed layer of concrete depends on the preservation of the adhesion between the reinforcement and the concrete and on the degree of corrosion of the reinforcement (Figure 7).

− Preparation of the complete concrete surface of the sides by dry sandblasting to obtain base for a new protective layer (cleaning and removal of smaller loose grains, dust deposits, biological deposits and other impurities), which provides the necessary roughness of the concrete surface and cleaning visible parts reinforcement from corrosion.

− Washing of prepared surfaces.

− Coating of "exposed" reinforcement bars to ensure better adhesion, which at the same time protects the reinforcement from corrosion.

− Setting the formwork to perform a new protective layer.

− Pouring of self-compacting concrete (SCC, two-fraction D_{max} = 8 mm) or applying of repair mortar (Figure 8).
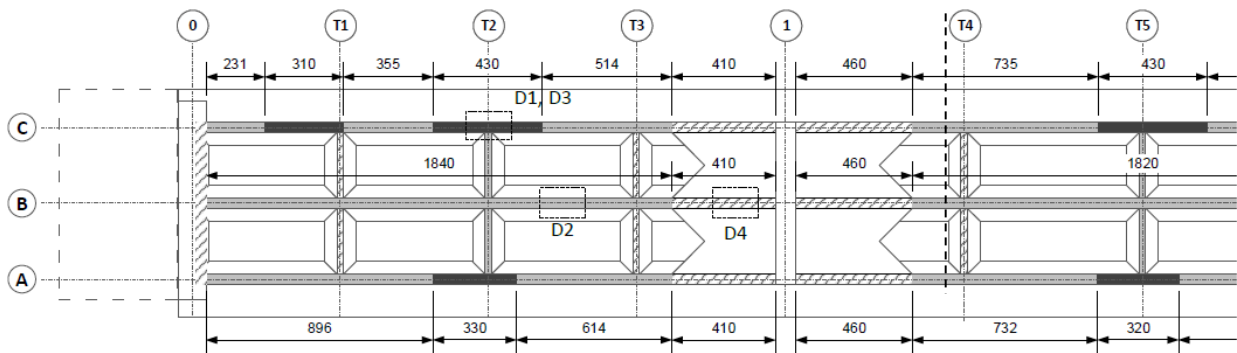
− Curing of concrete.

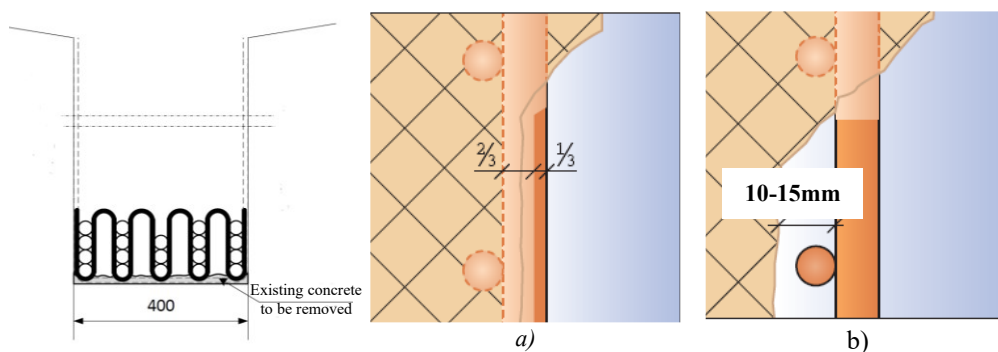*Figure 6.. Repair solutions for longitudinal and transverse girders*

Figure 7. Removal of the existing protective layer of concrete: a) removed layer of concrete if the reinforcement bar is partially affected by the corrosion process, and the adhesion is preserved; b) removed layer of concrete if the reinforcement bar is affected by the corrosion process along the entire circumference, and the adhesion with the concrete is disturbed
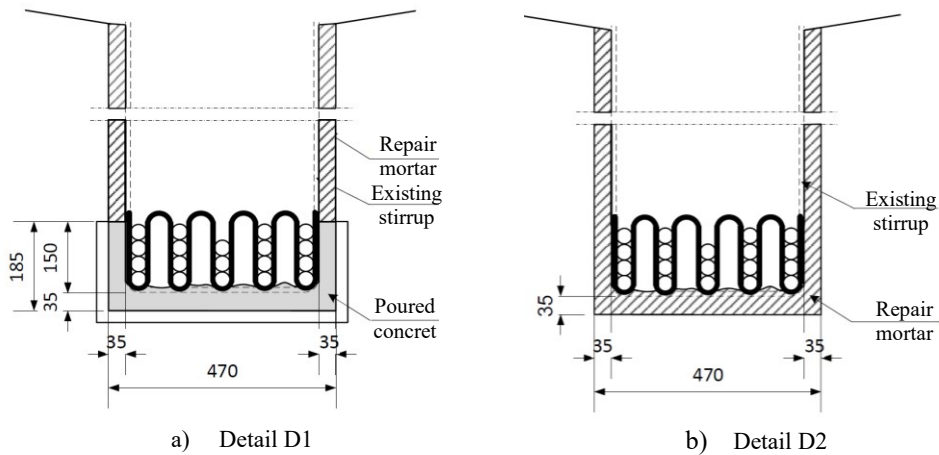
a)   Detail D1   b)   Detail D2

Figure 8. New protective concrete cover

4.1.2 D1: Replacement of bars of the main reinforcement and stirrups affected by strong corrosion and execution of a new protective layer

Replacement of corroded bars is applied in places of strong corrosion of reinforcement and significant reduction of cross section (Figure 9).

Replacement of corroded reinforcement bars includes the following operations:

− Marking of zones for replacement of corroded reinforcement bars. The zones should be of regular geometric shape and be at least 50 cm wider on both sides in relation to the damaged zone.

− Removal of concrete around the corroded reinforcement bars in the first row in order to release them and in height up to the first "healthy" reinforcement bar. "Healthy" rods should be stripped to ≈1/3 of the cross-sectional circumference. Concrete removal is performed by manual chipping or by pneumatic hammers. The depth of the removed layer of concrete depends on the number of bars affected by strong corrosion and is at least 5 cm in the zone of middle bars and 8 cm in the zone of corner bars.

− Removing concrete around the stirrups, to cut and weld to continue the stirrups. Concrete is removed at a length equal to the length of the corroded part of the stirrup increased by 20 cm or at a length of at least 20 cm from the upper edge of the removed concrete (if the stirrups have not corroded).

− Preparation of the remaining vertical concrete surfaces of the beams by dry sandblasting

− Cutting of corroded reinforcement bars and stirrups around the longitudinal reinforcement, in the replacement zone. When cutting the reinforcement that continues, at least 50 cm of free "healthy" reinforcement remains on both sides of the damaged zone. The stirrups are cut along the entire length on which the concrete was removed.

− Cleaning of the remaining visible parts of the reinforcement by dry or wet sandblasting.

− Washing of prepared surfaces.

− Continuation of reinforcement bars with garters made of rolled L profile or reinforcement bars and installation of new stirrup parts by overlapping with single-sided welding.

− Coating of "exposed" reinforcement bars to ensure better adhesion, which at the same time protects the reinforcement from corrosion.

− Setting three-sided formwork to the lower surface of the pedestrian cantilever slab. The formwork is placed in such way to ensure the continuity of the cross-section with the zones where the structural repair was not performed.

− Concreting of the new protective layer and the missing parts of the section with concrete under pressure.
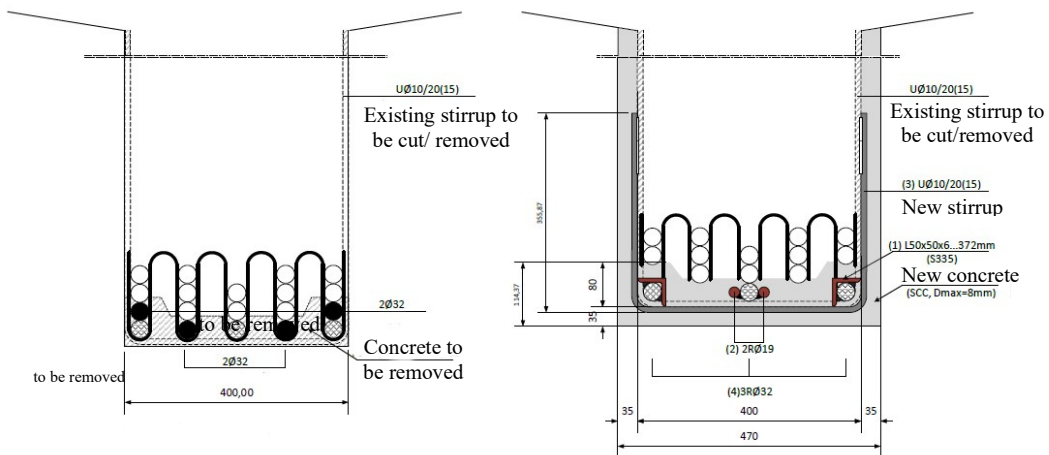
− Curing of concrete.

Figure 9. Repair solution D1 – replacing existing corroded reinforrcement

4.1.3 D3: Strengthening with CFRP strips

Strengthening with CFRP strips includes both zones, with strong corrosion and zones in which the load-bearing capacity with the existing reinforcement is not satisfied (according to static calculation). Detail of strengthening is given in Figure 10.

When placing CFRP, the following technical requirements are prescribed:
- Proof of achieved concrete compressive strength ($f_c \geq 30MPa$);
- Determination of bond strength / adhesion for concrete surface (Pull-of method, $f_{ath} \geq 1.5MPa$);
- Control of flatness / roughness of surfaces;
- Dew point control (surface temperature must be higher than dew point temperature increased by 3°C);
- Surface humidity control (surface humidity must not exceed 4%);
- Outdoor temperature (10°C -35°C);
- Principle of applying CFRP (preparation for gluing, applying glue and gluing) should be done according to the manufacturer's instructions;
- Control of performed works;

- Control of empty spaces in the glue. Gaps in the middle reinforcement zones can be injected with epoxy resin under low pressure, while in the case of gaps at the ends, the strips must be removed and re-glued.

4.2 Replacement of bearings

For the purpose of replacing the existing "pendulum" bearings with new, elastomeric ones, it is planned to raise the structure by ~ 10 mm at the column location S0 (Figure 11).

Lifting is performed by placing the press under the supporting transverse girder, in the phase after repairing the lower zone of the main girders, but before concreting the additional layer of the RC slab from the top side. The presses are placed next to the main girders, outside the zones of the new support so that the procedure of repair of the bearing surfaces and replacement of the bearing can be executed.

After lifting, the structure rests on temporary supports. Edge presses required for lifting must have a capacity of at least 350t, while the required capacity of medium presses is at least 120t.
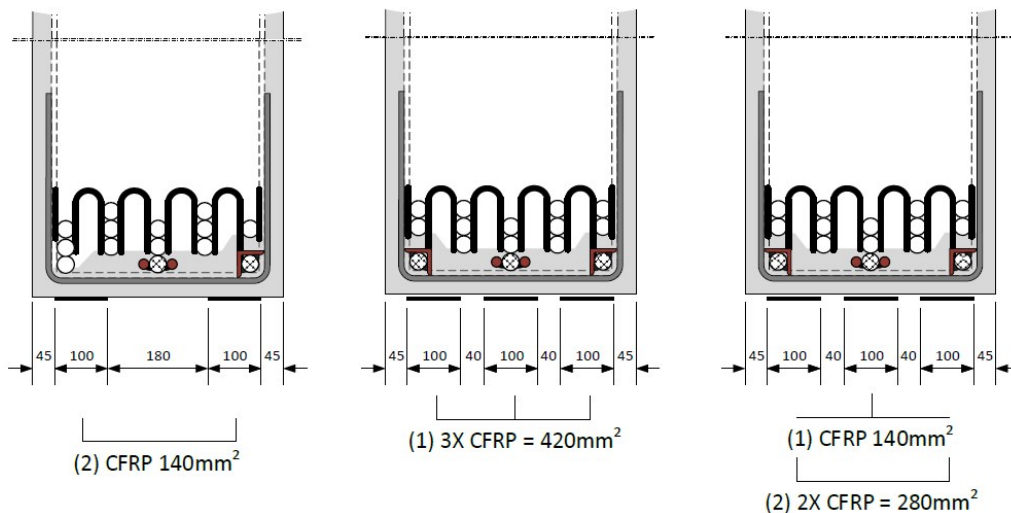
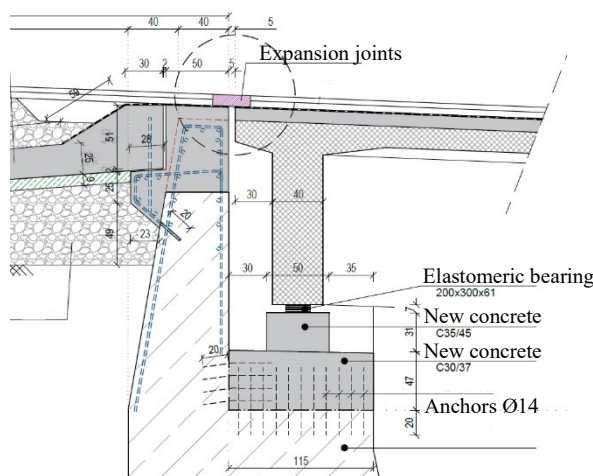Figure 10. Repair slution D3 – replacing existing corroded reinforrcement

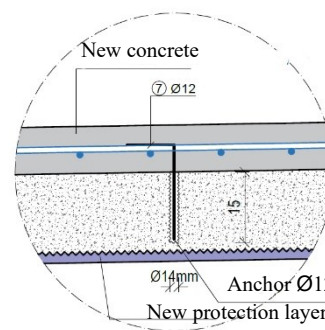Figure 11. Replacing of existing pendulum bearings

Figure 12. Repair solution of top side of RC slab

After the formation of new bearing blocks and the repair of the lower zone of the beam, the construction is lowered down on the new elastomeric bearings.

4.3 RC slab

4.3.1 Repair solution of top side of bridge deck

The method of repairing of top side of the bridge deck (Figure 12) includes the installation of anchors for ensuring composite action of new and old concrete (principle 4, method 4.2) and execution of a new concrete layer (principle 4, method 4.4).

These repair solution is applied to the entire top surface of the slab and includes the following operations:

− Preparation of the complete concrete surface by sandblasting for the application of bonding primer (cleaning and removal of smaller loose grains, dust deposits and other impurities), which also provides the necessary roughness of the concrete surface.

− Drilling holes with a diameter of Ø18, cleaning, dusting and pouring the mass to ensure adhesion between the anchors and the old concrete.

− Installation of Ø14 (B500B) concrete steel adhesion anchors in the prepared holes.

− Washing the top surface of the slab

− Installation of additional reinforcement.

− Applying a bonding primer immediately before concreting (if the coating is polymer-based)
Concreting of the additional concrete layer (Dmax = 16mm).

4.3.2 SP1 and SP2: Repair solution of bottom side of bridge deck

The method of repairing the RC bridge deck from the bottom includes: local repair of corroded reinforcement bars (principle 7, method 7.2), surface impregnation to prevent general corrosion of reinforcement (principle 11, method 11.3) and application of a protective coating which partially compensates the insufficient thickness of the concrete protection layer (principle 1, method 1.2) and execution of a new protective layer (principle 7, method 7.1).

Depending on the degree of damage to the lower surface of the slab, two groups of repair procedures are defined:

− SP1 is applied on slab areas that lack a protective layer, and has only local corrosion of reinforcement, erosion of concrete and concrete honeycombs and includes local repair of corroded reinforcement bars, surface impregnation and application of a protective coating

− Procedure SP2 is applied to slab areas that lack a protective layer, but have severe corrosion of reinforcement and other types of damage and includes the repair of corroded reinforcement bars and the execution of a new protective layer.

The position of the slab areas according to the repair solution is given on Figure 13.

5 Conclusion

Development of repair design was iterative, as there were several factors to consider. The investor had two requests that limited possible repair solutions. The first one was ensuring that one-half of the bridge would be available for pedestrian use during repair works. The other one was related to the fact that there is an active railway track below the bridge and because of that, it was not possible to significantly change the height of the main girders and to use supporting scaffolding.

Also, repair design for main girders according to solution D3 implies phase execution, in terms of sequential remove and replace of corroded reinforcement, due to significant reduction of the load-bearing capacity of their cross-section.
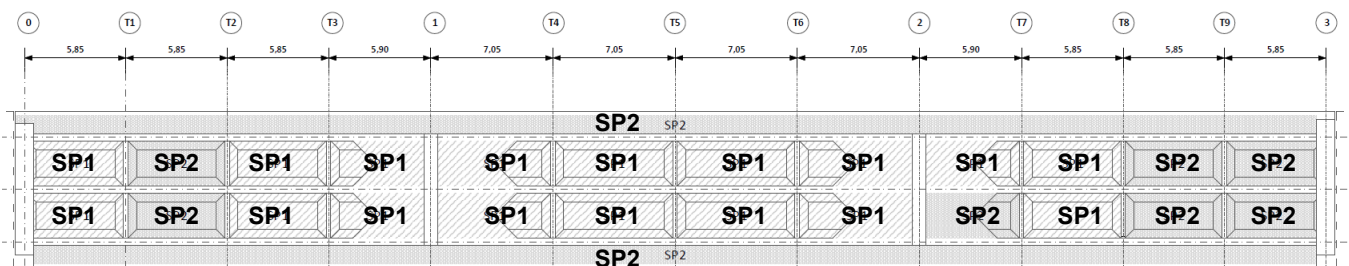
Figure 13. Areas with different repair solution for bottom side of RC slab

References

[1] Radonjanin V., Malešev M., Lukić I., Šupić S.: Study on the assessment of the road-pedestrian bridge over the river Lepenica in Kragujevac (in serbian), FTN – Department of Civil Engineering and Geodesy, Novi Sad, 2019.

[2] Radonjanin et al. (2019): Repair design of the construction of the road-pedestrian bridge over the river Lepenica in Kragujevac (in serbian), Joint venture (JV): Project Biro Utiber d.o.o. (Leader), FTN Departma za građevinarstvo i geodeziju (Partner), Centralna putna laboratorija d.o.o (Partner), Novi Sad, 2019.

[3] Malešev M., Šupić S., Radonjanin V., Lukić I.: Assessment of RC structure of road-pedestrian bridge over Lepenica river in Kragujevac, Association of Structural Engineers of Serbia, International Symposium 2020, Proceedings, pp. 263-272.

[4] Radonjanin V., Malešev M., Lukić I., Šupić S.: Repair of rc structure of road-pedestrian bridge over Lepenica river in Kragujevac, Association of Structural Engineers of Serbia, International Symposium 2020, Proceedings, pp. 279-288.

INSTRUCTIONS FOR AUTHORS

Acceptance and types of contributions

The Building Materials and Structures journal will publish unpublished papers, articles and conference reports with modifications in the field of Civil Engineering and similar areas (Geodesy and Architecture).The following types of contributions will be published: original scientific papers, preliminary reports, review papers, professional papers, objects describe / presentations and experiences (case studies), as well as discussions on published papers.

Original scientific paper is the primary source of scientific information and new ideas and insights as a result of original research using appropriate scientific methods. The achieved results are presented briefly, but in a way to enable proficient readers to assess the results of experi-mental or theoretical numerical analyses, so that the research can be repeated and yield with the same or results within the limits of tolerable deviations, as stated in the paper.

Preliminary report contains the first short notifications on the results of research but without detailed explanation, i.e. it is shorter than the original scientific paper.

Review paper is a scientific work that presents the state of science in a particular area as a result of analysis, review and comments, and conclusions of published papers, on which the necessary data are presented clearly and critically, including the own papers. Any reference units used in the analysis of the topic are indicated, as well as papers that may contribute to the results of further research. If the reference data are methodically systematized, but not analyzed and discussed, such review papers are classified as technical papers.

Technical paper is a useful contribution which outlines the known insights that contribute to the dissemination of knowledge and adaptation of the results of original research to the needs of theory and practice.

Other contributions are presentations of objects, i.e. their structures and experiences (examples) in the construction and application of various materials (case studies).
In order to speed up the acceptance of papers for publication, authors need to take into account the Instructions for the preparation of papers which can be found in the text below.

Instructions for writing manuscripts

The manuscript should be typed one-sided on A-4 sheets with margins of 31 mm (top and bottom) and 20 mm (left and right) in Word, font Arial 12 pt. The entire paper should be submitted also in electronic format to e-mail address provided here, or on CD. The author is obliged to keep one copy of the manuscript.

As of issue 1/2010, in line with the decision of the Management Board of the Society and the Board of Editors, papers with positive reviews, accepted for publication, will be published in Serbian and English, and in English for foreign authors (except for authors coming from the Serbian and Croatian speaking area).

Each page should be numbered, and the optimal length of the paper in one language is about 16 pages (30.000 characters) including pictures, images, tables and references. Larger scale works require the approval of the Board of Editors.

The title should describe the content of the paper using a few words (preferably eight, and up to eleven). Ab-

breviations and formulas should be omitted in the title. The name and surname of the author should be provided after the title of the paper, while authors' title and position, as well as affiliation in the footnote. The author should provide his/her phone number, e-mail address and mailing address.

The abstract (summary) of about 150-250 words in Serbian and English should be followed by key words (up to seven). This is a concise presentation of the entire article and provides the readers with insight into the essential elements of the paper.

The manuscript is divided into chapters and sub-chapters, which are hierarchically numbered with Arabic numerals. The paper consists of introduction and content with results, analysis and conclusions. The paper ends with the list of references. All dimensional units must be presented in international SI measurement units. The formulas and equations should be written carefully taking into account the indexes and exponents. Symbols in formulas should be defined in the order they appear, or alternatively, symbols may be explained in a specific list in the appendix. Illustrations (tables, charts, diagrams and photos) should be in black and white, in a format that enables them to remain clear and legible when downscaled for printing: one to two columns (8 cm or 16.5 cm) in height, and maximum of 24.5 cm high, i.e. the size of the letters and numbers should be at least 1.5 mm. Original drawings should be of high quality and fully prepared for copying. They also can be high-quality, sharp and contrasting photo¬copies. Photos should be in black and white, on quality paper with sharp contours, which enable clear reproduction.

The list of references provided at the end of the paper should contain only papers mentioned in the text. The cited papers should be presented in alphabetical order of the authors' first name. References in the text should be numbered with Arabic numerals in square brackets, as provided in the list of references, e.g. [1]. Each citation in the text must be contained in the list of references and vice versa, each entry from the list of references must be cited in the text.

Entries in the list of references contain the author's last name and initials of his first name, followed by the full title of the cited article, the name of the journal, year of publication and the initial and final pages cited (from - to). If the doi code exists it is necessary to enter it in the references. For books, the title should be followed by the name of the editor (if any), the number of issue, the first and last pages of the book's chapter or part, the name of the publisher and the place of publication, if there are several cities, only the first in the order should be provided. When the cited information is not taken from the original work, but found in some other source, the citation should be added, "cited after ..."

Authors are responsible for the content presented and must themselves provide any necessary consent for specific information and illustrations used in the work to be published.

If the manuscript is accepted for publication, the authors shall implement all the corrections and improvements to the text and illustrations as instructed by the Editor.

Writings and illustrations contained in published papers will not be returned. All explanations and instructions can be obtained from the Board of Editors.

Contributions can be submitted to the following e-mails: sneska@imk.grf.bg.ac.rs or miram@uns.ac.rs
Website of the Society and the journal: www.dimk.rs

Financial support

MINISTRY OF EDUCATION, SCIENCE AND
TECHNOLOGICAL DEVELOPMENT OF
REPUBLIC OF SERBIA

UNIVERSITY OF BELGRADE FACULTY OF
CIVIL ENGINEERING

INSTITUTE FOR TESTING OF MATERIALS-
IMS INSTITUTE, BELGRADE

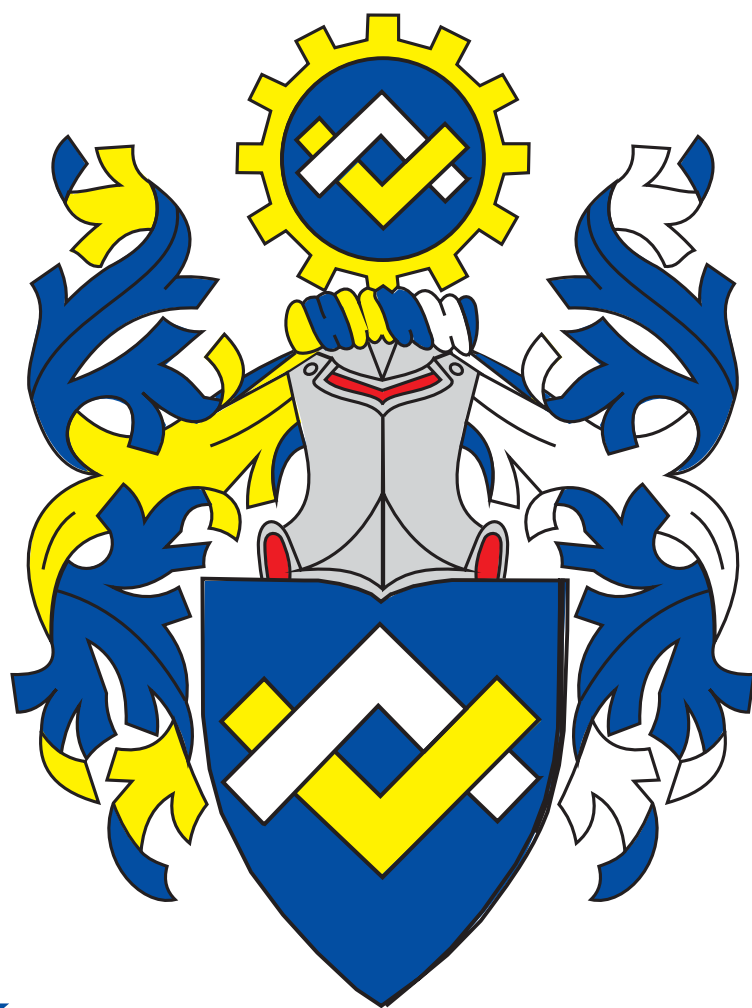FACULTY OF TECHNICAL SCIENCES,
UNIVERSITY OF NOVI SAD, DEPARTMENT
OF CIVIL ENGINEERING

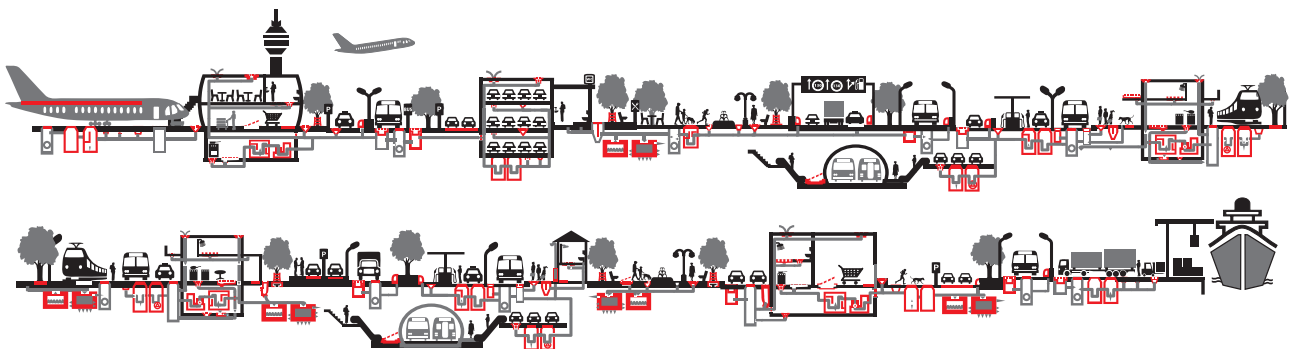SERBIAN CHAMBER OF ENGINEERS

INŽENJERSKA
KOMORA
SRBIJE

INSTITUT IMS a.d.

Institut za ispitivanje materijala IMS, sa tradicijom od 1929. godine, predstavlja najstariju naučno-istraživačku instituciju u Srbiji. Osnovna ideja prilikom osnivanja bila je potreba za jedinstvenom institucijom koja bi se osim istraživanja bavila i kontrolom građevinske industrije.

Delatnost Instituta IMS obuhvata laboratorijska ispitivanja građevinskih materijala, sertifikaciju proizvoda, nadzor nad izvođenjem radova i ispitivanje različitih tipova konstrukcija, izradu projektne dokumentacije, kao i naučno - istraživački rad u svim oblastima građevinarstva.

Poslovni centri Instituta IMS :
- Centar za puteve i geotehniku
- Centar za materijale
- Centar za metale i energetiku
- Centar za konstrukcije i prednaprezanje

INSTITUT IMS a. d.
Bulevar vojvode Mišića 43
11 000 Beograd
Tel: 011-2651-949
Faks: 011-3692-772
office@institutims.rs
www.institutims.rs

Institut IMS sertifikovao je sistem kvaliteta prema zahtevima standarda SRPS ISO 9001:2001. Svoju kompetentnost je potvrdio najvećim obimom akreditacije kod Akreditacionog tela Srbije (ATS) i Sertifikacionog tela.

Kadrovsku strukturu Instituta IMS čine doktori nauka, diplomirani inženjeri sa licencama Inženjerske komore Srbije i stručni tehnički kadar. Inženjeri Instituta IMS aktivno učestvuju na naučno-stručnim skupovima u zemlji i inostranstvu.

Institut IMS kontinuirano unapređuje kvalitet poslovanja na svim nivoima, kako u okviru terenskih i laboratorijskih ispitivanja, tako i na izradi projektno-tehničke dokumentacije s ciljem uspešne realizacije postavljenih zadataka.
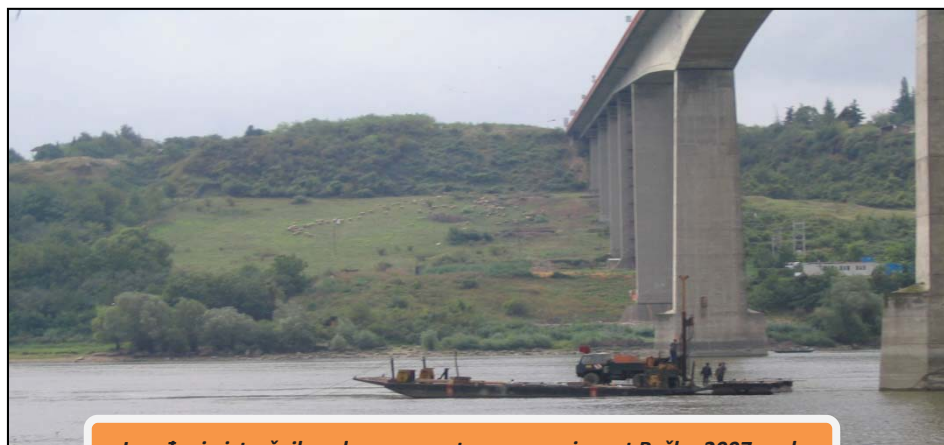
Izvođenje istražnih radova sa pontona za novi most Beška,2007.god.

Geotehnička istraživanja i ispitivanja – in situ

Od terenskih istražnih radova izdvajamo izvođenje istražnih bušotina (IB), standardnih penetracionih opita (SPT), statičkih penetracionih opita (CPT i CPTU), opita dilatometarskom sondom (DMT i SDMT), ispitivanja vodopropustljivosti tla različitim terenskim metodama (VDP), ugradnja pijezometara i dr.

Terenske metode ispitivanja šipova zauzimaju značajno mesto u našoj delatnosti, a na tržištu se izdvajamo kao lideri u toj oblasti u protekloj deceniji.

Ispitivanje šipova

SLT metoda (Static load test) ispitivanje nosivosti šipova statičkim opterećenjem;

DLT metoda (Dynamic load test) ispitivanje nosivosti šipova dinamičkim opterećenjem;

PDA metoda (Pile driving analysis) omogućava praćenje i optimizaciju procesa pobijanja prefabrikovanih betonskih i čeličnih šipova u tlo;

PIT (SIT) metoda (Pile(Sonic) integrity testing) koristi se za ispitivanje integriteta izvedenih šipova (dužine, prekida, suženja ili proširenja).
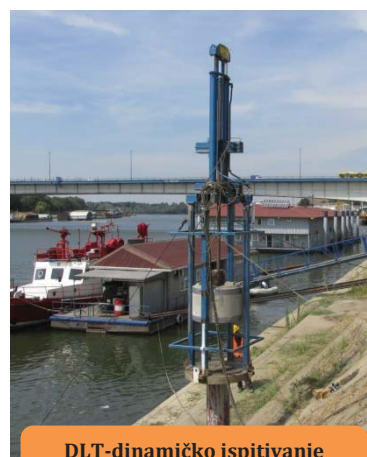
DLT-dinamičko ispitivanje šipova

CPT/CPTU opiti

Aktivno klizište
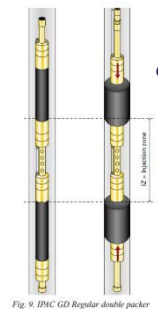
oprema za ispitivanje vodopropusnosti stena pod pritiskom do 10 bar-a metodom LIŽONA

Fig. 9. IPAC GD Regular double packer

Laboratorija za puteve i geotehniku

Laboratorija za puteve i geotehniku akreditovana je kod Akreditacionog tela Srbije – ATS prema SRPS ISO/IEC 17025:2006. U njoj se vrše ispitivanja tla (identifikaciono–klasifikaciona ispitivanja, fizičko–mehanička modelska ispitivanja), kamenog agregata i brašna, bitumena i bitumenskih emulzija, asfaltnih mešavina. U okviru laboratorijskih ispitivanja na terenu vrši se kontrola kvaliteta ugrađenog materijala i izvedenih radova (prethodna, tekuća, kontrolna ispitivanja i izvođenja opita in situ).

Projektovanje puteva i sanacija klizišta

U okviru projektovanja značajno mesto u radu zauzimaju geotehnička istraživanja terena i projekti sanacije klizišta - nestabilnih kosina useka i nasipa puteva i prirodno nestabilnih padina . Značajna su i projekovanja svih vrsta fundiranja specijalnih geotehničkih konstrukcija. Ističe se i iskustvo u oblasti putarstva, na projektovanju novih, rehabilitacija i rekonstrukcija postojećih puteva svih rangova sa pratećim objektima i dimenzionisanjem kolovoznih konstrukcija.

Nadzor

Naši inženjeri imaju veliko iskustvo u kontroli i proveri kvaliteta izvođenja svih vrsta radova, kontroli građevinske dokumentacije i praćenju radova u skladu sa njom, kao i rešavanju novonastalih situacija tokom izvođenja radova.

Najlepši krov u komšiluku

Continental Plus Natura je premium crep u natur segmentu! Dobro poznatog oblika, trajan i veoma otporan, a povrh svega pristupačan, naprosto oduzima dah svima. Čak i vašim komšijama!

Continental Plus Natura crep potražite kod ovlašćenih Tondach partnera.

Wienerberger

UZ **MAPEI** SVE JE **OK**

Kada birate, birajte tehnološki napredna rešenja, stručnost i **Mapei proizvode** najvišeg kvaliteta. Za izgradnju novih, sanaciju i rekonstrukciju postojećih ili konzervaciju istorijskih građevina. **Napravite razliku, odaberite Mapei – vašeg partnera u izgradnji.**

Više na: **mapei.rs** i **mapei.com**

MAPEI®
GRAĐEVINSKI LEPKOVI • HIDROIZOLACIONI SISTEMI
HEMIJSKI PROIZVODI ZA GRAĐEVINARSTVO

PUT INŽENJERING

Put inženjering d.o.o punih 25 godina radi kao specijalizovano preduzeće za izgradnju infrastrukture u niskogradnji i visokogradnji, kao i proizvodnjom kamenog agregata i betona. Preduzeće se bavi i transportom, uslugama građevinske mehanizacije i specijalne opreme.

Za spravljanje betona koristimo drobljeni krečnjački agregat sa našeg kamenoloma, deklarisanih frakcija, kontrolisane vlažnosti. Kompletan proces proizvodnje i kontrole kvaliteta vršimo prema važećim standardima.

Kao generalni izvođač radova, vršimo koordinaciju svih učesnika na projektu, planiranje, praćenje i nabavku materijala, kontrolu kvaliteta izvedenih radova, poštujući zadate vremenske rokove i finansijski okvir investitora.

Obradu armature vršimo brzo, stručno i kvalitetno, sa kompjuterskom preciznošću i dimenzijama po projektu.

Osnovni princip našeg poslovanja zasniva se na individualnom pristupu svakom klijentu i pronalaženje najoptimalnijeg rešenja za njegove transportne i logističke potrebe.

Koristeći inovativne tehnike i kvalitetan građevinski materijal iz sopstvenih resursa, spremni smo da odgovorimo na mnoge zahteve naših klijenata iz oblasti niskogradnje.

Naša kompanija u oblasti visokogradnje primenjuje sistem prefabrikovnih betonskih elemenata koji u odnosu na klasičnu gradnju ima brojne prednosti.

Usluge građevinskom mehanizacijom vršimo tehnički ispravnim mašinama, sa potrebnim sertifikatima kako za rukovaoce građevinskim mašinama tako i za same mašine.

Osnovna prednost prefabrikovane konstrukcije jeste brzina kojom konstrukcija može biti projektovana, proizvedena, transportovana i namontirana.

Prednapregnute šuplje ploče su konstruktivni elementi visokog kvaliteta, proizvedeni u fabrički kontrolisanim uslovima.

Raspolažemo opremom i mašinama za sve zemljane radove, kipere i dampere za rad u teškim terenskim uslovima, automiksere i pumpe za beton, autodizalice, podizne platforme.

Izvodimo hidrograđevinske radove u izgradnji kanalizacionih mreža za odvođenje atmosferskih, otpadnih i upotrebljenih voda, izvođenjem hidrograđevinskih radova u okviru regulacije rečnih tokova, kao i izvođenjem hidrotehničkih objekata.

Izrađujemo betonske "New Jersey profile" koji se u svetu koriste za preusmeravanje saobraćaja i zaštitu pešaka u toku izgradnje puta, kao i Betonblock sistem betonskih blokova.

Sakupljanje i privremeno skladištenje otpada vršimo našim specijalizovanim vozilima i deponujemo na našu lokaciju sa odgovarajućom dozvolom. Kapacitet mašine je 250 t/h građevinskog neopasnog otpada.

Površinski kop udaljen je 35 km od Niša. Savremene drobilice, postrojenje za separaciju i sejalica efikasno usitnjavaju i razdvajaju kamene agregate po veličinama. Tehnički kapacitet trenutne primarne drobilice je 300 t/h.

Uslugu transporta vršimo automikserima, kapaciteta bubnja od 7 m³ do 10 m³ betonske mase. Za ugradnju betona posedujemo auto-pumpu za beton, radnog učinka 150 m³/h, sa dužinom strele od 36 m.

NIŠ
Knjaževačka bb, 18000 Niš - Srbija
+381 18 215 355
office@putinzenjering.com

BEOGRAD
Jugoslovenska 2a, 11250 Beograd – Železnik
+381 11 25 81 111
beograd@putinzenjering.com

www.putinzenjering.com

MOBECO

MATEST
YOUR PARTNER IN TESTING

iT TECH

INELAS ERECO d.o.o

MATEST "iT TECH" KONTROLNA JEDINICA

ITOUCH
TECHNOLOGY

JEDNA TEHNOLOGIJA MNOGO REŠENJA

IT Touch Techlogy je Matestov najnoviji koncept koji ima za cilj da ponudi inovativna i user-friendly tehnologiju za kontrolu i upravljanje najmodernijom opremom u domenu testiranja građevinskih materijala

Ova tehnologija je srž Matestove kontrolne jedinice, software baziran na Windows platformi i touch screen sistem koji je modularan, fleksibilan i obavlja mnoge opcije

iT TECH pokriva
| INOVATIVNOST
| INTERNET KONEKCIJA
| INTERFEJS SA IKONICAMA
| INDUSTRIJALNA TEHNOLOGIJA

SISTEM JEDNOG RAZMIŠLJANJA   JEDNOM SHVATIŠ - SVE TESTIRAŠ

NAPREDNA TEHNOLOGIJA ISPITIVANJA ASFALTA

| GYROTRONIC - Gyratory Compactor
| ARC - Electromechanical Asphalt Roller Compactor
| ASC - Asphalt Shear Box Compactor
| SMARTRACKER^{tm} - Multiwheels Hamburg Wheel Tracker, DRY + WET test environment
| SOFTMATIC - Automatic Digital Ring & Ball Apparatus
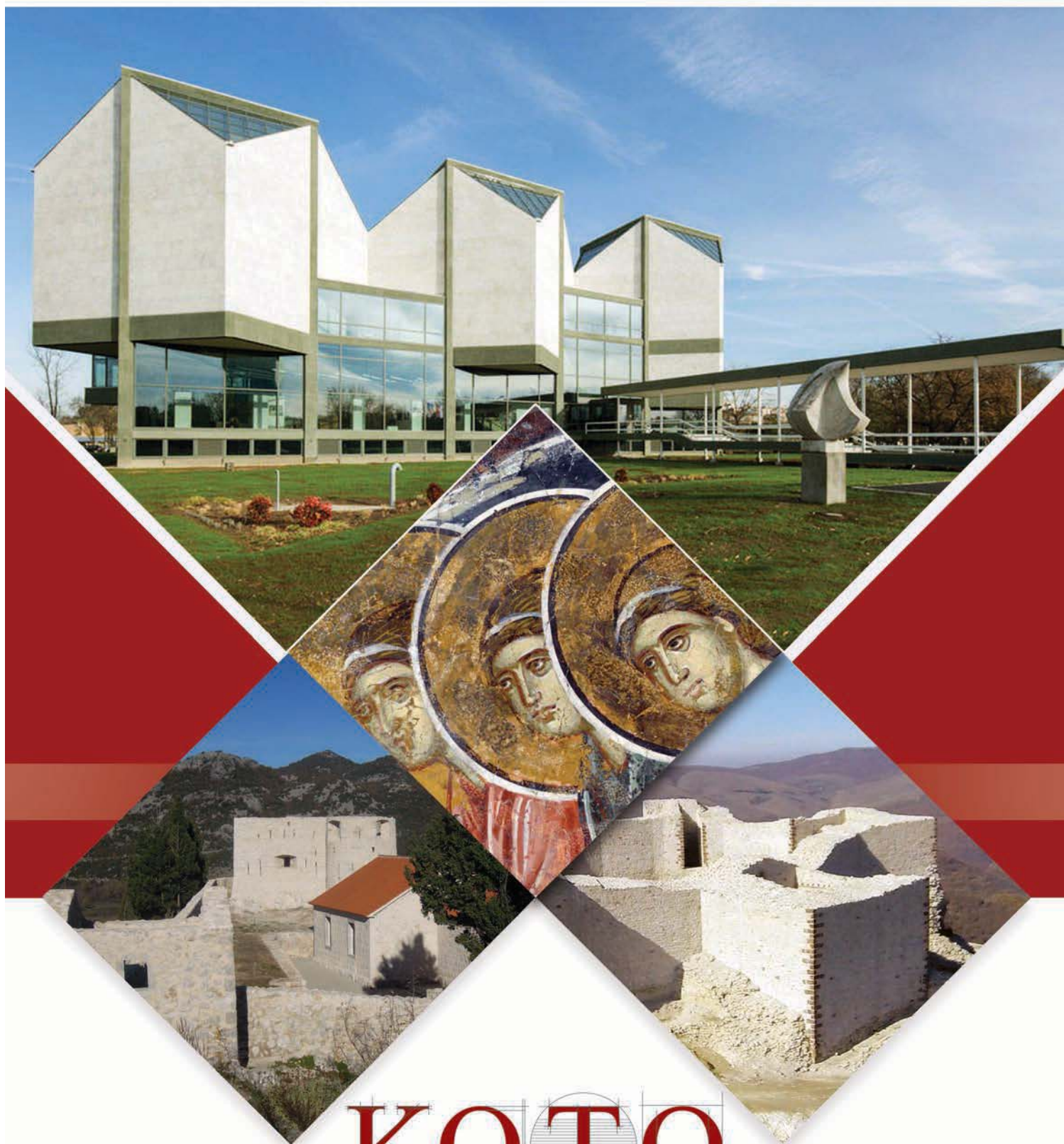| Ductilometers with data acquisition system

MULTIFUNKCIONALNI RAMOVI ZA TESTIRANJE

| CBR/Marshall digital machines
| Universal multispeed load frames
| UNITRONIC 50kN or 200kN Universal multipurpose compression/flexural and tensile frames

OPREMA ZA GEOMEHANIČKO ISPITIVANJE

| EDOTRONIC - Automatic Consolidation Apparatus
| SHEARLAB - AUTOSHEARLAB - SHEARTRONIC Direct / Residual shear testing systems
| Triaxial Load Frame 50kN

MIXMATIC - Automatic Programmable Mortar Mixer

INELAS ERECO D.O.O
Tošin bunar 274a, 11070 , Novi Beograd   tel. +381 11 2284 574 email. info@inelasereco.rs